DEVELOPMENT OF ADHESION FORCE MICROSCOPY FOR SURFACE CHARGE ANALYSIS OF COLLAGEN FIBRILS *IN VIVO* AND *IN VITRO*

by

Vinayak Mull

Submitted in partial fulfillment of the requirements
for the degree of Master of Science

at

Dalhousie University
Halifax, Nova Scotia
June 2023

This thesis is dedicated to my beloved late grandmother, a heart as big as whose I can only aspire to have and whom I couldn't be with during her final moments. I extend this dedication to my entire family, whom I had to leave behind to embark on this journey. The boundless love you all have for me is what keeps me going. I miss you every single day.

Table of Contents

List of Tables

List of Figures

Abstract

Collagen fibrils are a key component of the extracellular matrix of mammalian tissues where they serve as structural elements and as a ligand for receptor-mediated signaling. As collagen molecules assemble into fibrils, *in vitro* or *in vivo*, they acquire a modulation of their molecular and electron densities called the D- band, with a 67 nm spacing, that can be visualized by cryo-electron microscopy. The D-band is composed of a gap region missing one-fifth of the molecules in the cross-section compared to the overlap region. This leads to the gap region having a positive potential and the overlap region a negative potential with respect to an n-doped silicon probe as observed by Kelvin Probe Force Microscopy. In this study, we use the adhesion force between an n-doped silicon probe and a collagen substrate to demonstrate the sensitivity of adhesion force towards charge distribution on the surface of collagen fibrils. We also map the charge distribution at the surface of single *in vivo* and *in vitro* assembled collagen fibrils and characterize the three-dimensional location and strength of three sub D-band regions that have been observed previously by cryo-electron microscopy. Our approach provides an adhesion fingerprint unique to each fibril type we analyzed and points to local charge variations at the sub D-band level even along a single fibril. We also demonstrate that this technique is capable of detecting changes on the surface of collagen fibrils as a result of glycation- a process which leads to the accumulation of sugar-induced crosslinks on the proteins' surfaces, responsible for complications observed in aging and diabetes. It opens the road for a detailed analysis of collagen fibrils surface charge modifications due to ligand binding or mechanical strain on a fibril by fibril basis.

Acknowledgements

I would like to acknowledge the endless support of my supervisor, Professor Laurent Kreplak, and the gratitude and respect for whom I cannot fully describe. From bringing me here during the peak of COVID and helping me understand the very basics of conducting research, to understanding my limitations and patiently assisting me to overcome them, solving my issues with the utmost promptness, accommodating the research timeline so that I can visit my family, and directing the path for my future, you have led me to grow not just academically, but also personally. Leaving home and learning the new way of life was challenging but you made it easier. From the bottom of my heart, I thank you for everything.

I also want to thank my committee members, Professor Sam Veres and Professor Andrew Rutenberg for their ideas and interest in my research and Kelsey Gsell for her support (SPIP is now all yours haha).

Chapter 1

Introduction

1.1 Collagen fibrils

1.1.1 What are collagen fibrils and what is their function in the body?

Collagen fibrils are a major component of the Extracellular Matrix (ECM), accounting for up to 30 $\%$ of the total protein mass in the body. While there are close to 30 types of collagen found yet, type I collagen is the most abundant and the main component of fibrils.[1] Collagen fibrils are one of the main building blocks of connective tissues, including tendons, ligaments, skin, and bones and serve several purposes in the body.

They provide tensile strength, flexibility, and structural support to tissues.[2] Collagen fibrils form a strong and flexible network that helps maintain tissue shape and resist mechanical stresses.[3] They also play a crucial role in the wound healing process. During tissue repair, fibroblasts synthesize and deposit collagen fibrils at the site of injury, forming a provisional matrix.[4] This matrix acts as a scaffold for cell migration, tissue regeneration, and helps in wound closure. Collagen fibrils are also a fundamental component of the bone matrix. They facilitate the mineralization process which gives bones their hardness, thus preventing fractures and ensuring their structural integrity.[5],[6]

Moreover, type I collagen is implicated in various human pathologies, such as cancer, fibrosis (excessive tissue scarring), and atherosclerosis (the buildup of plaque in arteries).[7] Collagen derived from animal sources is extensively utilized as a biomaterial for manufacturing scaffolds used in bone regeneration.[8] It is also employed in the production of hemostats (substances that promote blood clotting), bandages, and patches for tendon repair.

1.1.2 Collagen fibrils *in vivo* assembly

Collagen fibrils are synthesized in the body by specialized cells called fibroblasts, which are found in many tissues throughout the body.[9] Collagen is first synthesized as procollagen, a triple helix composed of three polypeptide chains (1 $\alpha 2$ and 2 $\alpha 1$ chains) and is stabilized

by hydrogen bonding.[5]

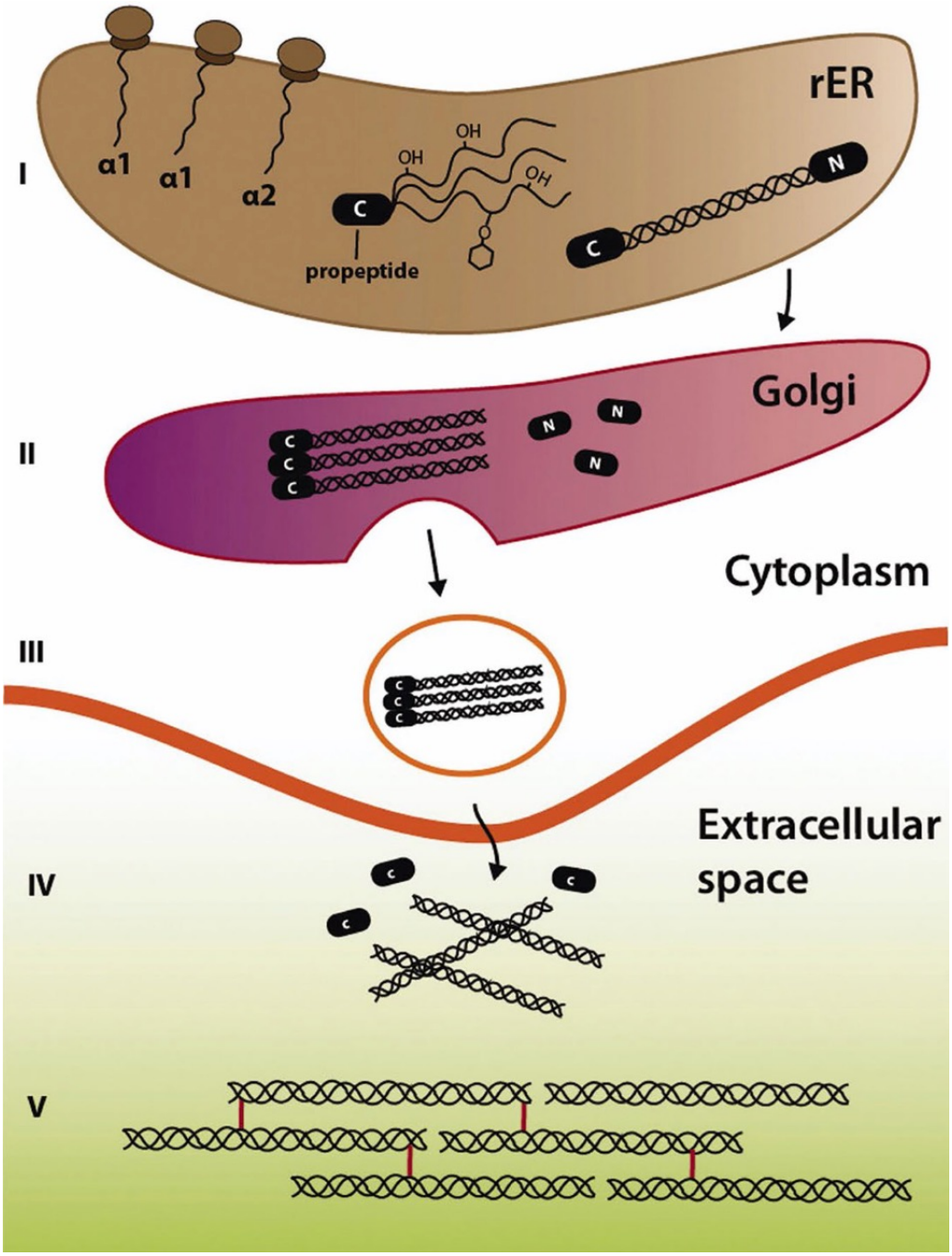

Figure 1.1: Collagen self-assembly *in vivo*, from the synthesis of procollagen to the formation of fibrils *Figure reprinted from [10]*

On either end of a procollagen molecule is a non-helical propeptide region terminating

with a carboxyl (C-terminal) or an amine group (N- terminal).[9] (Figure 1.1)

Once synthesized, procollagen molecules are packaged into vesicles and transported to the extracellular space.[11] The N- and C-terminal propeptides of procollagen are cleaved by specific enzymes, called N- and C- proteinase, respectively, yielding collagen monomers of a little over 300-nm long. These monomers then undergo an entropy-driven self-assembly process called fibrillogenesis, in which collagen monomers spontaneously self-assemble into quasi-hexagonal packed higher-order structures known as collagen fibrils.[12](Figure 1.1) The precise mechanisms and time scale of fibrillogenesis are not fully understood. The current accepted model states that five monomers assemble in a quarter-staggered fashion to form the microfibril, the basic subunit of the collagen fibril. The quarter staggering of the molecules within the microfibril structure results in a 67 nm periodic fluctuation in its linear density, which is called the D-band.[13] Each D-band or D-period is made up of an overlap and gap region, where the latter lacks 20 % molecules than the former.(Figure 1.1)

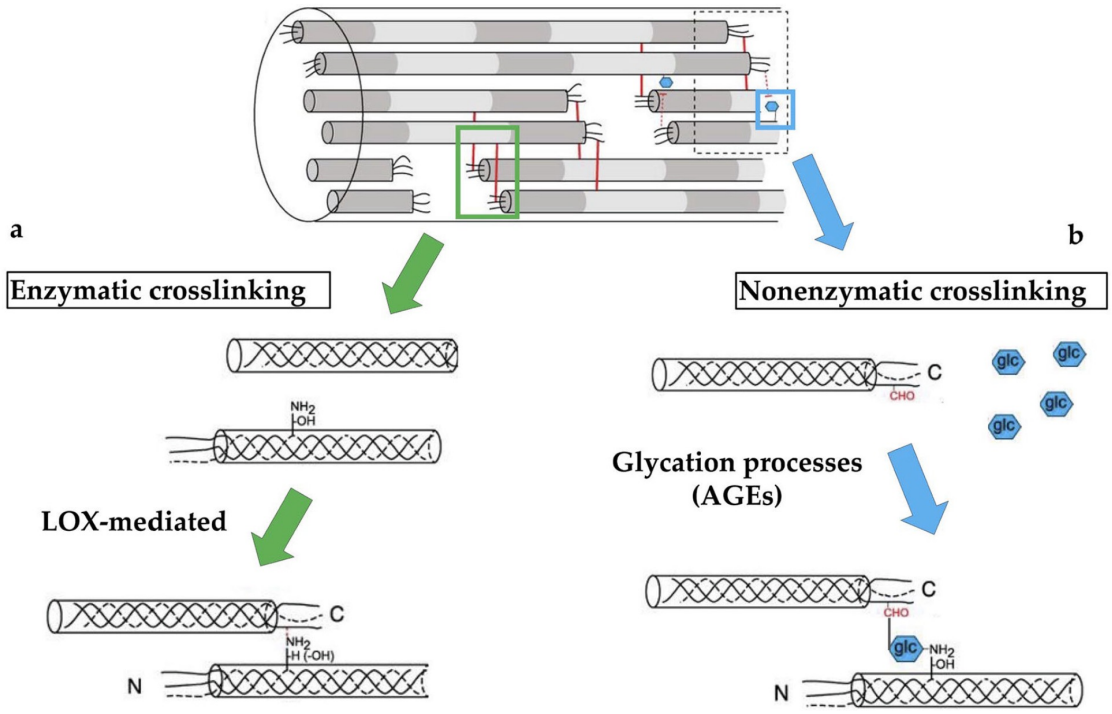

Figure 1.2: (a) Enzymatic and (b) Non-enymatic crosslinking in collagen fibrils *Figure reprinted from [14]*

The assembly of fibrils is completed by enzymatic cross-linking of collagen molecules within the fibril.[15](Figure 1.2a) This involves the formation of covalent bonds between

specific amino acid residues, such as lysine and hydroxylysine, within adjacent collagen molecules. Cross-linking is mediated by enzymes called lysyl oxidases responsible for the formation of mature cross-links, such as pyridinoline and deoxypyridinoline which enhance the stability, mechanical strength, and resistance to degradation of the collagen fibrils.[14]

As collagen fibrils are assembled and aligned, they become integrated into the ECM, where they interact with other ECM molecules, cells, and growth factors to influence tissue structure and function.

1.1.3 Collagen fibril *in vitro* assembly

Collagen fibrils can also be assembled *in vitro*. This process involves extracting collagen from animal tissues, followed by purification methods to isolate collagen molecules. Incubation of these molecules in acidic or neutral buffer in optimal conditions leads to fibrillogenesis. This process is typically monitored by turbimetry or electron microscopy. Whether or not fibrils form and the properties of the fibrils, such as appearance of D-band, fibril shape and width, depend on many factors, such as ionic strength, pH, temperature[16], [17] and concentration of the buffer.[18]

The fibril assembly pathway has also been shown to depend on the initiation procedure used.[19] When a cold, acidic collagen solution is heated before neutralization (warm start), the initial stages of reconstitution show the presence of numerous ”early fibrils.”(Figure 1.3 C) These fibrils are tapered in shape and exhibit a distinctive band pattern with a periodicity of 67 nm (the D-band). This has been observed even at turbidity close to zero. In contrast, if the collagen solution in acid is neutralized first and then warmed (neutral start), the assembly process initially results in a mesh of long thin non-banded filaments.(Figure 1.3 D) The appearance of D-periodic fibrils is observed later in the assembly process. When neutralization and warming are carried out simultaneously, similar ”early fibril” intermediates are observed. This suggests that the filamentous intermediate assemblies are initiated in the transient cold neutral solution. The end result of either pathway is the formation of D-banded fibrils.(Figure 1.3 E, F) While these fibrils may look similar to the *in vivo* assembled fibrils, one difference is that *in vitro* collagen molecules retain extrahelical telopeptides at the ends when it is extracted with acetic acid solution,[20] the potential consequences of which will be discussed later.

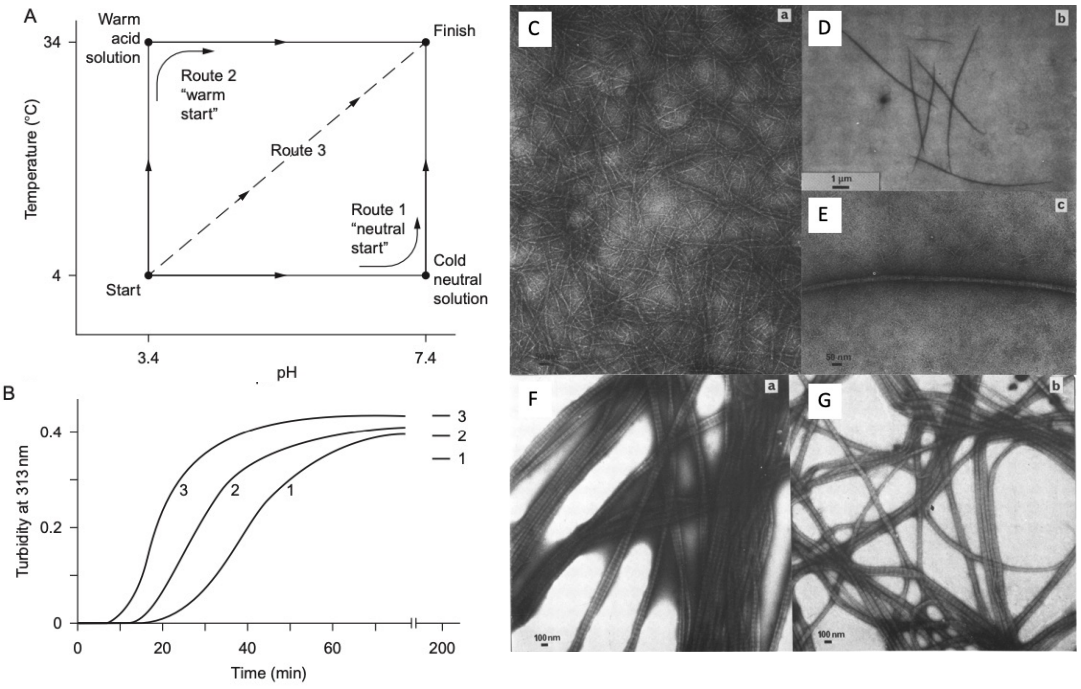

Figure 1.3: Alternative assembly routes observed in the reconstitution of type I collagen fibrils from purified solution. *(A) Diagram to show three initiation routes to transfer the collagen from a cold acid solution to a warm neutral solution. Routes 1 and 2 involve a warming step and a neutralization step. Route 3 is a combined single step achieved by adding a warm buffer solution to the initial collagen solution. (B) Turbidimetric curves to show a comparison in the kinetics of fibril formation between the three routes.(C) Typical loose fibrous assemblies of collagen that accumulate after the route 1 (neutral start) initiation procedure. (D and E) Typical early fibrils found after route 2 (warm start) initiation procedure. These are compact, clearly D-periodic, and have smoothly tapered tips. (F and G) TEM images of the final collagen fibrils using the neutral-start and warm-start initiation procedures, respectively. Figure adapted from [19]*

1.2 Charge distribution on the surface of collagen fibrils

Every polypeptide chain contains a high quantity of ionizable residues.[21] Under physiological conditions, there are about 230 acidic and 250 basic residues on the collagen molecule which are mostly charged.[22] This gives rise to a charge distribution within and at the surface of collagen fibrils.

Understanding the surface charge distribution is important for various reasons. Collagen is known to be a hub for binding of many proteins, such as integrin and fibronectin.[23] The binding of these proteins is critical for the maintenance of tissue structure and function. The surface charge profile of collagen, as well as other ECM proteins, plays an essential role in

cell adhesion.[24, 25] This is because these proteins that interact with the ECM typically have a specific electrostatic charge distribution on their surface. Therefore, the charge distribution on the collagen surface can influence the strength and specificity of the interaction with these proteins.[26, 27] Moreover, the fibrils, which undergo varying mechanical loads, are known to show direct and converse piezoelectric effects.[28]-[32] Hence, this surface charge profile is fundamental for the function of the fibrils, not only as nanoscale cables, but also as scaffolds vital for tissue development, and repair.

Changes in the surface charge of collagen fibrils can have significant consequences for tissue function and homeostasis. For example, mutations in collagen genes that alter the charge distribution on the collagen surface can cause diseases such as osteogenesis imperfecta, a condition characterized by brittle bones and other connective tissue abnormalities.[33] Similarly, changes in the surface charge of collagen fibrils due to environmental factors, such as pH and temperature, can affect tissue properties and lead to pathologies.[34, 35] Therefore, understanding the surface charge of collagen fibrils is critical for gaining insight into the fundamental mechanisms underlying tissue maintenance over the organism' lifespan and disease. It also has important implications for tissue engineering, drug delivery, and other biomedical applications that involve the manipulation of collagen-based materials, since the creation of new tissue relies on optimal cell response which is governed by the electro-mechanical properties of the material.

1.3 Glycation in collagen fibrils

Since the surface charge distribution of collagen fibrils is so important, processes which alter it can cause deleterious effects throughout the body. One such process is glycation.

1.3.1 What is glycation?

As organisms age, they are more prone to complications such as susceptibility to injury, loss of elasticity in tissues and reduced healing capacity.[36] These complications get worse in patients of type II diabetes. These effects have linked to the accumulation of Advanced Glycation End-products (AGEs) on proteins such as collagen fibrils as a result of glycation.

Glycation is a spontaneous, non-enzymatic reaction that takes place in all living systems. It involves the chemical reaction between the carbonyl groups found in reducing sugars and

the amine groups present in proteins, lipids, or nucleic acids.[37, 38] The process of glycation begins by forming a reversible Schiff base when a carbohydrate, typically glucose, reacts with an amino group in a protein, such as a lysine side-chain in collagen. This initial Schiff base is unstable and subsequently transforms into a stable intermediate called a keto amine, commonly referred to as an Amadori product. Over the course of months or even years, a complex series of reactions occurs, resulting in various metabolic by-products of non-enzymatic glycolysis. These by-products include glyoxal, methyl glyoxal (MGO), and 3-deoxyglucosone. When these by-products interact with extracellular proteins, they form Advanced Glycation End-products (AGEs).[39]-[43](Figure 1.2b) Certain AGEs have the ability to create connections between the free amino groups of adjacent proteins, resulting in inter-molecular crosslinks. These crosslinks contribute to structural changes in tissues. Other AGEs, referred to as ”adducts,” only affect a single protein, leading to modifications within that protein.[44] Among the various types of AGEs, glucosepane, a specific type of crosslink that forms between lysine and arginine residues, has been identified as the most prevalent in collagen tissues.[45]

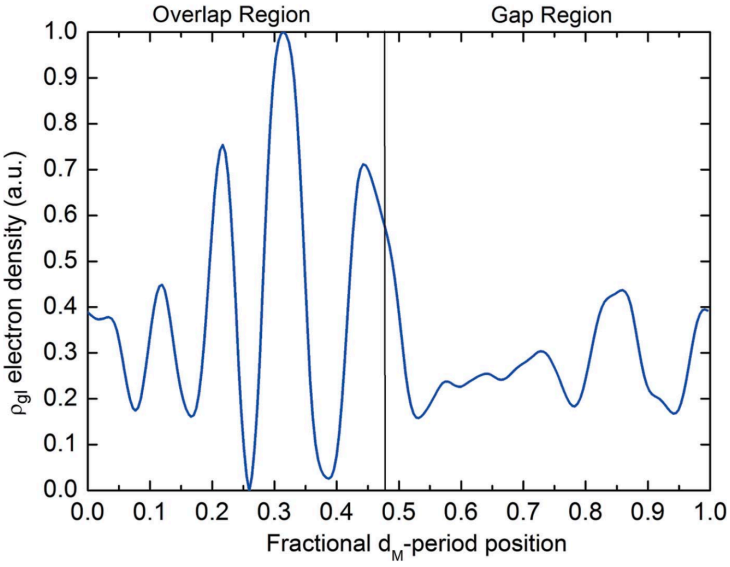

Figure 1.4: The alteration in electron density (ρ_{gl}) resulting from glycation along a single D-band (noted d_M) of a fibril as determined by Fourier difference synthesis of Small Angle X-ray Scattering (SAXS) patterns of glycated and non-glycated tendons. *Figure reprinted from [46]*

The effects of glycation have been studied extensively for decades and the specific

binding sites for the AGEs on collagen fibrils have been suggested in different studies.[46]-[48] Figure 1.4 shows the change in electron density caused by glycation along a single D-band of a fibril obtained by Fourier difference synthesis computed from SAXS patterns of glycated and non-glycated tendons. Note that the accumulation of AGEs is significantly larger in the overlap than the gap.[46](Figure 1.4)

1.3.2 Effects of glycation

The arrangement of collagen molecules within collagen fibrils is influenced by multiple non-covalent interactions, with charge-charge interactions playing a significant role.[49]-[52] When the lysine sidechains in collagen undergo glycation, the length of the sidechain and the distribution of charges on it are changed due to the addition of sugar adducts.[53] These modifications are expected to disturb the molecular organization within collagen fibrils. Changes in both the molecular and fibrillar charge distributions are likely to impact the interaction between collagen fibrils and the surrounding extracellular matrix (ECM) components. Consequently, this can have a cascading effect on the ECM network as a whole, leading to significant alterations in the cellular microenvironment.

As a result, glycation has been linked to multitude of biological changes in collagen fibrils. The formation of AGEs (adducts or crosslinks) on specific amino acids involved in intermolecular recognition has been shown to diminish collagen-proteoglycan binding and weaken cell adhesion.[54] This is likely because most of the lysines involved in the formation of glucosepane are also binding sites for heparin, proteoglycans and integrin.[48] Furthermore, it has also been observed that the fibril becomes more negatively-charged because of glycation.[55] Glycation has a significant impact on cell-matrix interactions, which ultimately results in impaired wound healing and increased inflammation.[54, 56] This is in line with the fact that the non-enzymatic crosslink at arginine involved in the formation of AGEs is close to the binding site of Matrix Metalloproteinase-1 (MMP-1)- an enzyme responsible for collagen maintenance.[48] This may lead to steric inhibition of MMP-1 binding and activity and decrease the susceptibility of collagen to degradation. It has also been observed that glycation reduces enzymatic cross-links both on the surface and the inner part of fibrils,[48] and expands the molecular packing.[57] Many studies have also linked glycation to bio-mechanical changes in fibrils and tissues,[58]-[62] out of which, an increase in tissue stiffness is the most discussed.[63]-[67] Furthermore, glycated collagen activates the

receptor for AGE products (RAGE) in cells. The activation of RAGE has been implicated to a myriad of pathologies and other physical conditions such as diabetic complications,[68] aging,[69] vascular disease,[38] Alzheimer's Disease,[70] and cancer.[71]

1.4 Characterization of the charge distribution along collagen fibrils

Due to the importance and abundance of collagen in the body, collagen fibrils have been studied extensively by different techniques, and some of these provide great insight on the electron density modulation and charge pattern in these fibrils.

1.4.1 Small Angle X-ray Scattering (SAXS)

SAXS works by shining a beam of X-rays on a sample and measuring the intensity and scattering angle of the photons scattered by the sample. Scattered X-ray photons provide information about the electron density distribution within a sample. In the case of collagen fibrils, the X-rays scatter off the repeating structure of the collagen molecules within the fibril.[72] This produces a characteristic pattern of peaks in the SAXS data, which can be analyzed to determine the D-periodicity of the fibril and the degree of order within the hierarchical network. This technique was used to obtain the only atomic model of the collagen fibril's interior.[73]

1.4.2 Transmission Electron Microscopy (TEM)

TEM is another technique that has be used to visualize the internal structure of collagen fibrils with high resolution. TEM works by passing a beam of electrons through a thin sample of the material being studied which results in the formation of an image based on the interaction (scattering, diffraction or absorption) of the electrons with the sample. While TEM provides high resolution images, it typically requires the sample to be fixed, dehydrated, and stained with heavy metals. In Cryo-EM, a variant of TEM, rather than fixing the sample, it is frozen on a grid using liquid ethane or propane. While this preserves the natural and hydrated state of the sample, it requires the sample to be maintained at cryogenic temperatures.[74] By using this technique on rat-tail tendon collagen fibrils, three major electron dense regions were observed within one D-period[75] (Figure 1.5), which were identified to be the previously discovered X1, X2 and X3 bands.[76] Fibrils stained

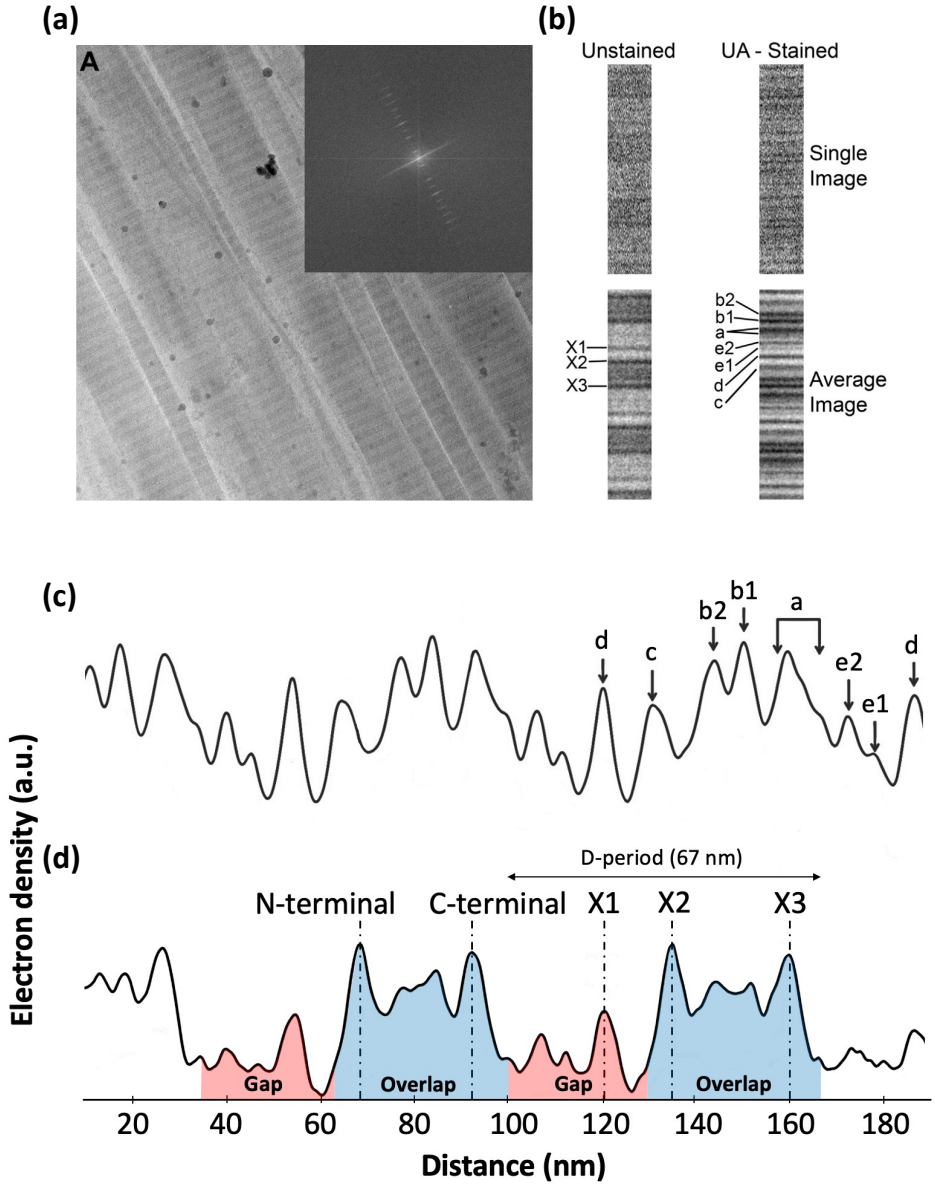

Figure 1.5: Electron density fluctuation along a rat-tail tendon (RTT) collagen fibril observed by cryo-electron microscopy *(a) Cryo-TEM micrograph of unstained RTT, with inset showing Fourier transform reflecting axial periodicity. (b) Single and averaged images from unstained and Uranyl Acetate (UA)-stained cryo-TEM images. Major bands observed in the unstained image are labeled X1, X2, and X3, which represent three main electron dense regions visible within the fibril. The positive staining bands (a–e) of are indicated for the UA-stained image, which reveal regions rich in negatively charged amino-acids within the fibril. Profiles from (c) UA-stained and (d) unstained images show the electron density fluctuation corresponding to these bands and their location within the D-band- the X1 in the gap region and the X2 and X3 in the overlap region coinciding with the N- and C-terminal domains of the collagen molecule, respectively. Figure adapted from [75]*

with uranyl acetate that binds to negatively charged amino acids, aspartate and glutamate, also show around 9 bands within a D-period. (Figure 1.5)

As explained earlier, the surface charge profile of collagen fibrils plays an important role in its functioning. While these techniques are effective, they are limited in the study of surface charge profile of collagen fibrils. Techniques like SAXS and TEM, while capable of providing a high resolution of around 6 nm, yield bulk electron density variation in the fibril. Since molecular remodeling is expected to alter the distribution at the surface of the fibril[77], the bulk and surface properties can be significantly different. Therefore, techniques like Atomic Force Microscopy (AFM) have been employed to study the surface of the fibrils.

1.4.3 Atomic Force Microscopy(AFM)

AFM is a technique which uses physical probe to scan a sample surface and obtain high-resolution images. A sharp tip or probe typically made of Silicon Nitride, attached at the end of a cantilever, is brought into close proximity or contact with the sample surface and systematically scanned across the surface in a raster pattern. The interaction between the probe and the sample surface leads to a high-resolution image with information about the topography, physical properties, like elasticity, and other surface interactions of the sample at the nanoscale.[78] Kelvin Probe Force Microscopy (KPFM) is a type of AFM which can image surface charges.[79] In the Amplitude Modulated-KPFM (AM-KPFM) mode, the probe first scans the topography of the sample with a simple scan under amplitude feedback while in contact with the surface. Then, the probe is lifted to a given height above the surface to perform a second scan at the natural resonant frequency of the cantilever, following the trajectory acquired during the topography scan, without feedback. During this second scan, a DC voltage is adjusted throughout to zero the oscillations induced because of the electrostatic force between the tip and the sample caused by the surface potential and applied alternating voltage. This leads to the measurement of the Contact Potential Difference (CPD)[80, 81] and in turn, the charge distribution at the surface. KPFM images of rat-tail tendon fibrils have revealed a surface potential modulation corresponding to the D-band where the overlap region is more negatively charged, i.e. lower potential, than the gap region.[34](Figure 1.6)

KPFM is effective in characterizing surface charges. However, as seen in Figure 1.6, the

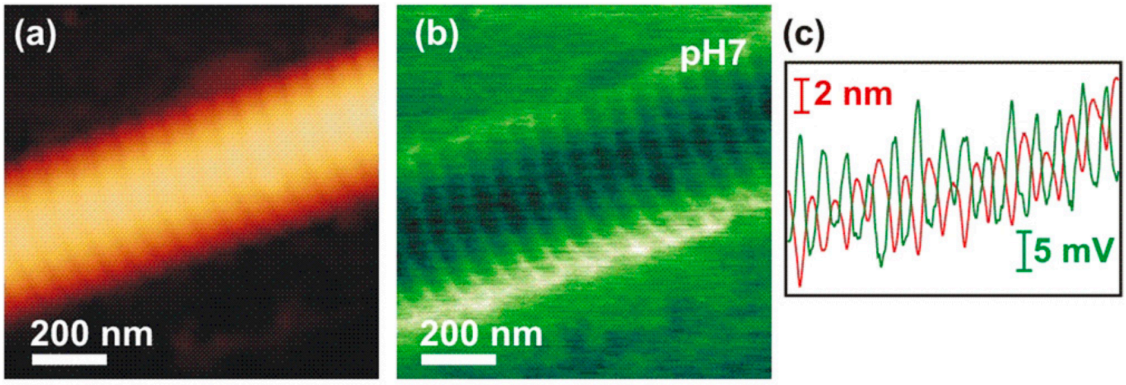

Figure 1.6: Charge contrast between overlap and gap regions as observed by KPFM *(a)AFM tapping-mode topography map (color scale range 150 nm). (b) KPFM surface potential map of the same area as in (a) (color scale range 150 mV). (c) Topography (red) and potential (green) profile through crest of the fibril in (a) and (b), respectively. Figure reprinted from [34]*

images lack sub D-band features seen by cryo-EM (Figure 1.5), which is likely because the measurement is not taken in contact with the sample and thus, the electrostatic force is not isolated to only the tip apex, as it also interacts with the tip pyramidal shape and the cantilever shaft. Since the CPD measurement is an average of all of these electrostatic contributions, this results in a low resolution of about 30 nm in current AM-KPFM measurements.[81] Other traditional techniques[82, 83], like zeta-potential measurements, which are commonly used to determine the electrical charge on suspended particles, are not suitable for collagen fibrils because these structures are not easily suspended in a liquid medium. Additionally, collagen fibrils are highly organized and tightly packed, which makes it difficult to access their surfaces for electrical measurements.

Therefore, a method that can offer a high resolution mapping of the spatial arrangement of charges on collagen fibrils is necessary. We believe that this can be achieved using adhesion force microscopy.

1.4.4 What is adhesion force microscopy?

During each scan performed by the AFM in Peak Force mode, the tip moves toward the sample (approach), physically interacts with the surface (contact) and then moves away from the sample (retract). (Figure 1.7) While the tip is retracting from the surface, just before the pull-off, the tip experiences the maximum attractive force. This force corresponds to

the adhesion force between the tip and the surface. (Figure 1.7) As the tip approaches the sample, the deflection of the cantilever increases up to a maximum interaction force (peak force). By controlling the peak force, different images showing the modulation of surface properties such as height or adhesion force can be obtained.[84]

The measurement of adhesion force by an AFM has been mostly restricted to spectroscopic applications such as measuring single-molecule or cell-cell adhesion forces.[85]-[89] However, in principle, for localized charges implanted at the surface of a dielectric material, it should be possible to map the charge distribution by simply measuring the adhesion force between the tip and the sample. One of the components that this adhesion force is dependent upon is the electrostatic force between the tip and the sample. This electrostatic interaction varies according to the charge distribution on the surface. In the case of a conductive tip and a conductive or naturally charged surface like mica, a voltage bias can be used to increase the adhesion force by several orders of magnitude through the attractive electrostatic interaction of opposite charges.[90] This effect has previously been observed on a hydrophilic surface at a low relative humidity of below 40% RH even in the presence of water absorption and the associated screening of the electric potential. In the absence of a voltage bias and at low relative humidity, it is still expected that the adhesion force between a charged silicon tip and a charged surface should depend on the spatial distribution of charges. Considering a

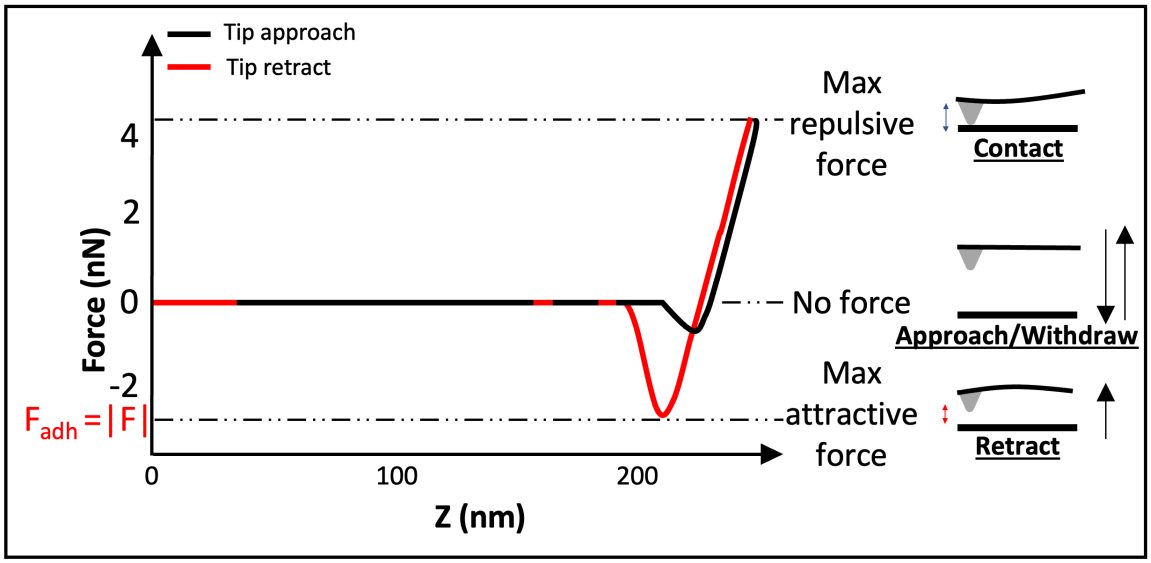

Figure 1.7: A typical force-distance curve captured by AFM shows the measurement of adhesion force at the point of pull-off from the surface. The AFM can be operated using the maximum repulsive force as feedback parameter (Peak Force mode).

negatively charged tip, a flat surface with bound charges, and ignoring the effect of surface roughness,[91] localized negative charges should yield a decrease in the total adhesion force whereas localized positive charges should yield an increase in the total adhesion force.

Leveraging this fact, we hypothesize that the measurement of the modulation of adhesion force as a function of surface charge can prove to be a powerful technique. It can overcome the limitations of previously discussed techniques as this method can map the surface charges at a high resolution without the application of an applied voltage.

1.5 Aim of the thesis

This thesis is divided in two main studies. The first study aims to validate the application of adhesion force microscopy to image the surface charges present on single collagen fibrils from different sources. The second study investigates if this technique can be applied to understand the impact of glycation on collagen fibrils from physiologically distinct tendons.

1.5.1 Is adhesion force microscopy sensitive to surface charge distribution along a single collagen fibril?

This study represents an in-depth rendition of our previously published article.[92] We acquire adhesion force maps of collagen fibrils in an ambient condition at a pixel resolution of 4 nm for four different types of collagen I fibrils, assembled *in vitro* from collagen molecules with and without their charged telopeptides (telo- and atelo-collagen, respectively), and extracted from two bovine leg tendons with functionally distinct nanostructures. We show that adhesion force fingerprints extracted from the images reveal three electron density sub-bands similar to the ones observed by cryo-electron microscopy (Figure 1.5) with significant variations in strength and position independent of height variations. Considering the main forces involved and upon observing consistency between our results and others', we hypothesize that the n-type silicon tip used in our experiment acts like a negative charge. Our results support the idea that the charge distribution at the surface of the fibril is significantly different from the interior of the fibril and depends on the presence of the telopeptides as well as the anatomical location of the fibril.

1.5.2 Can adhesion force microscopy detect glycation induced changes at the collagen fibril surface?

Bovine leg tendons were cryo-sectioned into 20 μm sheets and the collagen fibrils within were imaged. Multiple segments of these tendons were also incubated in separate solutions of 0.2 M ribose in PBS or PBS only, for a period of upto 3 weeks, during which one segment was retrieved each week, cryosectioned and imaged. This was done to observe the gradual effect of ribose-induced glycation on the fibrils. We show that extracted fibrils differ from fibrils in tendon sections, significantly in the case of extensor and minimally in the case of flexor. The accumulation of AGEs is also shown to be more pronounced and faster in extensor fibrils than flexor fibrils, which we attribute to the differences in their surface properties. We also observe that the effect of long-term incubation of PBS on the surface of fibrils at 35°C may be non-negligible, and needs to be studied further.

Chapter 2

Materials and Methods

2.1 Sample Preparation

2.1.1 Sources of tendons and collagen solutions

For the study of extracted collagen fibrils, a matched pair of Common Digital Extensor (CDE) and Superficial Digital Flexor (SDF) tendons were procured from the leg of a steer, around 1 to 2 years old, at a local abattoir. Similarly, for the study of fibrils within tendon sections, a matched pair of CDE and SDF from a another steer was used. These tendon pairs were stored dry at -80 °C, and were cut and used as needed.

For the study of collagen fibrils assembled *in vitro*, Type-I atelo- and telocollagen solutions in 0.01 N HCl, extracted from bovine hides (Advanced Biomatrix, USA), were used.

2.1.2 *Ex-vivo* Collagen fibrils extraction

For *in vivo* collagen fibril extraction, a pair of CDE and SDF tendons were used as follows. (Figure 2.1a) A frozen tendon piece was quickly transferred in a petri dish in 500 μL of Phosphate Buffered Saline (PBS), and then scrapped with the help of blade and tweezers to isolate collagen fibrils from the tendon into the solution. The tendon was discarded and the solution was transferred to a glass-bottom petri dish where it was incubated for 30 minutes at room temperature to let the fibrils adhere to the bottom of the dish. The solution was discarded and the dish was rinsed four times with 5 mL of ultrapure water and finally dried with nitrogen gas.

2.1.3 Collagen fibrils self-assembly

In vitro collagen fibril assembly was carried out using 3 mg/ml Type-I atelo- or telocollagen solutions in 0.01 N HCl, respectively. (Figure 2.1b). First, the collagen solution in acid and PBS were warmed separately in a water bath at 37°C for 5 minutes. The two solutions

were mixed together to final concentrations of 200 μg/ml for telocollagen and 300 μg/ml for atelocollagen, transferred to a glass-bottom petri dish, and incubated at 37°C for 18 hours. The solution was then gently pipetted out and the dishes were gently rinsed with 5 mL of ultrapure water four times, followed by drying with nitrogen gas.

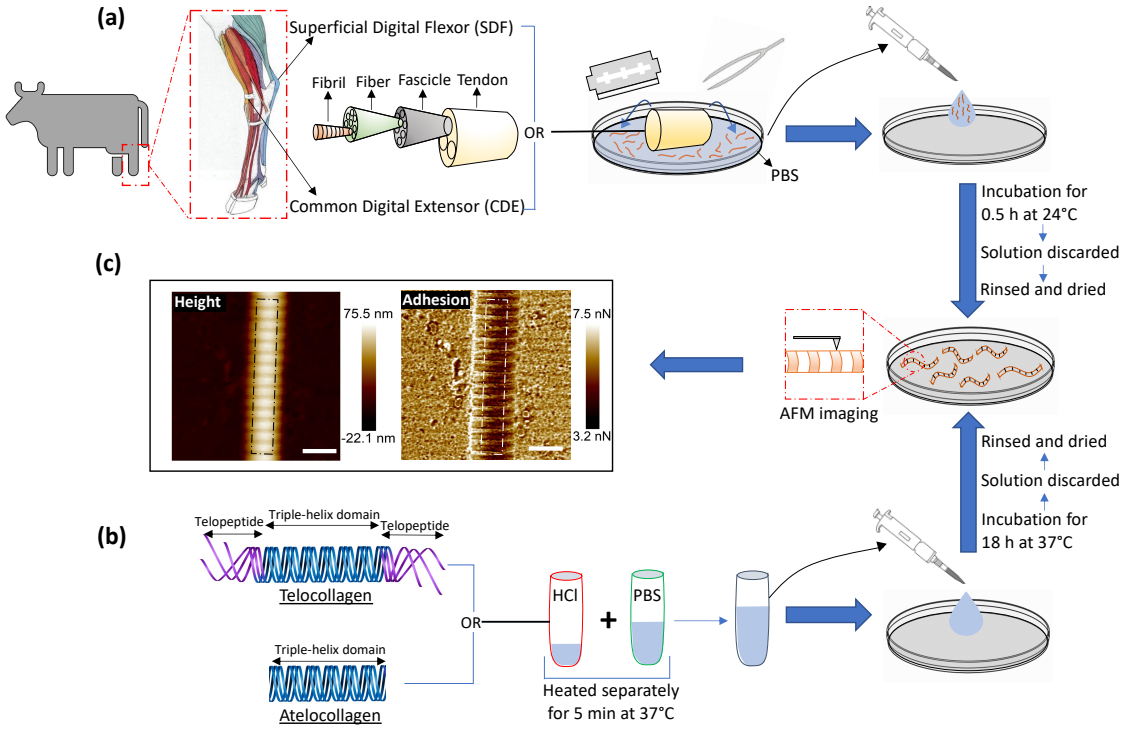

Figure 2.1: Preparation of *in vivo* and *in vitro* collagen fibrils *(a) Collagen fibrils are extracted by scraping either Superficial Digital Flexor (SDF) or Common Digital Extensor (CDE) tendons in PBS. The solution containing fibrils is transferred to a petri dish for incubation at 24°C for 30 min, which thereafter is discarded and the dish is rinsed with ultra pure water and dried with N_2 gas. (b) Atelo- or telocollagen molecules stored in 0.01 N HCl and PBS solution are heated separately at 37°C for 5 min, then mixed and incubated in a petri dish at 37°C for 18 h. Similar to (a), the solution is thereafter discarded and the dish is rinsed and dried. (c) Collagen fibrils adhered at the bottom of the dish are imaged by atomic force microscopy in peak-force mode. Several pixel wide profiles (white dotted lines) are extracted from these images for analysis.(Scale bar= 200nm)*

2.1.4 *In vitro* glycation

To observe the effect of glycation, tendon segments of both CDE and SDF types were incubated separately in a solution of 0.2 M Ribose in PBS and in a control solution of just

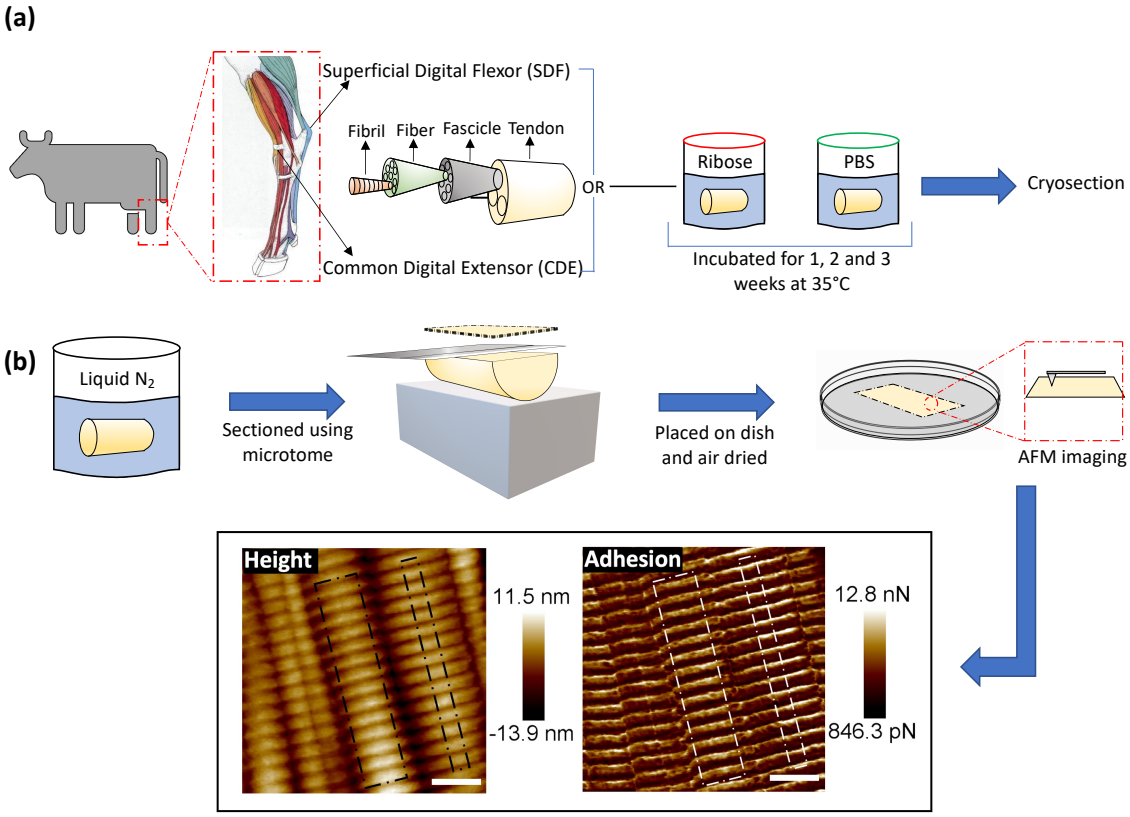

Figure 2.2: Glycation and Cryosection *(a) Mutiple CDE or SDF tendons are incubated in PBS (control) and a ribose solution for increasing incubation periods, followed by cryosectioning and imaging. (b) A tendon segment is frozen in liquid nitrogen, then mounted on a steel block and cryosectioned using a microtome to produce 20-um thick collagen sheets. These sheets are imaged using AFM and wide and narrow profiles are extracted from height and adhesion images (Scale bar= 200nm)*

PBS, along with 1% Antibiotic-antimycotic solution (Sigma Aldrich) for 3 weeks at 35°C. (Figure 2.2a) During this 3-week experiment, one tendon segment, 2-3 cm in length from all four solutions was taken out every week, cut half longitudinally and cryosectioned. The sections thus formed where then imaged using AFM.

2.1.5 Cryosectioning

A 2-3 cm segment of CDE or SDF tendons was cut in half longitudinally and mounted on a steel block using optimal cutting temperature compound (Fisher Healthcare, Ottawa, ON) and frozen in liquid nitrogen. Then they were cryosectioned using a Leica SM2000R sliding microtome to produce 20 μm thick sheets of collagen. These sections were transferred to

a petri dish containing ultrapure water, immediately followed by a dry petri dish and air dried. The sections were then imaged using the AFM. (Figure 2.2b)

2.2 Atomic Force Microscopy

Collagen fibril samples were imaged on a Bioscope catalyst (Bruker, USA) atomic force microscope mounted on an IX71 inverted optical microscope (Olympus, USA) and operating in Peak Force Quantitative Nanomechanical Mapping mode (Peak Force QNM). The cantilevers used were made of silicon nitride and had an n-doped Silicon pyramidal tip with a nominal radius of 2 nm and a half angle of 18° (SCANASYST fluid +, Bruker USA). Note that in this architecture, the pyramidal tip behaves as an insulated conductor that is not necessarily grounded. The spring constant was calibrated for each cantilever before imaging using the thermal noise method[93] and ranged from 1 to 1.5 N/m. 1 μm images were acquired with 512 pixels per line at a scan rate of 0.5 Hz, peak force setpoint of 5 nN, cantilever oscillating frequency of 1 kHz and corresponding vertical tip velocity of 0.6 mm/s. Two channels were recorded for analysis, the height and the adhesion force between the tip and the substrate (Figure 2.2c). For all the images, the humidity in the room was between 15 and 20 $\%$RH.

2.3 Data analysis

2.3.1 Extracting profiles from images

For the height images, a 1st order plane fit followed by a 1st order line by line polynomial fit, with the fibril masked, was applied using NanoScope Analysis (Bruker, USA) in order to flatten the image. A several pixels wide profile, ranging from 28 pixels to 107 pixels depending upon the fibril diameter, along the length of the fibril was extracted using SPIP (Image Metrology, Denmark) (Figure 2.3a, solid line). For the analyzing the fibrils in sections, a narrow profile of about 10 pixels, as shown in Figure 2.2a, was also extracted along the fibril.

2.3.2 Converting raw profiles into fingerprints

The following analysis was done using a Python Script[94]. An adjacent average of the height profile with a window size of 103 pixels, which is equivalent to 3 D-band repeats,

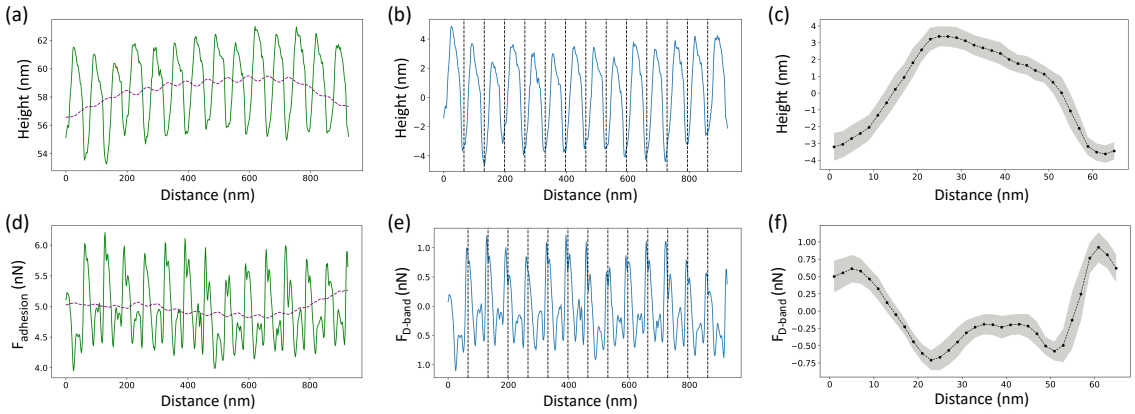

Figure 2.3: D-band averaging. *(a) A profile extracted along the length of the fibril (solid line) is used to calculate an adjacent average with a window of size equivalent to 3 D-band repeats of 67 nm each (dotted line). (b) The filtered profile (solid line), obtained by subtracting the adjacent average from the extracted profile, is Fourier transformed to calculate the value of D-band repeat and then divided into individual D-band periods (dashed lines). (c) All individual periods are averaged together to obtain a height fingerprint of the D-band. (d) A profile synchronized with the one taken from the height image is extracted from the adhesion image (solid line), which measures the total adhesion force, $F_{adhesion}$ experienced by the tip. Following the same process, an adjacent average is calculated (dotted line) and subtracted from the extracted profile. (e) The resultant filtered profile (solid line) corresponding to the adhesion force due to the D-band only, $F_{D\text{-}band}$, is divided into individual D-periods (dotted lines) using the value of the D-band repeat obtained from the paired height profile. (f) The D-periods are averaged together to create the adhesion fingerprint of the D-band.The grey shading in (c) and (f) represents the standard deviation of the D-band periods with respect to the fingerprint.*

67 nm each, was computed (Figure 2.3a, dashed line) and then subtracted from the profile to remove previously reported long-range fluctuations in height not associated with the D-band repeat.[95] The obtained filtered profile (Figure 2.3b) was Fourier transformed to obtain the value of the D-band repeat and sliced into individual D-band periods (Figure 2.3b, dashed lines). Finally, all the individual height profiles were averaged together to obtain the height fingerprint of the D-band (Figure 2.3c). A similar process was followed for analyzing adhesion images except that the value of the D-band repeat obtained from the paired height profile was used for slicing the D-band periods of the adhesion profile (Figure 2.3e-g). This was possible because the profile extraction from the height and adhesion images was synchronized using SPIP. The final adhesion fingerprint obtained by removing the adjacent average from the adhesion profile displays the change in adhesion force, $F_{D\text{-}band}$ attributed to the D-band only.

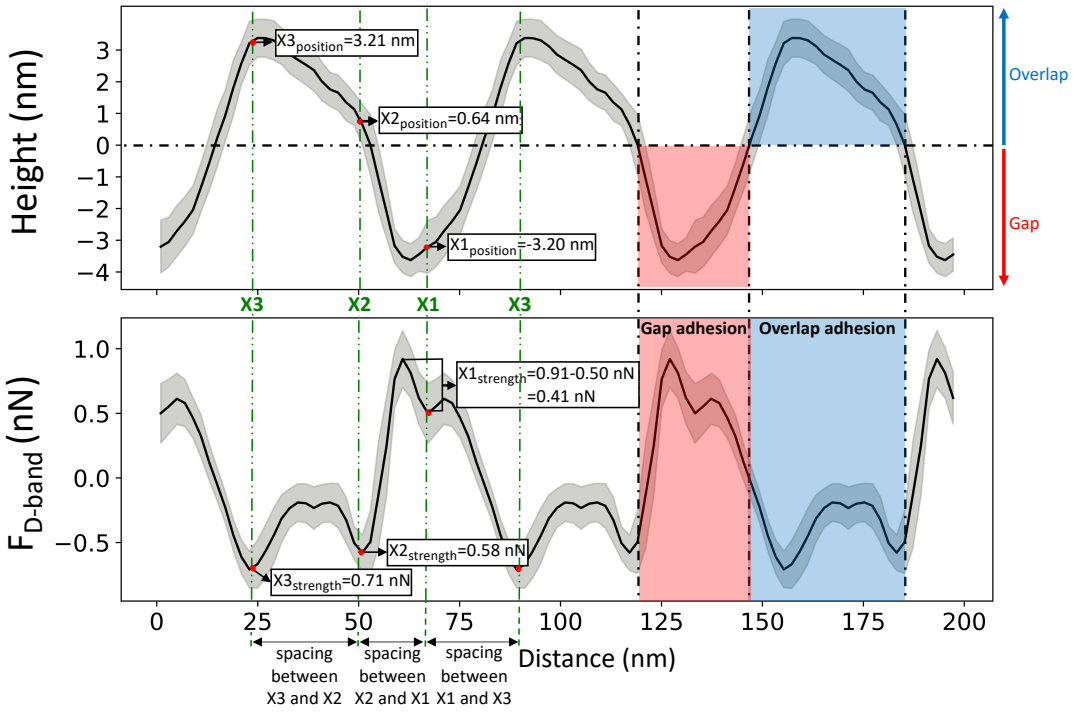

Figure 2.4: Calculation of different parameters from fingerprints *Mean adhesion of the overlap (blue region above 0 in height) and gap (red region below zero in height) is calculated for each fibril, along with the vertical position, strengths and distances between X1, X2 and X3 bands as shown.*

2.3.3 Calculation of various adhesion values from from fingerprints

The overlap and gap regions were defined using the height fingerprint as the regions above and below 0 nm, respectively and the average adhesion in these regions was defined as overlap and gap adhesion, respectively (Figure 2.4). The difference between these mean adhesion values for the overlap and gap region of a fibril yields the overlap-gap adhesion contrast. Electron density bands, X1, X2, and X3 (dotted lines) were marked by locating appropriate dips in the adhesion force and the spacing between them was calculated. Height location of these bands was measured by matching their location in the adhesion fingerprint. Absolute values of adhesion force for the X2 and X3 bands were regarded as their strengths. For the X1 band, its strength is estimated as the reduction in adhesion with respect to the maximum adhesion force recorded in the gap region.

2.3.4 Statistical tests

Significant difference between measured quantities was assessed by Welch's anova using the Pingouin package in python. If a p-value of less than or equal to 0.05 was obtained, independent two-sample t-test was performed. The samples with the p-value of equal or less than 0.05 were considered significantly different.

Chapter 3

Results and Discussion

3.1 Adhesion force microscopy is sensitive to the charge distribution at the surface of single collagen fibrils

In this study, collagen fibrils extracted from two tendon types, SDF and CDE, and fibrils self-assembled *in vitro* from atelo- and telocollagen molecules (Figure 2.2), were imaged by adhesion force microscopy at a relative humidity between 15 and 20%. The fibrils had a wide range of height, between 11 nm and 149 nm, and exhibited the expected D-band repeat with a period of 67 nm (SD=3 nm) (n=30).

3.1.1 The adhesion force along a collagen fibril is insensitive to nanoscale topography

Height fingerprints (Figure 3.1) were obtained by a process of filtering and averaging of profiles extracted from height images (Figure 2.3). The D-band amplitude, measured using these height fingerprints, showed a positive correlation with the height of the fibril- flatter, *in vitro* fibrils have smaller D-band amplitude as compared to the taller, *ex-vivo* fibrils (Figure 3.2a). An almost identical trend of D-band amplitude with fibril height has already been reported for collagen fibrils extracted from bovine corneal and scleral tissues.[96] As the height of the fibril and the amplitude of the D-band decrease, the overlap region of the height profile displays clearer ridges, as seen by comparing the CDE and atelocollagen examples (Figure 3.1). This increase in visibility of sub D-band features with a decrease in height is in agreement with a previous imaging study on 3 nm tall self-assembled collagen tapes, which revealed up to twelve sub D-band features within a single repeat.[97] The adhesion measurements, however, did not reflect a similar trend with height. (Figure 3.2b) There was no significant difference between the mean adhesion of each fibril type, except for telocollagen, whose mean adhesion was significantly lower than the others. This difference is not a height effect considering that atelo- and telocollagen have almost identical height

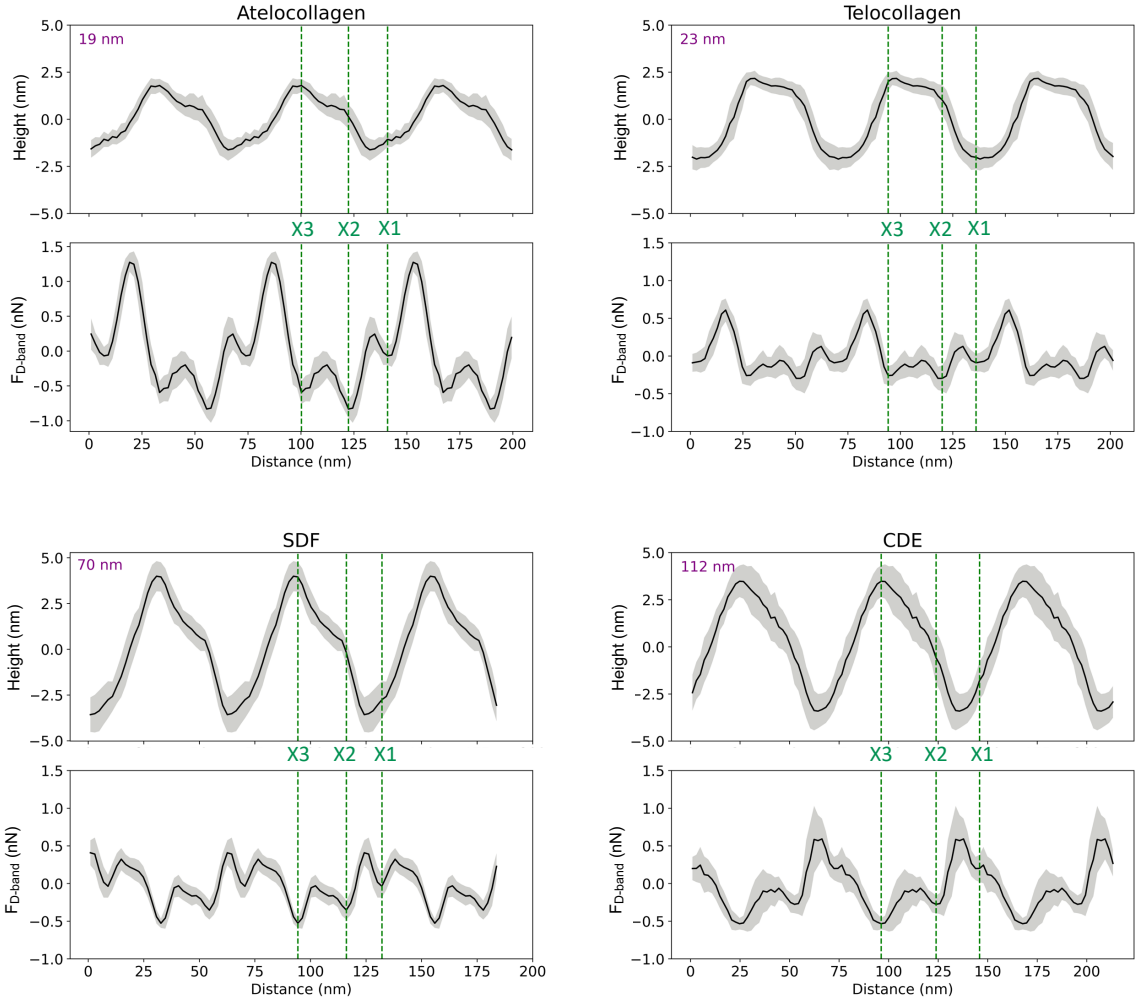

Figure 3.1: Height and Adhesion fingerprints for four different collagen fibrils obtained from atelocollagen, telocollagen, SDF and CDE samples. *Each fingerprint is repeated over three D-band periods for clarity and includes the average of all the D-periods along the fibril (solid line) as well as the standard deviation between individual D-periods (grey shade).In addition, the average height of the fibril is indicated as well as the proposed positions of the three main electron density bands, X1, X2 and X3 (dotted lines) observed by cryo-electron microscopy.*[75]

ranges (Figure 3.1a).

Using the adhesion fingerprints, the adhesion force experienced by the tip in the overlap and gap regions of the D-band (Figure 3.2c) and the overlap-gap adhesion contrast (Figure 3.2d) was calculated as shown in Figure 2.4.

The average resultant adhesion force, $F_{D\text{-band}}$ was positive for the gap and negative for the overlap region (Figure 3.2c). There was no significant difference between the fibril

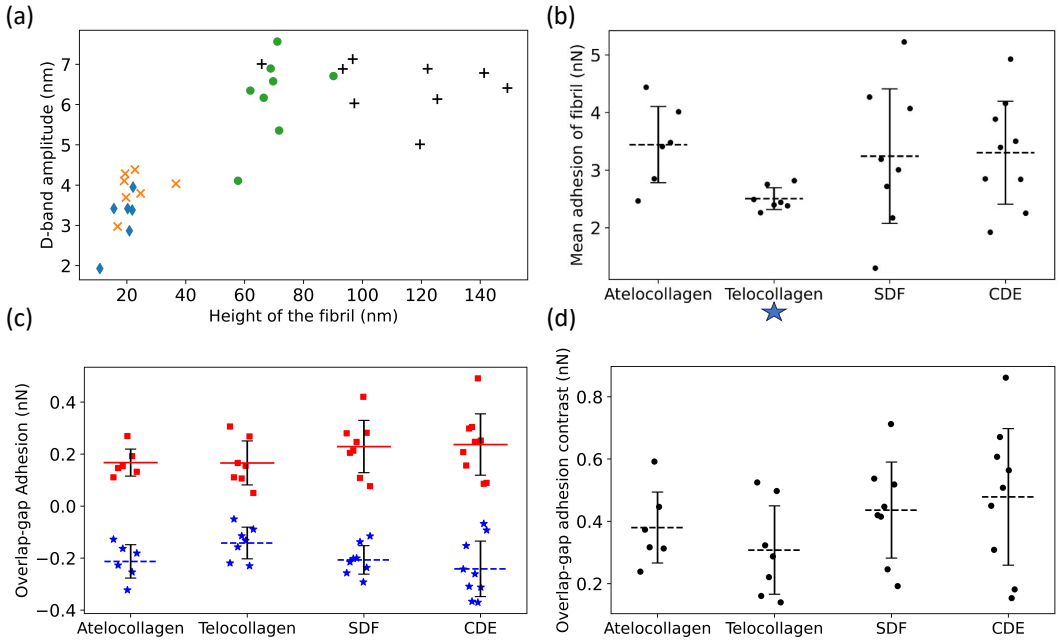

Figure 3.2: (a) Increase in D-band amplitude with height of the fibril. *atelocollagen (◆), telocollagen (✖), SDF (●), and CDE (+).*(b) Mean adhesion of fibrils. *Telocollagen significantly different from others, as marked by star (⋆)* (c) Overlap adhesion (⋆) and Gap adhesion (■). (d) Overlap-gap adhesion contrast

types in terms of either overlap and gap adhesion or the overlap-gap adhesion contrast.

In principle, this adhesion force measured by the AFM between the tip and the fibril is governed by three forces- the Van Der Waal's force (F_{vdW}), the Capillary force (F_c), and the Electrostatic force (F_e) as represented by the equation below:

$$F_{\text{D-band}} = F_{\text{vdW}} + F_{\text{c}} + F_{\text{e}} \tag{3.1}$$

Any of these forces, separately or together, can result in the adhesion contrast observed between the overlap and gap. The Vander Waal's force, F_{vdW}, is expected to be modulated by the molecular density, for which the electron density in Figure 1.5 is a proxy. So, the higher the electron density, the greater F_{vdW} should be. If $F_{D\text{-band}}$ is purely governed by F_{vdW}, the adhesion force should be greater in the overlap compared to the gap region, as the overlap is denser than the gap.(Figure 1.5) However, this is the opposite of our experimental data (Figure 3.2c). So, F_{vdW} does not appear to be the prime factor responsible for this contrast. Next, the capillary force, F_c, is a function of humidity in the air[98] and should play a role in modulating $F_{D\text{-band}}$ as follows. Because of the tip geometry and the trough created in the gap region, water absorption is higher in the gap compared to the overlap,[98]

resulting in a greater capillary force in the former than the latter. Hence, F_c contributes to a higher adhesion in the gap than the overlap region, which is qualitatively consistent with our results (Figure 3.2c). However, as the height difference between the gap and overlap regions increases, the capillary force in the gap region should increase. Yet, the mean adhesion values of the overlap and gap regions are not significantly different among the fibril types even though they cover a wide range of D-band amplitudes (Figure 3.2). Therefore it is unlikely that F_c alone drives the observed spatial modulation of the adhesion force.

Since neither F_{vdW} nor F_c can fully explain the results, the hypothesis we put forward is that the n-doped Silicon tip used in our experiment is acting like a negative charge. Since it has been previously shown using KPFM that the overlap (gap) region is negatively (positively) charged,[34] following the hypothesis, the tip would be repelled (attracted) by the overlap (gap) region, hence yielding a negative (positive) adhesion. This is consistent with the results (Figure 3.2c). So, the Electrostatic force between the tip and the sample, F_e can be one of the forces to be accounted for the adhesion pattern observed and is likely the main contributor to the observed sub-D-band force dips.

3.1.2 Molecular assignment of fibril type specific adhesion fingerprints

Three adhesion force dips are consistently visible in the fingerprints of all four fibril types. We attribute these dips to the X1, X2, and X3 bands-the three main electron-dense regions observed by Quan and Sone using Cryo- EM (Figure 1.5). Other, less conspicuous bands were also visible, albeit less frequently in the fingerprints as compared to the unprocessed profiles as they are often lost due to averaging (Figure 3.3).

The respective spacing between the three main bands for all fibril types approximately matches the ones observed by Cryo-EM (Figure 1.5, 3.4a). However, we also observe that each individual fibril has a unique set of spacing and that on average, each fibril type differs in spacing by a few nanometers. Taking advantage of the registration between the adhesion and height fingerprints, it was possible to locate the height position of each adhesion force dip along the D-band topography (Figure 3.4b and 2.4).

It has been well-documented that during fibril formation, a 3.8 nm lattice plane of collagen molecules orients radially, which causes the C-terminal telopeptide to be jutted outwards, causing it to be at the apex of the fibril's corrugated surface, and the N-terminal telopeptide

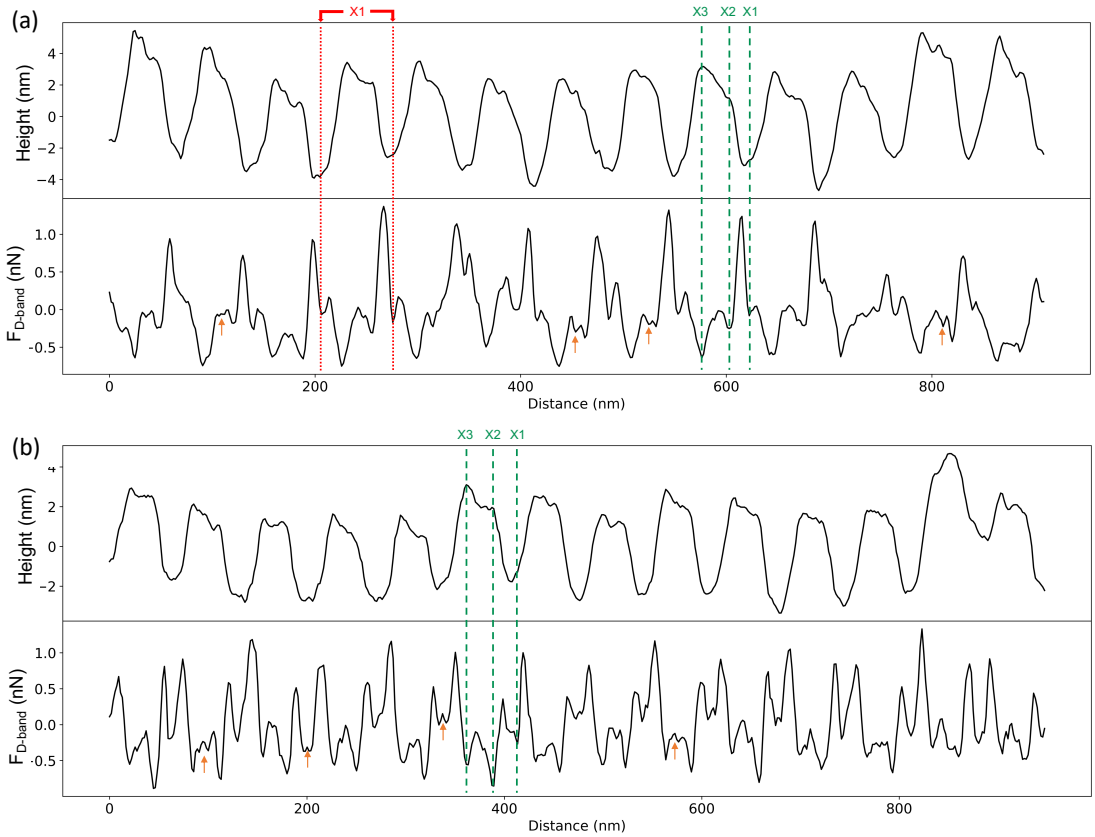

Figure 3.3: Appearance of minor sub-bands and instances of asynchronization of height and adhesion in the filtered profiles from an (a) SDF fibril and (b) Telocollagen fibril *The 3 major bands in this profile along with multiple smaller dips corresponding to sub-D-bands are visible (orange arrows) that are often not visible in an averaged fingerprint. Red dotted lines in (a) show an asynchronization in the visibility of X1 band in height and adhesion- while the one with a visible peak in height exhibits a less intense dip in adhesion, the other with no peak in height displays a stronger dip in adhesion. Also, while the X3 band shows a taller peak in height than X2 does in both (a) and (b), the dip in adhesion caused by the X3 band is stronger than that of X2 in (a) and vice-versa in (b).*

to be buried underneath the fibril surface.[99, 100] Hence, the X3 band, which corresponds to the C-terminus of the collagen molecule, is located at the apex of the D-band repeat with the X2 band, corresponding to the N-terminus, located a few nanometers underneath (Figure 3.4b), validating our band assignment.

From the results so far, these dips in the adhesion force, $F_{D\text{-band}}$ can be attributed to two forces-the capillary force, F_c, which is dependent on the topography, or the Electrostatic force, F_e, which is dependent on the surface charge. One possibility is that the visibility of

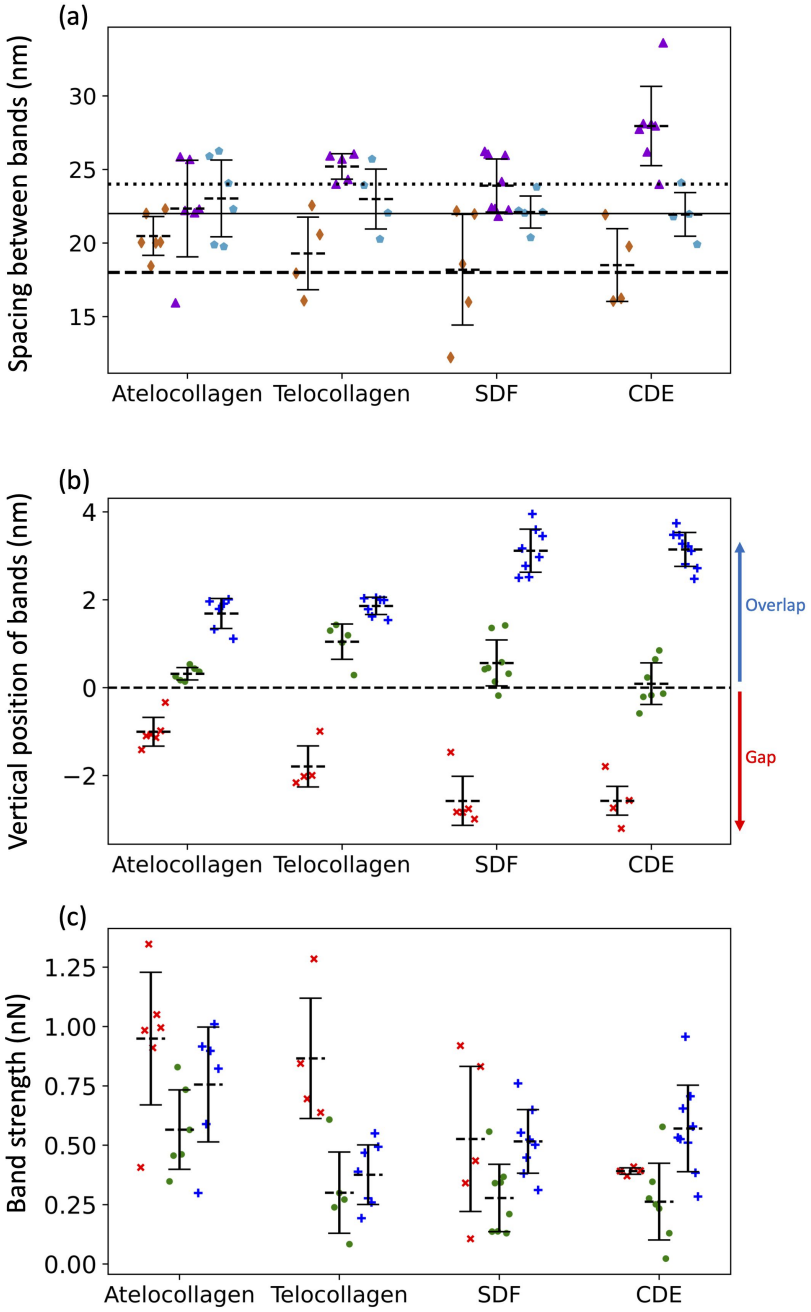

Figure 3.4: (a) Band spacing. *Average spacing between X1 and X2 bands (◆), X2 and X3 bands (▲) and X3 and X1 bands (⬟) along with the spacing between X1 and X2 bands (dashed line), X2 and X3 bands (solid line) and X3 and X1 bands (dotted line) calculated using cryo-TEM data.*(b) Height location of bands, X1 (✖), X2 (●) and X3 (+). *Negative height position (X1) indicates that the band is located in the gap region whereas positive height position (X2 and X3) indicates that the band is located in the overlap region.*(c) Adhesion strengths of X1 (✖), X2 (●) and X3 (+) bands. *See Figure 2.4 for details.*

these sub D-band features is a result of the modulation of F_c alone. While the most intense dips in adhesion match the electron-dense peaks, since F_c is dependent on topography, each dip in adhesion should be accompanied by a proportional variation in height.[98] This, however, is not the case since there are many instances where the dips in the adhesion profile associated with the characteristic bands, X1, X2, and X3, are not accompanied by any peaks in the height profile (Figure 3.1, 3.3). Moreover, F_c is also expected to be weaker in shallower dips of shorter, atelocollagen fibrils as compared to deeper dips of taller, CDE fibrils. But, since this was not observed in the results, variations in capillary force are unlikely to be the explanation for the detection of these sub-bands. Accounting for the other possibility, the X1, X2, and X3 bands marked in Figure 3.1 also correlate to *d, c, and a* peaks, respectively, observed in the Uranyl Acetate stain profile (Figure 1.5). These peaks represent regions with a high number of negative charges within the fibril. If they were net negatively charged, these regions would repel a negatively charged tip and thus decrease the electrostatic force, F_e, resulting in a dip in adhesion force, $F_{D\text{-band}}$. Hence, in addition to explaining the adhesion contrast observed between the overlap and gap, F_e could also be responsible for the visibility of these sub-bands.

3.1.3 Fibril types have intrinsic differences in the surface charge pattern

To compare the differences in adhesion measured among the fibril types at a higher resolution, adhesion strength for the three bands was measured, as described in Figure 2.4. It was revealed that in addition to a unique set of spacing between the X1, X2, and X3 bands, each fibril type has a unique set of adhesion strengths for the three bands (Figure 3.4c).

Assuming that adhesion is purely governed by electrostatic force and interpreting adhesion band strength as a proxy for the net negative surface charge, we observe that the X2 band (N-terminus) is on average less negatively charged than the X3 band (C-terminus) for all fibril types (Figure 3.4c) and that there is significant intra-fibril variation (Figure 3.1 gray shading and 3.3). Comparing across fibril types, the strengths of the X2 and X3 bands are basically identical for SDF and CDE fibrils (Figure 3.4c). This is expected considering that in both cases the N- and C-telopeptides are engaged in crosslinks with adjacent collagen molecules.[73] The telocollagen fibrils have an X2 band identical to the SDF and CDE fibril but a lower X3 band (Figure 3.4c). This is consistent with the idea that the N-terminal

telopeptide is buried under the fibril surface even for *in vitro* assembled fibrils whereas the C-terminal telopeptide is exposed at the surface and interacting with adjacent molecules in a non-native way.[101] In the atelocollagen case, where both telopeptides are missing, the X2 and X3 bands are stronger than for the three other types indicating a unique conformation of the collagen molecules at the fibril surface in two regions that host interacting sequences with several key collagen partners such as keratan sulfate, metalloproteinases, fibronectin and integrins.[100]

The strength of the X1 band is also worth analyzing because it is the *in vivo* interaction site for another proteoglycan, decorin.[102] For all fibril types, the X1 is a negative dip in adhesion force superimposed on one side of the positive adhesion force peak characteristic of the gap region (Figure 3.1). Because we use the maximum adhesion force in the gap region as our reference (Figure 2.4), we likely overestimate the strength of the X1 for all fibril types, including CDE. Nonetheless, all fibrils are analyzed in the same way, so the decrease in strength of the X1 band for the SDF and CDE fibrils compared to the *in vitro* assembled ones may be due to the presence of decorin molecules at the surface of the SDF and CDE fibrils. Decorin is composed of a positively charged core protein domain that covers the X1 band and one negatively charged chondroitin sulfate chain.[103] The mechanical extraction of the fibrils from the SDF and CDE tendons is expected to remove some if not all chondroitin sulfate chains, leaving only the decorin core covering the X1 band. We propose that the CDE fibrils have had their chondroitin sulfate chains consistently removed, thus producing an X1 band of low but very well-defined strength (Figure 3.4c). SDF fibrils in comparison have a much broader range of X1 band strength that is likely a result of the higher cohesiveness between fibrils in this tissue,[104] thus requiring a more forceful extraction than in the CDE case. Finally, the increase in strength of the X1 band for the *in vitro* assembled fibrils compared to the SDF and CDE (Figure 3.4c) is likely due to the absence of the decorin core protein.

There are different reasons which can be responsible for a discrepancy between our results and the ones obtained by Quan and Sone using Cryo-EM.[75] The electron density used as reference (Figure 1.5) was measured on a single fibril extracted from a rat tail tendon which is similar to a bovine CDE tendon. As explained above, there are many intrinsic differences between fibrils of different types and hence, results obtained from each of them

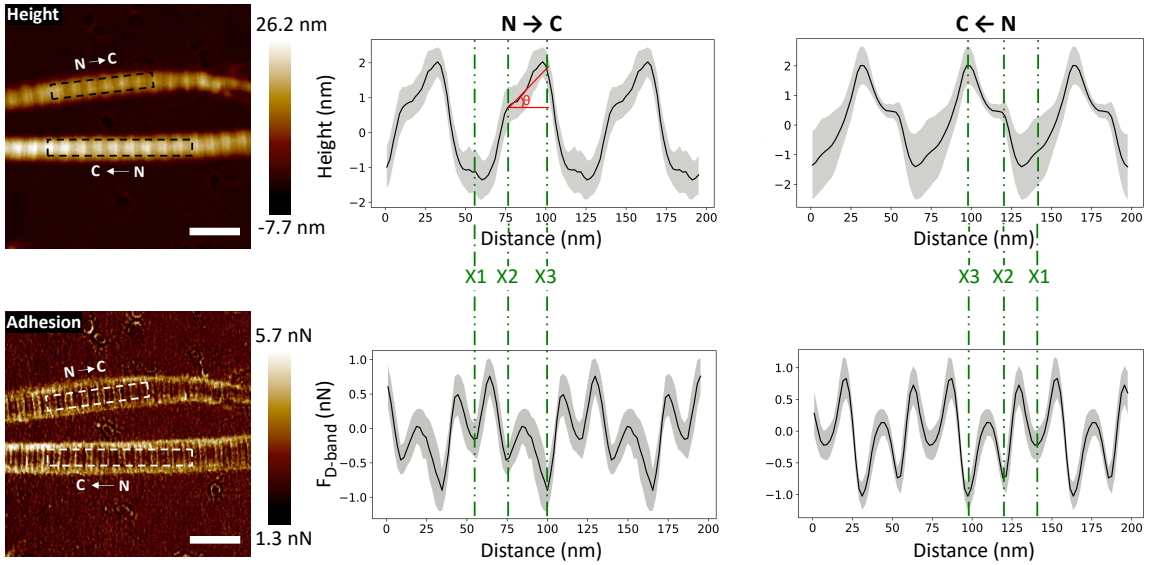

Figure 3.5: Height and adhesion images of two atellocollagen fibrils with opposite polarity. *The arrows on each image indicate the orientation from the N-terminus to the C-terminus of the collagen molecules within the fibrils. Height and adhesion fingerprints extracted from left to right in the broken line boxes are presented with the assignment of the X1, X2 (N-terminus) and X3 (C-terminus) bands. The angle of out-of-plane molecular tilt between the N- and C-termini, (θ), is defined as shown.(Scale bar= 200nm)*

cannot be expected to be entirely similar. Moreover, cryo-EM reveals details in the bulk of a material unlike the AFM, which displays surface properties. So, a discrepancy between the results obtained by the two methods can be an indication of how the charge distribution on the surface of the fibril is different from its interior.

3.1.4 Fibril orientation and out-of-plane molecular tilt

Within a collagen fibril, all the molecules are oriented in the same direction, making the structure polar.[105] Assessing this polarity on a fibril-by-fibril basis is experimentally challenging. Negative staining electron microscopy,[106] Piezoelectric Force Microscopy[29] and second harmonic generation microscopy[107, 108] are the three main techniques capable of identifying polarity, absolutely in the first case and comparatively in the other two cases. Leveraging our assignment of the X1, X2 and X3 bands in the height and adhesion fingerprints, it is possible to define the polarity of a collagen fibril in absolute term (Figure 3.5) without staining.

In principle, this approach could be combined with imaging of tissue cryo-sections to

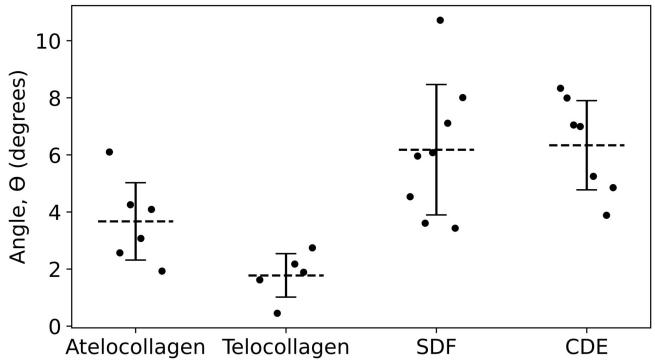

Figure 3.6: Angle of out-of-plane molecular tilt between the N- and C-termini (Figure 3.5) for the four different fibril types.

characterize the polarity of collagen fibril bundles in skin or tendons.[109] Furthermore, with the polarity identified, it is possible to measure the out-of-plane molecular tilt, predicted by Orgel and coworkers,[73] using the positions of the X2 and X3 bands in the height fingerprint as shown in Figure 3.5. Telocollagen fibrils have the lowest average out-of-plane molecular tilt, approximately 2°, followed by atelocollagen fibrils with similar height but an average tilt of 4° (Figure 3.6). This factor of two in molecular tilt further demonstrates the subtle differences in fibril structure induced by the deletion of the telopeptide as already observed with the adhesion strength of the three bands (Figure 3.4c). The two types of *ex-vivo* fibrils have the largest average out-of-plane molecular tilt, 6 ° (Figure 3.6) which is likely set by the presence of enzymatic cross-links at the C-terminus.[100] In all four cases, the measured angle is affected by changes in the shape of the fibrils as they dry on the glass substrate.[110]

3.2 *Ex-vivo* fibrils in sections

CDE and SDF tendons were cryosectioned and then imaged using AFM. (Figure 2.2a) The tendon sections were studied as they are expected to be a more natural representation of fibrils in the body as compared to the extracted and self-assembled fibrils. As fibrils in sections appear closely packed, while there were only 1 or 2 fibrils present in a 1 μm image of the extracted fibrils' sample, (Figure 2.1c) an image of a section contained at least 4-5 fibrils. (Figure 3.7, 3.8) The D-band pattern was exhibited by all fibrils, with a period of 64 nm (SD=4nm) (n=25). As explained in section 2.3.1, both narrow and wide profiles were extracted from these fibrils to analyze the effect of averaging. (Figure 2.2a) As expected,

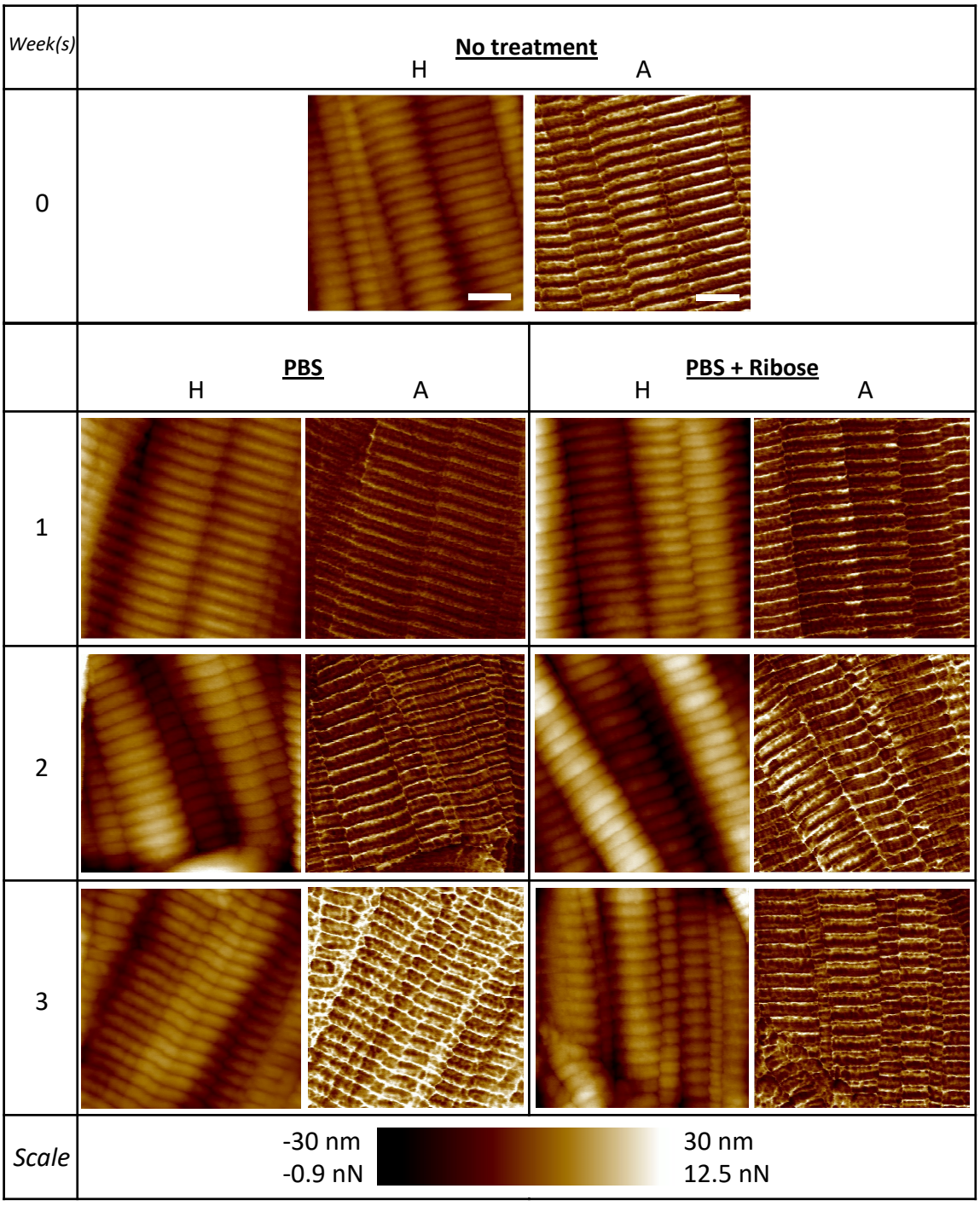

Figure 3.7: Height (H) and Adhesion (A) images of CDE samples at different stages of the experiment. *Scale bar=200m*

wide profiles lacked some definition that narrow profiles possessed. However, the data acquired from a profile too narrow is often accompanied with noise. Therefore, for a fair

comparison between extracted fibrils and fibrils in sections, only the wide profiles similar in width to those used in extracted fibrils were used for this study.

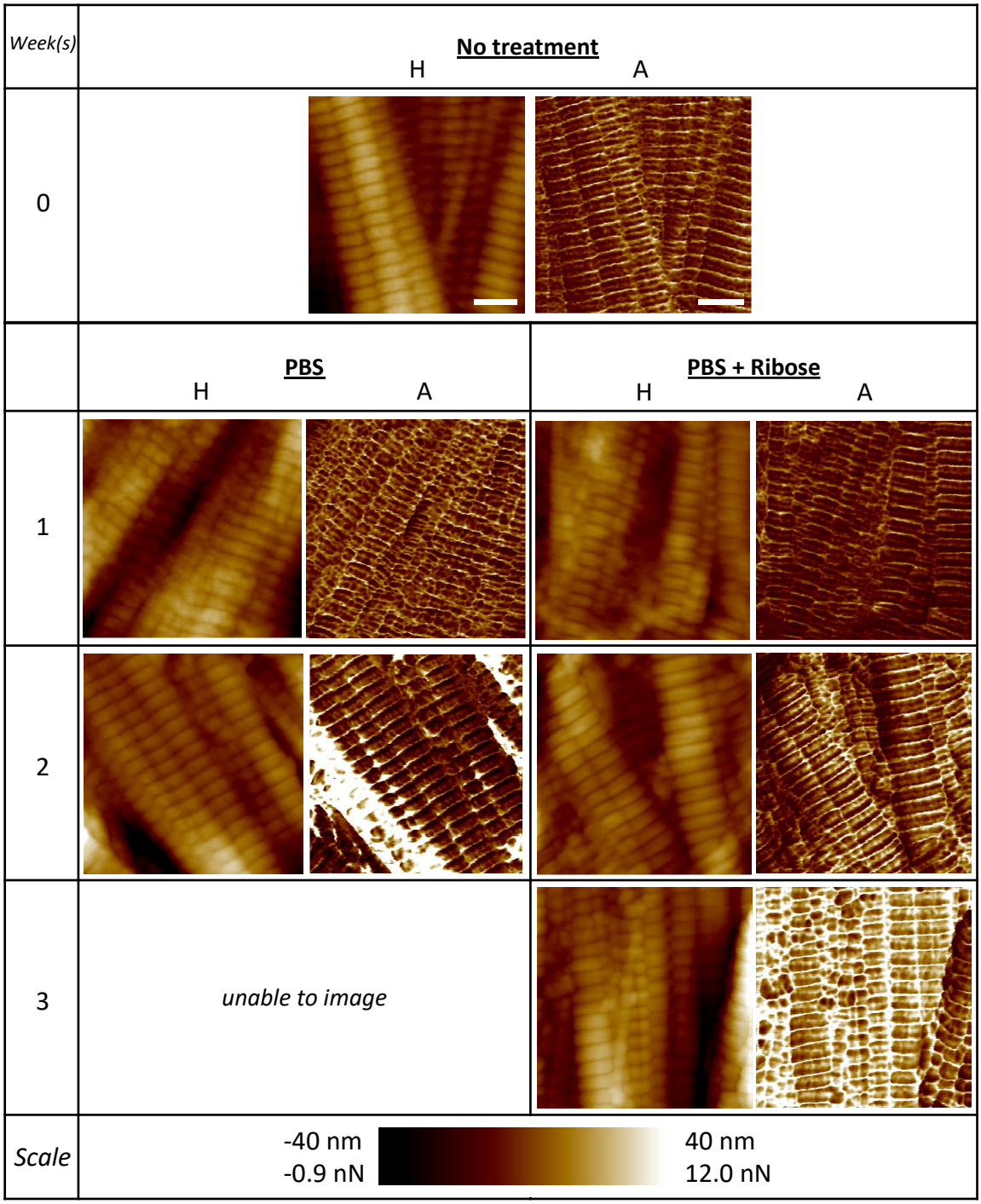

Figure 3.8: Height (H) and Adhesion (A) images of SDF samples at different stages of the experiment. *Features were not clearly visible in the images of the control sample at week 3. Scale bar=200m*

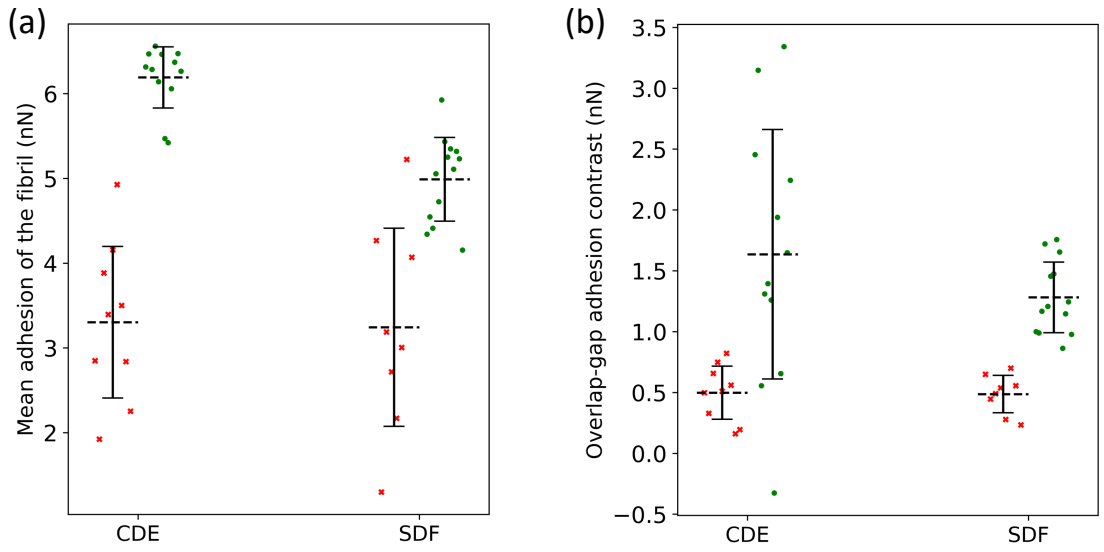

Figure 3.9: (a) Mean adhesion and (b) Overlap-gap adhesion contrast of *ex-vivo* extracted fibrils (✖) and fibrils in sections (●)

3.2.1 Mean adhesion values of fibril types from sections are significantly different

The fibrils from CDE and SDF tendon sections had significantly different mean adhesion values, (Figure 3.9a) with CDE being more adhesive than SDF. This is in contrast with the extracted fibrils where CDE and SDF had comparable adhesion values. (Figure 3.2d) Moreover, the mean adhesion of fibrils in sections was greater than extracted fibrils for both fibril types. However, the variation in the mean adhesion amongst the fibrils in both section samples was lower than that for extracted fibrils. (Figure 3.9a)

Following the same approach as in the study of extracted fibrils, (Figure 2.4) the mean adhesion of the overlap and gap regions, along with their contrast, was calculated for fibrils in sections.(Figure 3.9b) The overlap-gap adhesion contrast was significantly higher in both CDE and SDF sections as compared to the respective samples of extracted fibrils. This was also accompanied by a greater variation in the overlap-gap adhesion contrast amongst the fibrils in both individual samples.

3.2.2 Fibrils in sections have less prominent sub-D-band features

Following the idea of attributing dips in adhesion as electron dense bands, X1, X2 and X3 as in extracted fibrils, the visibility and strength of these bands were also studied in fibrils

from sections. In extracted fibrils, whereas the X1 band was rarely visible, the X2 and X3 bands were distinctly visible in the adhesion profile.(Figure 3.1) Often, the X2 and X3

Week(s)		**Extracted fibrils**	**Untreated section**
0	**H**	Tall peak and a shoulder/short peak in overlap, corresponding to X3 and X2 bands, respectively, and a rare, negligibly short peak in gap, corresponding to X1 band.	Different height shapes in overlap observed: Tall peak with shoulder, triangular or rectangular shape; No peak corresponding to X1 band.
	A	Two dips in overlap corresponding to X2 and X3 bands, respectively; Tall peak between X2 and X3 band; A rare, shallow dip in gap corresponding to X1 band.	Strong dip for X3 band, but shallow (less strong) dip for X2 band; No dip visible for X1 band.
		PBS treated section (control)	**PBS + ribose treated section**
1	**H**	Features like extracted fibrils.	Features like untreated section.
	A	Features like extracted fibrils.	X2 and X3 bands less prominent since the tall peak between X2 and X3 band decreased in intensity or was completely absent in 19% cases, leading to a flat adhesion pattern in overlap; X1 band rarely visible in gap
2	**H**	Features like extracted fibrils.	Features like untreated section.
	A	Features like extracted fibrils.	Flat adhesion pattern (like 1 week ribose) seen in 40% cases. In some cases, tall peak between X2 and X3 band replaced by multiple small peaks, indicating accumulation; X1 band rarely visible.
3	**H**	Features like extracted fibrils.	Features like untreated section.
	A	Features like extracted fibrils.	Flat adhesion pattern (like week 2 ribose) seen in 32% cases; X1 more frequently visible.

Table 3.1: Summary of qualitative changes observed in Height (H) and Adhesion (A) profiles in all CDE samples.

bands did not show the same strength, as one of the bands was more adhesive than the other. While the bands appear as dips in adhesion, they are often accompanied by a peak in height. Although this peak is rarely commensurate to the depth of the dip in adhesion, this synchronization of height and adhesion profiles is important for correct band assignment. These bands are located using the dips in the adhesion profile, however, their identification is only successful using the corresponding features in the height profile.

The profiles obtained from images of fibrils in sections were analyzed using this technique (summarized in Table 3.1, 3.2). The visibility of all three bands diminished in fibrils

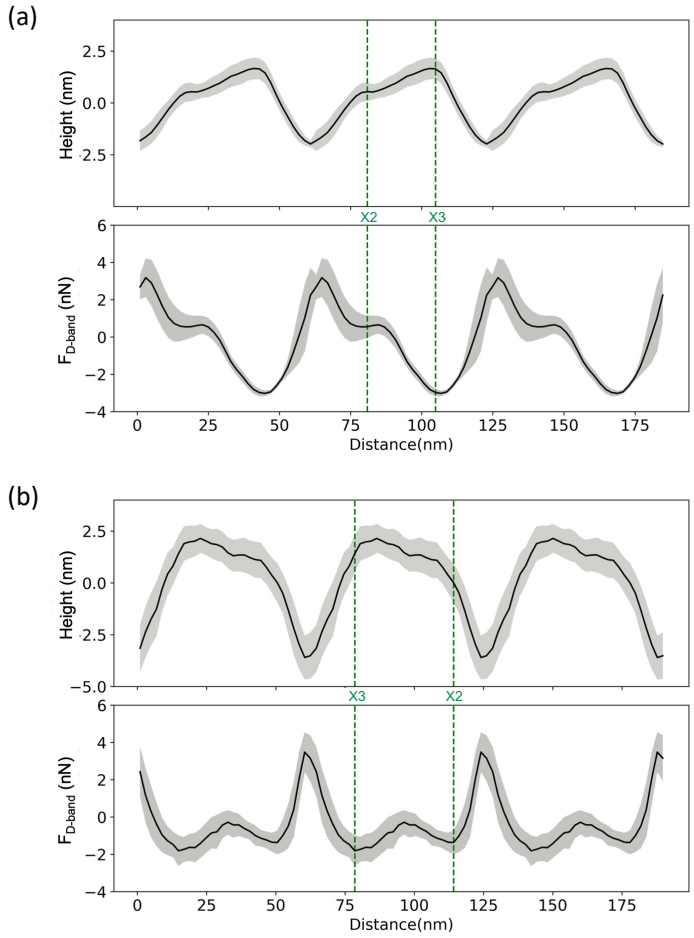

Figure 3.10: Height and corresponding adhesion fingerprint profiles of a fibril from (a) CDE and (b) SDF tendon section

from sections as compared to that of extracted fibrils. In fibrils from CDE sections, the X1 band was not visible in any fibrils. While the X3 band was visible in all the fibrils, fewer instances of visibility of the X2 band were observed. Even in most of the cases where the

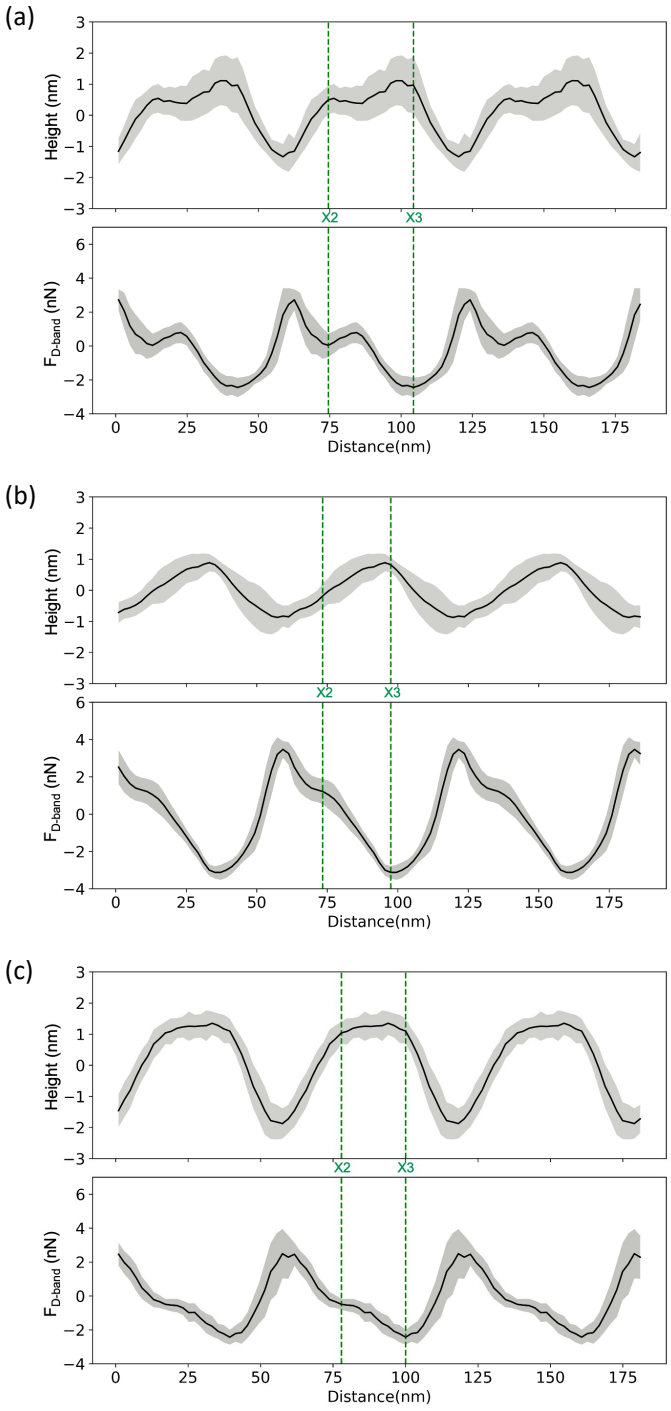

Figure 3.11: Different height profiles and their corresponding adhesion profiles observed in the overlap region of fibrils in the untreated CDE section *(a) A peak with a shoulder previously observed in extracted fibrils (b) Triangular profile (c) Rectangular profile*

X2 band was visible, the dip in adhesion caused by it was very shallow as compared to that

of the X3 band. (Figure 3.10a)

The shape of the height profile also varied as compared to the extracted fibrils. The previously observed height profiles in the extracted fibrils displayed a tall peak, corresponding to the X3 band, along with a shoulder or a shorter peak, corresponding to the X2 band. In the fibrils in sections, while a similar shape was observed in many height profiles (Figure 3.1,3.11a), there were cases where the height was triangular with only a single peak present corresponding to the X3 band in the overlap region.(Figure 3.11b) In addition, the height profile also rarely displayed two peaks of equal height for the X2 and the X3 bands, giving rise to a rectangular shape (Figure 3.11c). While the triangular shape of the height profile was often accompanied by a partial or complete loss of the X2 band in the adhesion profile, there were cases where it was observed even when the X2 band was present. (Figure 3.11b) Therefore, as observed earlier, while there is a degree of correlation between the modulation in height and adhesion, one is not completely governed by the other.

There are a number of differences in the preparation of the samples of extracted fibrils and sections that can potentially explain the fact that a loss of strength of the X2 band was only observed in the fibrils in sections. Samples of extracted fibrils is prepared via mechanical extraction whereas the fibrils in sections do not undergo such a process. Mechanical extraction can potentially remove non-collagenous proteins, like the proteoglycans, from the surface of the fibrils, as mentioned earlier. It is possible that during the mechanical extraction of the fibrils, keratan sulphate, one of the proteoglycans which binds at the location of the X2 band[111] is removed, revealing the X2 band's negative charges and therefore yielding a stronger dip in adhesion in the case of extracted fibrils. This should result in the mean adhesion of the extracted fibrils to be lower than the fibrils in sections, which aligns with the results. (Figure 3.9a) Moreover, at the end of the extraction process, samples are dried with Nitrogen gas, whereas, tendon sections are left to dry naturally. This can potentially lead to extracted fibrils exhibiting surface properties altered due to drying, similar to the changes observed as a result of vacuum drying. [112] Furthermore, it is possible that in cryosectioning, some sections are cut through the fibrils, revealing the inner part of the fibrils. As the interior of the fibril is expected to be different than its surface, images of such fibrils can be different from those of extracted fibrils. Finally, it is important to acknowledge the aspect that despite comparing the extracted fibrils and fibrils in sections from similar tendon types, they were obtained from distinct animals.

In the case of SDF, however, the visibility of these sub-D-band features did not change as much between extracted fibrils and fibrils in sections.(Table 3.2) Like for extracted SDF

Week(s)		**Extracted fibrils**	**Untreated section**
0	**H**	Tall peak and a shoulder/short peak in overlap, corresponding to X3 and X2 bands, respectively, and a rare, short peak in gap, corresponding to X1 band.	Features like extracted fibrils.
	A	Two dips in overlap corresponding to X2 and X3 bands, respectively; Tall peak between X2 and X3 band; A shallow dip in gap corresponding to X1 band.	Features like extracted fibrils.
		PBS treated section (control)	**PBS + ribose treated section**
1	**H**	Features like extracted fibrils.	Features like control.
	A	Features like extracted fibrils.	Features like control.
2	**H**	A partial or total loss of peak corresponding to X2 band in many cases	Features like extracted fibrils.
	A	Strong dip for X3 band, but shallow (less strong) dip for X2 band; No dip visible for X1 band in almost all cases.	Features like extracted fibrils.
3	**H**	*Unable to image sample.*	Features like extracted fibrils.
	A		Flat adhesion pattern in overlap (like CDE ribose samples) seen in 15% cases; X1 rarely visible in gap.

Table 3.2: Summary of qualitative changes observed in height (H) and adhesion (A) profiles in all SDF samples.

fibrils, the visibility of X1 band was rare for SDF fibrils in sections. And although the X2 and X3 bands were not as prominent as in the extracted fibrils, they were still visible in almost all fibrils. (Figure 3.10b) Moreover, the difference between the mean adhesion of fibrils in sections and extracted fibrils was not as large as in the case of CDE. (Figure 3.9a) Therefore, contrary to CDE, for SDF, fibrils in sections and extracted fibrils appear

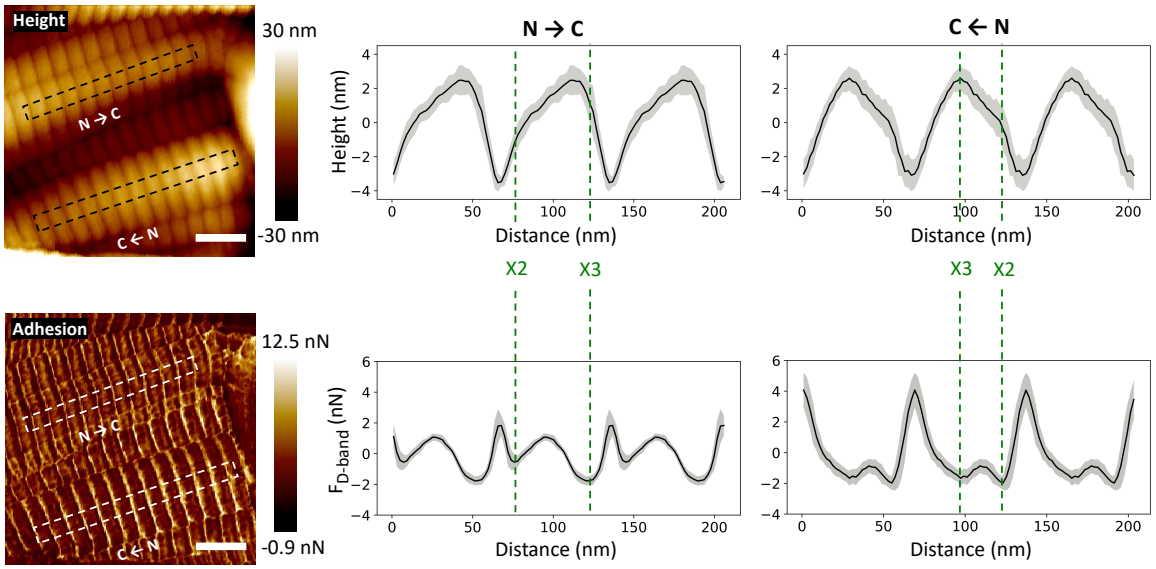

Figure 3.12: Height and adhesion images of two fibrils from CDE tendon section with opposite polarity. *The arrows on each image indicate the orientation from the N-terminus to the C-terminus of the collagen molecules within the fibrils. Height and adhesion fingerprints extracted from left to right in the broken line boxes are presented with the assignment of the X2 (N-terminus) and X3 (C-terminus) bands. (Scale bar= 200nm)*

the same. This can again be attributed to the higher cohesiveness between fibrils in SDF compared to CDE,[104] which would result in an almost pristine surface after mechanical extraction.

Similar to extracted fibrils, using the dips in adhesion and the corresponding peaks in height for the identification of bands, the orientation of fibrils was determined. (Figure 3.12) In the extracted fibrils, since the features in both profiles were clearer, the determination of the orientation was simple. However, as described earlier, for the sections, since there were many cases where these dips (peaks) in adhesion (height) profiles were missing, in about half of the cases in CDE, the orientation of the fibril could not be ascertained. In SDF, this ratio was smaller, i.e. approximately one-third, due to a higher visibility of these sub-D-band features in both profiles.

3.3 Glycation of fibrils within tendons

The effect of glycation on fibrils was studied using ribose over a period of 3 weeks. CDE and SDF tendon segments were incubated at 35°C in a solution of either 0.2 M ribose in PBS, or PBS only, which acted as a control. The concentration of ribose was 0.2 M following

the study conducted by Tanaka et. al, where they observed the effect of glycation linearly increasing with time for the first 2-3 weeks at this concentration, followed by a gradual plateauing.[57] A tendon segment of each type was taken out each week, cryo-sectioned and imaged using AFM. (Figure 2.2) This enabled us to observe the gradual effect of PBS and ribose on collagen fibrils.

Instead of wide profiles, narrow profiles were extracted from the images for this experiment, as described in section 2.3.1. This was done to observe the minute changes in the fibrils' surface and not lose them to averaging done in the wide profiles. The D-band period observed in the fibrils was 65 nm (SD=5nm). While most fibrils in all the samples had acceptable D-band periods, some of them exhibited periods as low as 50 nm, and as high as 80 nm. These anomalous values were not exclusive to fibrils of any specific samples or stage of the experiment. During the dry imaging of a tendon section, if layers of fibrils are loosely bound to each other, this can cause drift and lead to distorted images. The peculiar D-band values were likely due to this distortion in the AFM images and were observed throughout the experiment. As a way to eliminate the outliers from the data set, the fibrils outside the range of one standard deviation from the mean, i.e. 60 nm to 70 nm, were removed. This yielded an average of 18 fibrils per sample. (Figure 3.7, 3.8)

3.3.1 Incubation in PBS changes surface properties of fibrils in sections

After the incubation of tendon segments in the control solution of PBS, the properties of fibrils in sections changed. The observed effects were different for CDE and SDF, and differed from week to week (qualitative changes summarized in Table 3.1, 3.2).

3.3.1.1 CDE

After 1 week of incubation in PBS, the mean adhesion of fibrils in the PBS-treated section significantly lowered as compared to that of fibrils in the untreated section. (Figure 3.13a) The variation in mean adhesion amongst the fibrils remained the same. There was no significant difference in the overlap-gap adhesion contrast between the treated and untreated samples. (Figure 3.13b) As mentioned earlier, fibrils in untreated sections did not display a prominent X2 band in the adhesion profile in most cases, and no X1 band in any case. In contrast, in almost all fibrils in the treated section, the X2 and X3 band was present in the adhesion profile and the X1 band was also visible in a few cases. (Figure 3.14a) The

shape of the height profile also had a lesser degree of variability, with most of the fibrils displaying the characteristic peak with a shoulder in the overlap region. (Figure 3.14a) These characteristics are similar to those observed in the extracted CDE fibrils. Moreover, while not equal, the mean adhesion value of fibrils in the treated section was closer to that of extracted fibrils, than to the fibrils in the untreated section. (Figure 3.9a, 3.13a)

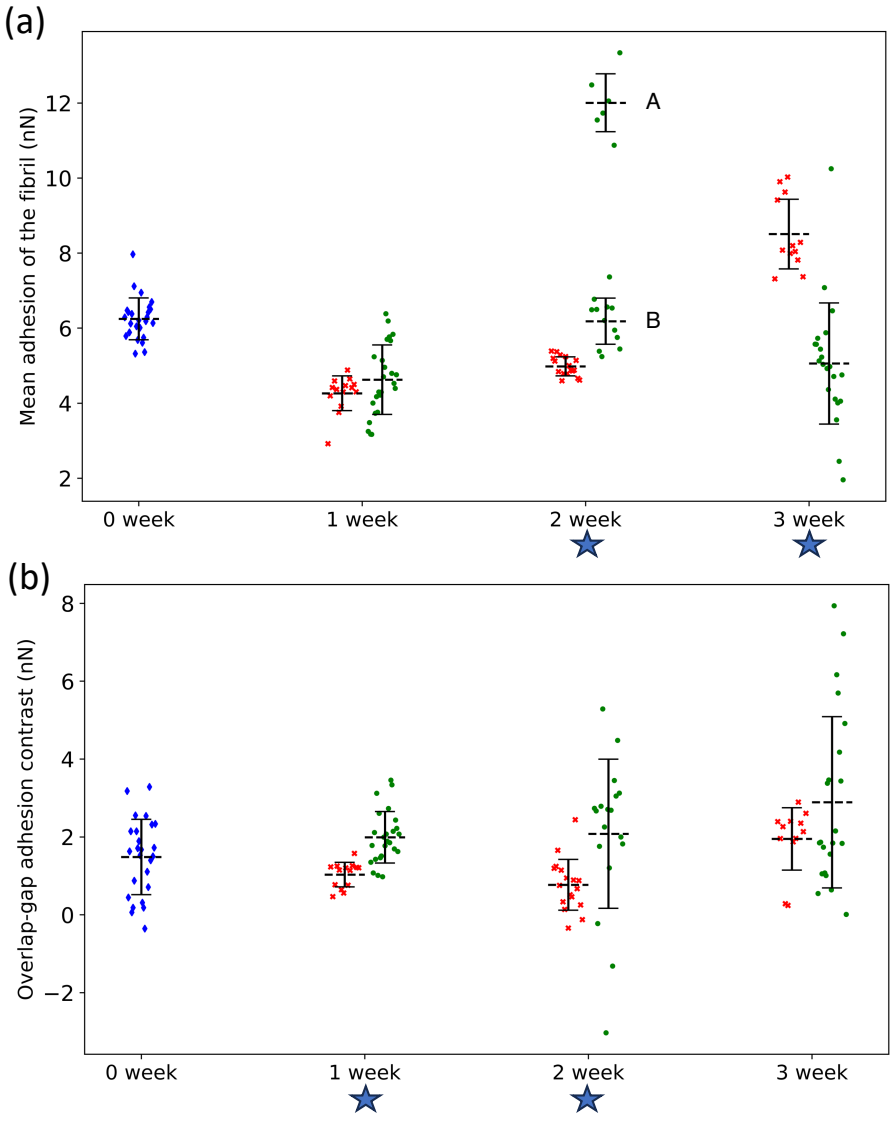

Figure 3.13: (a) Mean adhesion and (b) Overlap-gap adhesion contrast of CDE fibrils at different weeks of the experiment. *Untreated sample (◆), control sample (✖), ribose sample (●). Fibrils were divided into groups A and B where bimodal distribution was observed. Instances of significant difference between control and ribose sample is marked by star (⋆).*

After 2 weeks of incubation in PBS, these characteristics did not show much alteration.

The mean adhesion was higher than the week 1 sample, but lower than the untreated section sample.(Figure 3.13a) The variation in mean adhesion amongst the fibrils was also lower. While the mean overlap-gap adhesion contrast lowered compared to the week 1 sample, the variation amongst the fibrils was larger, thus leading to no significant difference between the samples.(Figure 3.13b) In terms of clarity of sub-D-band features, whereas the fibrils in the sections treated for 1 week showed significant improvement from the untreated section, the fibrils in the sections treated for 2 weeks did not show any change as compared to the week 1 sample. (Figure 3.14b) The X2 and X3 bands were still visible in the adhesion profile of most fibrils, with rare visibility of the X1 band. The height features also remained the same, with most fibrils displaying the tall peak corresponding to the X3 peak, along with a shoulder, corresponding to the X2 peak.

After 3 weeks, while the visibility of sub-D-band features remained the same for the most part, the adhesion values of the fibrils changed significantly. (Figure 3.13a) The mean adhesion of fibrils was significantly higher than all the previous weeks' samples. This was accompanied by a doubling of the variation in the mean adhesion amongst the fibrils. The overlap-gap adhesion contrast was also the highest compared to the previous weeks. (Figure 3.13b) Like the week 2 sample, the X2 and X3 bands were distinctly visible in the adhesion profile of most fibrils. (Figure 3.14c) There were also no significant changes in the height features observed.

To summarize the changes observed in the fibrils due to incubation of the tendon segments in PBS over 3 weeks, the most significant change was observed after 1 week. Unlike the fibrils in the untreated section, the fibrils in the 1 week treated section displayed characteristics in both height and adhesion profiles that were similar to the ones of extracted fibrils. (Figure 3.1, 3.11, 3.14a) Unless the addition of antimycotic solution led to any changes, it appears that long-term incubation in PBS affected the surface of the fibril in some manner. This result is intriguing because an incubation in a neutral buffer is not expected to change the fibril surface significantly.[34] However, considering that the surface properties of the fibrils incubated in PBS are similar to the ones of extracted fibrils than to the fibrils in untreated sections, it is speculated that PBS incubation led to the removal of some of the non-collagenous material which is known to be bound on the surface of the fibril. [113]-[116] Due to this effect of chemical extraction, the bands became clearer in both height and adhesion profiles, and the mean adhesion of the fibril also decreased, which is

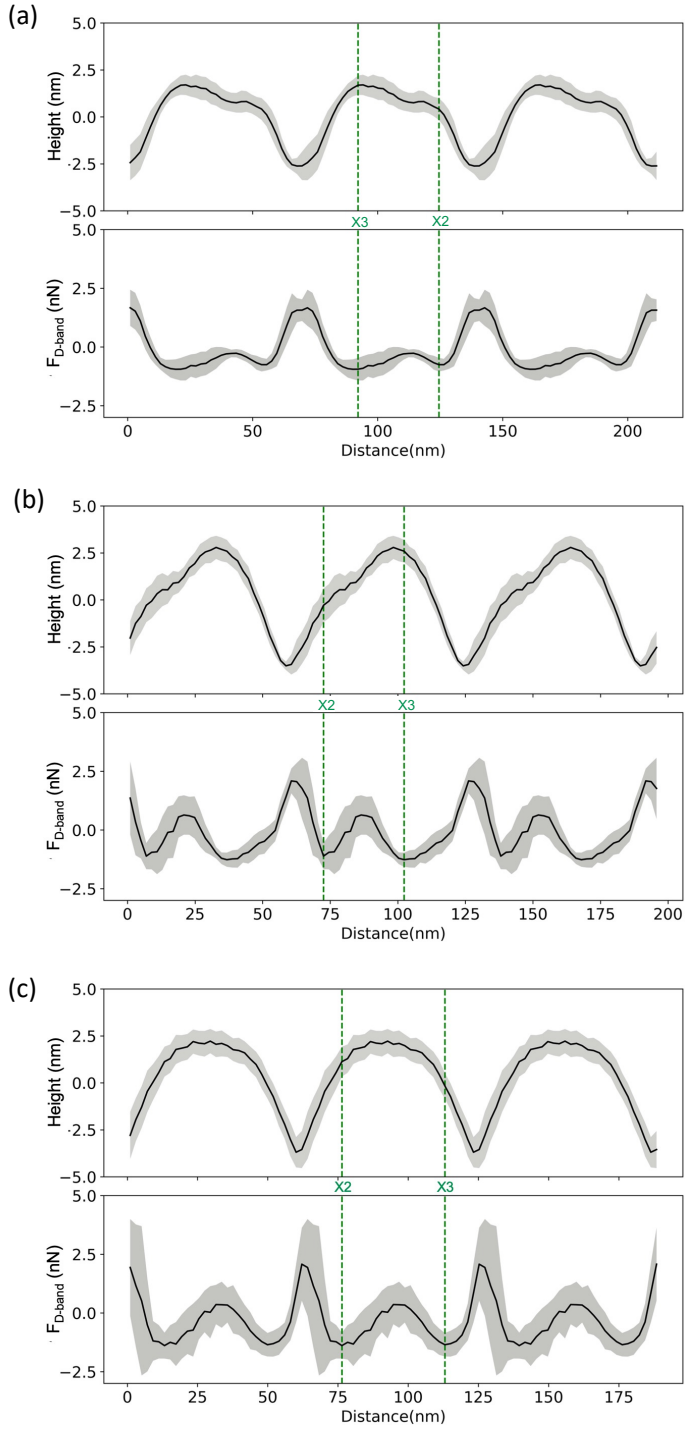

Figure 3.14: Height and corresponding adhesion profiles from fibrils in CDE section after (a) 1 week, (b) 2 weeks, and (c) 3 weeks of incubation in PBS. *Both X2 and X3 bands are distinctly visible in the fibrils like previously observed in extracted CDE fibrils (Figure 3.1)*

expected with the appearance of negatively-charged regions at the fibril surface. Since the fibrils in sections incubated for more than 1 week did not change much in terms of visibility of these sub-D-band features, it appears that this effect of PBS plateaus in less than a week. However, this is contrary to the quantitative analysis because the adhesion values continue to change after weeks 2 and 3 of incubation. (Figure 3.13) One source of concern is that the solutions in the later weeks showed an increasing fungal growth, with the week 3 samples showing the highest growth. Although 1% Antibiotic-antimycotic solution was used in all the samples, it appears that the concentration was not enough to prevent the fungal growth, and repeated opening of the sealed samples in a non-isolated environment aggravated this problem. Therefore, the change in the adhesion values at weeks 2 and 3 can be due to changes in the fibril surface caused by bacterial and/or fungal action.

3.3.1.2 SDF

After 1 week of incubation in PBS, in mean adhesion, there was no significant difference compared to that of fibrils in the untreated section, even so the average value increased. (Figure 3.15a) The variation in the mean adhesion amongst the fibrils decreased. However, the average value of and the variation in the overlap-gap adhesion contrast did not change. (Figure 3.15b) In addition, there also was no significant change in the visibility of the sub-D-band features. (Figure 3.16a)

After 2 weeks of incubation, the distribution of mean adhesion values across the sample appears to be bimodal. (Figure 3.15a) However, this bimodality is not real, since it was only observed after the removal of fibrils with extreme D-band values, as explained earlier. Therefore, the fibrils were considered a single group. The average value of and the variation in the mean adhesion of the fibrils increased significantly as compared to the week 1 sample. However, due to the large variation, there was no significant difference between the mean adhesion of fibrils in sections treated for 1 week and 2 weeks. A similar rise was observed in the overlap-gap adhesion contrast. (Figure 3.15b) The adhesion and height profiles also showed some changes. Unlike in the fibrils observed after 1 week incubation, the height profile often showed a partial or total loss of a shorter peak corresponding to the X2 band. Moreover, the strength of the X2 band reflected in the adhesion profile was lower than the strength of the X3 band. (Figure 3.16b) The X1 band was also absent in almost all the fibrils. Due to these reasons, the band assignment in this sample was difficult.

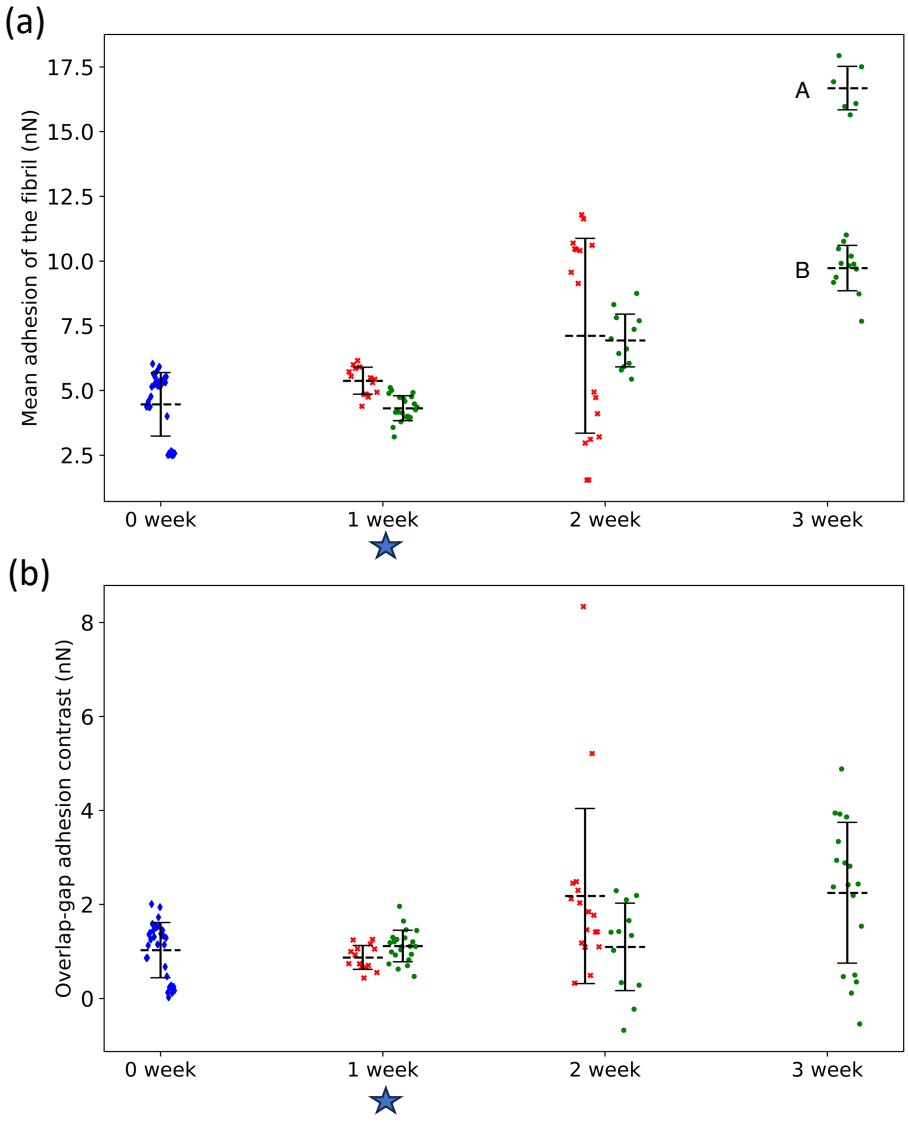

Figure 3.15: (a) Mean adhesion and (b) Overlap-gap adhesion contrast of SDF fibrils at different weeks of the experiment. *Untreated sample (◆), control sample (✖), ribose sample (●). Fibrils were divided into groups A and B where bimodal distribution was observed. Instances of significant difference between control and ribose sample is marked by star (★).*

After 3 weeks, imaging of the fibrils was unsuccessful. When attempted, while the fibrils and the D-band was still vaguely visible, the fibrils often showed material accumulated on top, which blemished almost all surface features in both height and adhesion images.

From these results, the changes in SDF fibrils due to the incubation in PBS seems to be entirely different than the CDE case. Unlike the CDE case, the fibrils were mostly similar in the untreated section and the section incubated for 1 week. Significant changes were

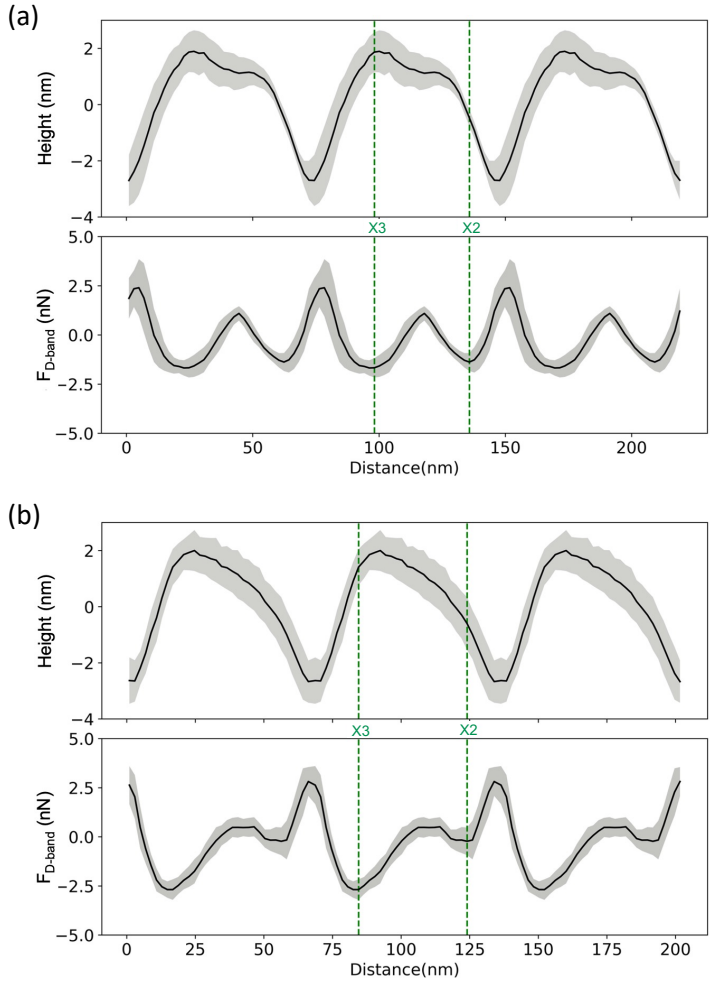

Figure 3.16: Height and corresponding adhesion profiles from fibrils in SDF section after (a) 1 week, and (b) 2 weeks of incubation in PBS. *While a prominent X2 band in adhesion is visible in the week 1 sample, similar to the untreated sample (Figure 3.9), it appears diminished in the week 2 sample*

observed in the fibrils after 2 weeks of incubation in PBS, where the visibility of the X2 band decreased in both height and adhesion profiles. And the changes in the sample after 3 weeks were more drastic, to the extent of being impossible to measure in both height and adhesion profiles.

There is a potential explanation for this discrepancy between SDF and CDE. Considering that PBS may be responsible for the removal of non-collagenous material from the surface of the fibril within a week of incubation, it appears that this effect is not so prominent on SDF fibrils. To recall, a similar disparity was observed when comparing the extracted fibrils and fibrils in untreated sections. While the fibrils in the untreated CDE sections varied from

the extracted fibrils, in the case of SDF, fibrils from both samples were mostly similar. (Figure 3.1, 3.10) It is speculated that the bound proteoglycan coverage on the surface of the CDE and SDF is different. To recall, the extracted CDE and SDF fibrils also showed a difference in the strength of the X1 band, which could be attributed to a possible difference in the coverage of decorin in the gap region. SDF has previously been shown to have a higher mRNA expression of these proteoglycans along with greater glycoamoinoglycan levels as compared to the CDE.[117]-[119] If indeed PBS is responsible for the removal of these proteogylcans, it appears that their higher coverage makes it difficult to remove them from SDF within a week of incubation.

It is possible that in SDF, it takes longer than a week for a full effect of PBS. However, after 2 weeks, the band visibility decreased instead of increasing, followed by a total loss of visibility after 3 weeks. The fungal growth observed in SDF samples was more pronounced than in CDE samples. Therefore, it is possible that the surface of SDF samples started showing signs of degradation and/or accumulation of fungal protein as a result of the microbial activity after 2 weeks, which started blemishing the sub-D-band features.

The change of surface properties of collagen fibrils due to long-term incubation in PBS has not been well documented in the literature. In the study of the effect of glycation on fibrils done by Tanaka et. al using X-ray diffraction and gel electrophoresis,[57] the fibrils undergone prolonged incubation in PBS did not show any alteration in fibril structure. This is in line with our results since all the fibrils incubated in PBS exhibited a clear D-band pattern and hence, the structure of the fibrils remained intact. However, if there were changes due to PBS on the surface of the fibril, X-ray diffraction would be unable to detect them, but AFM could. There are some other studies as well which have used PBS as a control solution for incubation of tendons. However, these studies either had different parameters (lower temperatures or shorter incubation period) or did not include an examination of the surface of the fibrils. In the current study, the results observed in both CDE and SDF sections demonstrate that the effect of PBS on adhesion measured by the AFM may not be negligible. While the samples did show signs of fungal growth, it was only visible in the weeks 2 and 3. However, significant changes in CDE and minor changes in SDF were observed after 1 week of incubation in PBS, even in the absence of visible fungal growth. Therefore, further study is required to confirm the effects of long-term incubation in PBS on the surface of collagen fibrils at or above 35°C.

3.3.2 Ribose changes the adhesion pattern along the fibrils in CDE sections, but not in SDF sections

To understand the effect of glycation on collagen fibrils using AFM, we analyzed the change in the surface properties of fibrils in tendon sections, especially the change in adhesion force, as a function of incubation time. (Figure 3.7, 3.8) Since incubation in PBS appears to affect the fibrils, the ribose treated samples were compared to the PBS treated control samples from each corresponding week.

It was observed that while the tendon segments in the control solution were white in color, the tendons, both CDE and SDF, exposed to ribose displayed a golden-yellow color whose intensity increased as the weeks progressed. This is consistent with previous observations of tissues in diabetic patients.[120] Apart from this, similar to the results obtained from the incubation in PBS, the changes observed from incubation in ribose were different for CDE and SDF.

3.3.2.1 CDE

After 1 week of incubation in ribose, as compared to the control sample, the mean adhesion showed no significant difference. (Figure 3.13a) The overlap-gap adhesion contrast, however, was significantly higher with a larger variation amongst the fibrils. (Figure 3.13b) Qualitatively, the features in the height profile remained the same as the control sample.(Table 3.1) While the X1 band was rarely visible, the X2 and X3 bands were visible in many cases. The prominence of the dips in adhesion due to the X2 and X3 bands, however, decreased or was completely lost in some cases. In fibrils not treated with ribose, whether assembled, extracted or in a section, between these two dips, a tall peak in adhesion has been observed (Figure 3.1, 3.10, 3.14a). This peak helps in the identification of the X2 and X3 bands, and also minor bands- a, b1 and b2, (Figure 1.5) since these minor bands appear superimposed on this peak as small dips. (Figure 3.1, 3.3) However, in this sample incubated for a week in ribose, in about 24% of the cases, (Table 3.3) this tall peak was absent, and therefore instead of the typical pattern of two dips in adhesion in the overlap region, it was just a single wide and flat dip in adhesion with no identifiable bands (Figure 3.17a).

After 2 weeks, a bimodal distribution was observed in the mean adhesion of the fibrils and therefore, the fibrils were divided into separate groups, A and B. (Figure 3.13a).

Interestingly, all the fibrils in group A belonged to the same image. While the mean adhesion of both groups was significantly higher than that of the control sample and had equal variability across the group, group A was almost twice as adhesive as group B. A similar bimodality was not observed in the overlap-gap adhesion contrast (Figure 3.13b). It did, however, show a similar rise, with both the average value and the variability across the sample being significantly higher than the control sample, but not significantly different from the week 1 sample. The features observed in height and adhesion profiles were similar to those observed in the week 1 sample. While the bands were visible in many cases, there were also instances (about 60%, Table 3.3) where a flattened adhesion pattern in the overlap region was observed in some fibrils in group B. (Figure 3.17b) Moreover, instead of a complete loss of the tall peak in adhesion between the X2 and X3 band and a flat adhesion pattern, some other fibrils in group B displayed multiple small peaks, thus giving an impression of something accumulating on top of the fibril at the position of the tall peak and thus diminishing its effect on adhesion. (Figure 3.18)

After 3 weeks, the mean adhesion of the sample and its variability amongst the fibrils significantly lowered from the week 2 sample.(Figure 3.15a) This was the same when compared to the control sample at week 3 except that the variability in mean adhesion was larger in the ribose sample than the control sample. The overlap-gap adhesion contrast of the ribose sample was not significantly different from either the control sample or the week 2 ribose sample due to the large variation across the sample.(Figure 3.15b) The visibility of

<table>
<tr><th rowspan="2">Week(s)
Tendon</th><th rowspan="2">0
(untreated)</th><th colspan="2">1</th><th colspan="3">2</th><th colspan="2">3</th></tr>
<tr><th>PBS</th><th>PBS+ribose</th><th>PBS</th><th colspan="2">PBS+ribose</th><th>PBS</th><th colspan="2">PBS+ribose</th></tr>
<tr><td rowspan="3">CDE</td><td rowspan="3">8 % (n=25)</td><td rowspan="3">0 %
(n=14)</td><td rowspan="3">24 %
(n=25)</td><td rowspan="3">0 %
(n=17)</td><td colspan="2">44 % (n=18)</td><td rowspan="3">8 %
(n=12)</td><td colspan="2" rowspan="3">32 % (n=22)</td></tr>
<tr><td>A</td><td>B</td></tr>
<tr><td>0 %
(n=6)</td><td>60 %
(n=12)</td></tr>
<tr><td rowspan="3">SDF</td><td rowspan="3">0 % (n=34)</td><td rowspan="3">0 %
(n=14)</td><td rowspan="3">4 % (n=22)</td><td rowspan="3">5 %
(n=17)</td><td colspan="2" rowspan="3">0 % (n=12)</td><td rowspan="3">-</td><td colspan="2">11 % (n=18)</td></tr>
<tr><td>A</td><td>B</td></tr>
<tr><td>33 %
(n=6)</td><td>0 %
(n=12)</td></tr>
</table>

Table 3.3: Percentage of fibrils in CDE and SDF samples at different stages of the experiment displaying a flattened adhesion pattern in the overlap region.

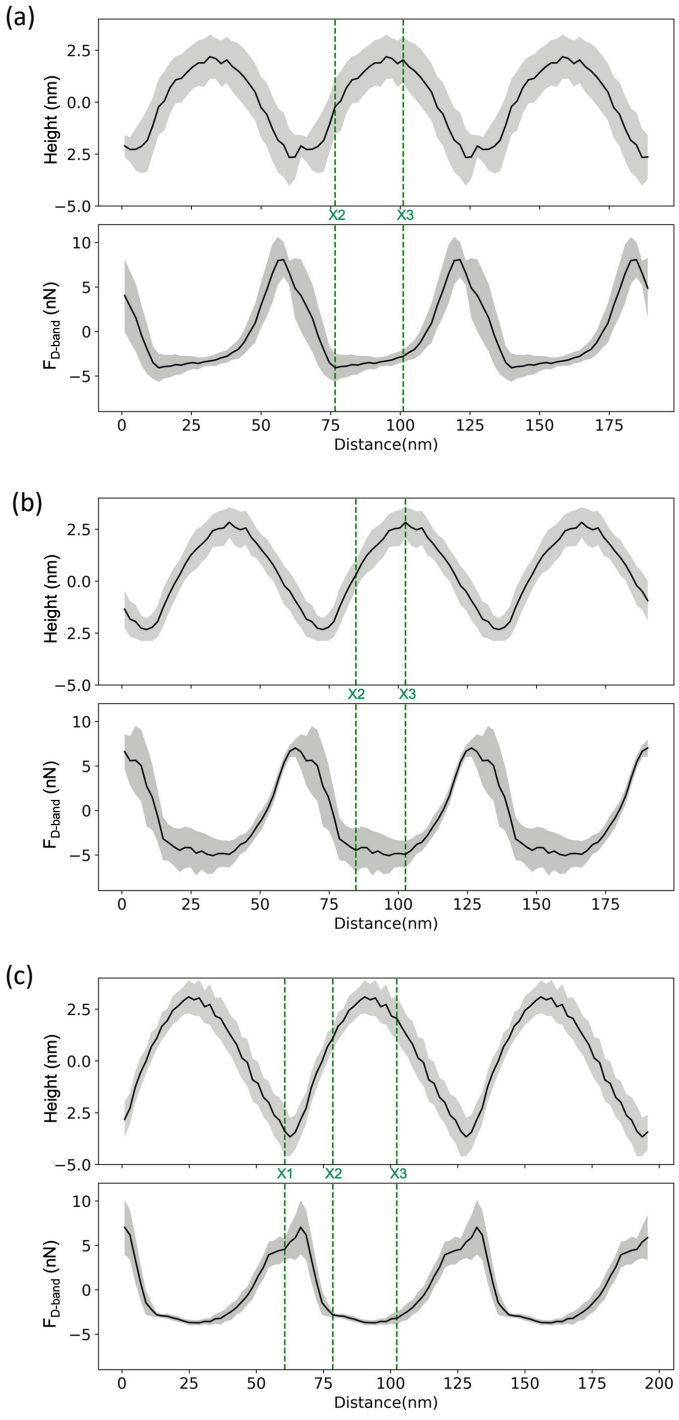

Figure 3.17: Flattened adhesion features in the overlap region observed in fibrils in ribose treated CDE sections at different stages *(a) After 1 week (b) After 2 weeks (c) After 3 weeks The tall peak in adhesion generally visible in the overlap region is consistently diminished*

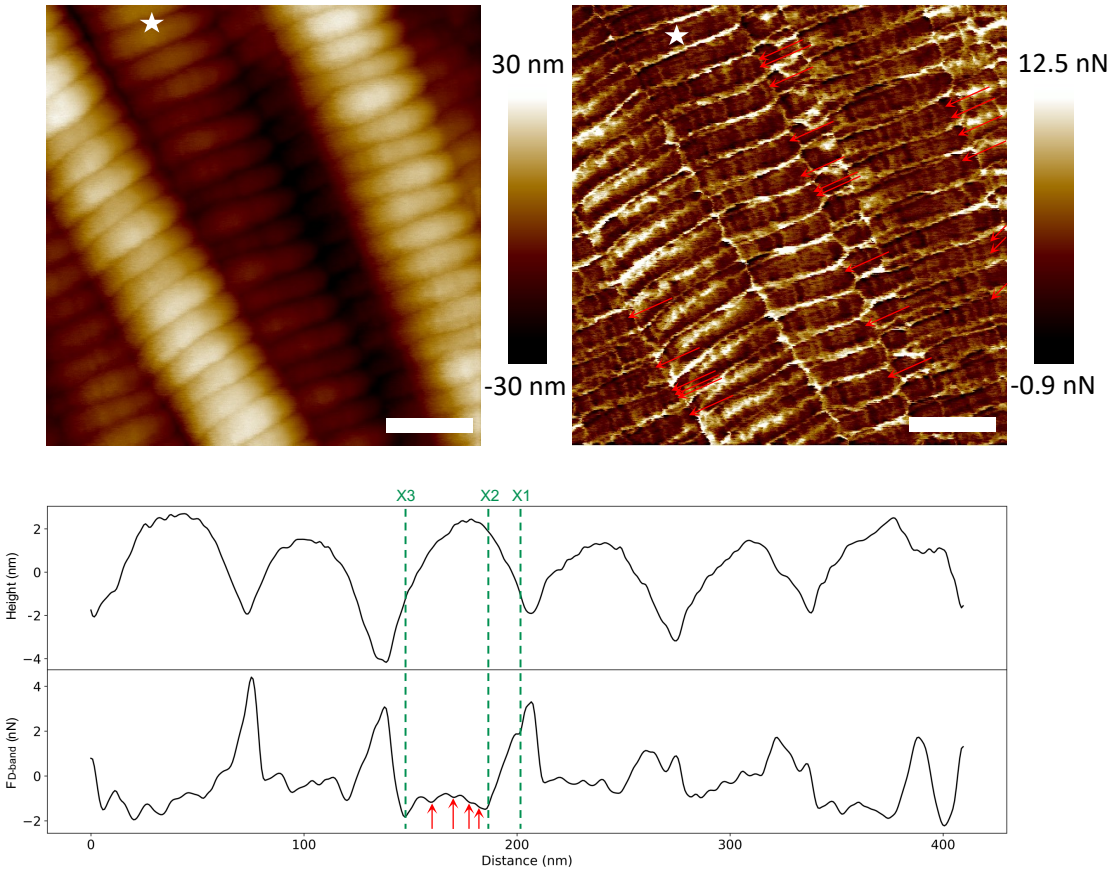

Figure 3.18: Sub-D-band features visible in Height (left) and Adhesion (right) images, and corresponding filtered profiles from a fibril (marked by star) from a CDE section treated with ribose for 2 weeks (group B, Figure 3.13) Thin lines of low adhesion (marked by red arrows) are seen in the adhesion image, that are also apparent in the filtered profiles, which may be due to the accumulation of AGEs on the fibril. *Scale=200 nm*

sub-D-band features was similar to the week 2 sample, with a few differences. Unlike the control and the week 2 ribose sample, the visibility and the strength of the X1 band were higher. In some fibrils, all three bands were distinctly visible. Like the other two ribose samples, this one also showed instances of flattened adhesion pattern in the overlap region, observed in about 32% of the fibrils (Table 3.3, Figure 3.17c)

3.3.2.2 SDF

After a week of incubation in ribose, fibrils in the SDF section showed no significant change in the mean adhesion as compared to the fibrils in the untreated section, with a greater variability amongst the fibrils.(Figure 3.15a) However, as compared to that of the

control sample, the mean adhesion was significantly lower, with an equal variability across the sample. The overlap-gap adhesion contrast for the ribose sample was similar to that of the untreated sample but was significantly greater as compared to the control sample.(Figure 3.15b) In terms of qualitative differences in the height and adhesion profiles, however, between the ribose sample and the untreated or control sample, there were none apparent. (Table 3.2; Figure 3.10b, 3.16, 3.19a)

After 2 weeks, the mean adhesion of the ribose sample was significantly higher than the week 1 sample, with greater variation across the sample.(Figure 3.15a) As compared to the control sample, the mean adhesion of the ribose sample did not have a significant difference due to the large variation observed in the control sample. The overlap-gap adhesion contrast displayed a large variation across the ribose sample, and therefore, there was no significant difference in the overlap-adhesion contrast of the ribose sample from either the week 1 sample, or the control sample. (Figure 3.15b) Moreover, the ribose sample did not show any prominent differences in the height and adhesion profiles from the week 1 sample. (Figure 3.19b)

After week 3 of the experiment, the mean adhesion values across the sample exhibited a bimodal distribution and were divided into two separate groups, A and B. (Figure 3.15a) Similar to the bimodality observed in CDE after 2 weeks, the group with higher adhesion, group A, consisted of fibrils only from one image. Like the trend observed in the previous week, the mean adhesion of both groups was significantly higher than that of the ribose sample after 2 weeks of incubation.(Figure 3.15a) For the overlap-gap adhesion contrast, a higher average value and a greater variability in the week 3 ribose sample than that of the week 2 ribose sample were observed.(Figure 3.15b) The visibility of the sub-D-band features in the height and adhesion profiles again did not show a significant change from the previous observations. (Figure 3.19c) There were, however, some cases in fibrils of group A (33%), where the adhesion pattern in the overlap region was flattened, just as observed in the CDE ribose samples (Table 3.3, Figure 3.17). In the absence of data for the 3 weeks control sample, a detailed analysis of the ribose effect after 3 weeks could not be completed.

3.3.2.3 Mean adhesion values do not align with expected results

There have been multiple studies using different techniques to observe the effect of glycation on collagen fibrils. Bansode et. al observed a decrease in the surface potential of the

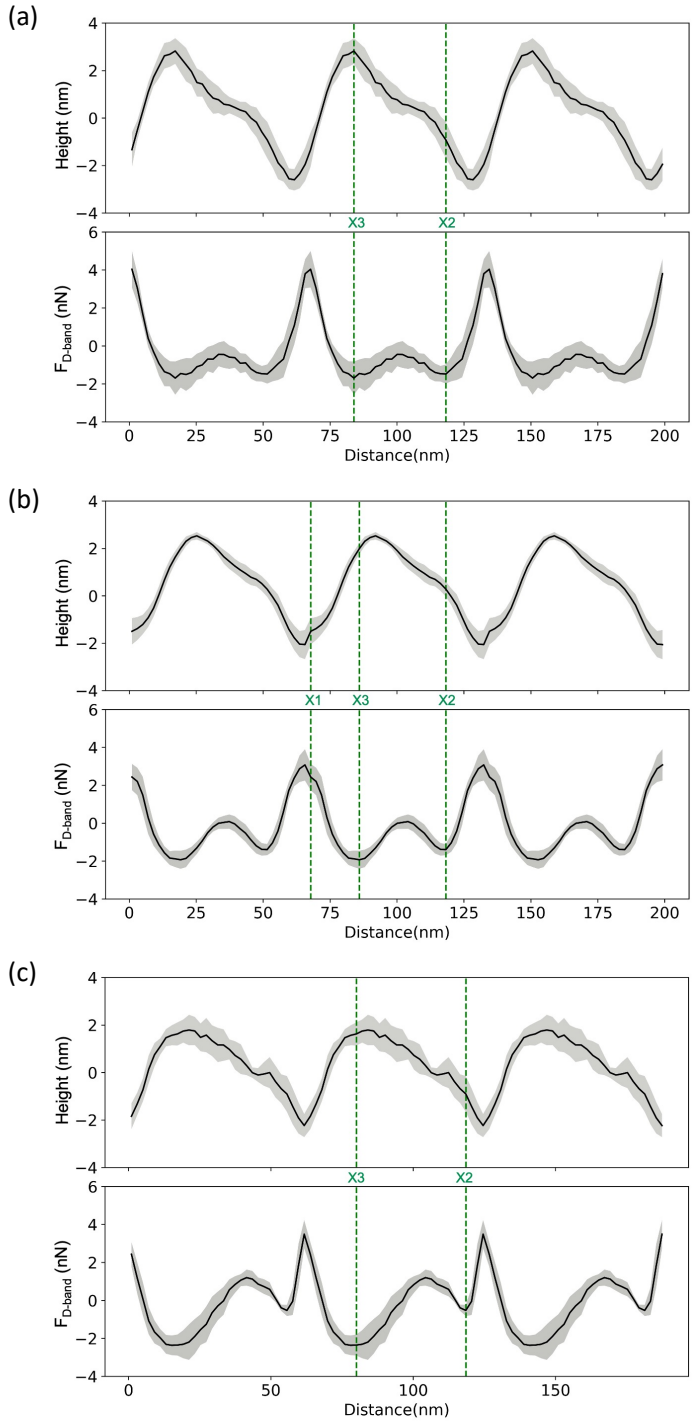

Figure 3.19: Height and corresponding adhesion profiles from fibrils in SDF section after (a) 1 week, (b) 2 weeks, and (c) 3 weeks of incubation in ribose. *The X2 and X3 bands are clearly visible in all fibrils, with features typically observed in SDF fibrils.*

fibrils after ribose-5-phosphate (R5P) glycation using KPFM, therefore stating that the fibril becomes more negatively-charged as a result of glycation.[55] They did not observe the change in surface potential being larger in the overlap than the gap or vice-versa, thus displaying equal lowering of surface potential in both regions. Following the idea of a negatively-charged tip, if the fibril becomes more negative overall, the mean adhesion should decrease.

In our results, however, we did not observe the mean adhesion of the fibrils lowering as a function of incubation time in ribose. In the CDE case, while the mean adhesion of the fibrils did decrease after 1 week of incubation in ribose, the same was observed for the control sample as well. The SDF samples seem to be showing a trend of increase in both the average mean adhesion value of the sample and the variation in that value observed across the sample as the incubation time with ribose increased. However, since the mean adhesion of the ribose samples and PBS-treated control samples do not always have a significant difference, and the data from the control sample after 3 weeks is absent, it is unclear what is governing this rise in mean adhesion.

There are multiple factors which can be responsible for this discrepancy between the expected and observed results.

First, the changes in mean adhesion measured in the ribose samples is not due to ribose alone but also influenced by the unknown effect of PBS.

Second, there is also a possibility of surface degradation caused by the microbial activity. As explained in section 3.1, the adhesion force measured by AFM is influenced by multiple forces. While it is likely that the electrostatic force between the tip and the surface is the primary factor modulating the adhesion force in our system, the adhesion force is still extremely sensitive to nanoscale changes on the surface and tip. Degradation of the surface and a resultant accumulation of material on the tip can introduce frictional interactions or change the effective contact area between the tip and the surface which can impact the adhesion force measurements.

Third, we also suspect that the effect of ribose is not uniform throughout the tendon section or along the length of the fibril. This is because there is a variation in heterogeneous crosslink density along the length of collagen fibrils.[95, 121] A tendon section used in the experiment can have surface area over 7 orders of magnitude larger than that of the four to five 1 μm images acquired from it. This fact along with a possible uneven effect of

ribose means it may be that the data acquired is insufficient for an unbiased analysis. This may be the reason behind the large variation in mean adhesion values in many samples. These factors can also explain why in the bimodal distribution in the mean adhesion values observed in the CDE and SDF ribose samples at week 2 and week 3, respectively, the more adhesive group, A, only consisted of fibrils only from a single image.

3.3.2.4 Qualitative features indicate accumulation of AGEs on the fibrils at previously observed sites

Using SAXS, Caro et. al created electron density maps that show the sites for glycation in one D-band along the fibril.[46] While the sites are present in both the overlap and gap regions, the likelihood for glycation is larger in the overlap than in the gap region. Since the results from the KPFM study show an overall decrease in the surface potential of the fibril as a result of glycation,[55] the binding of Advanced Glycation End-products (AGEs) is expected to result in localised dips in adhesion at the sites described by Caro et. al. A similar effect is observed in our data.

In the CDE case, the ribose samples from all three weeks display a flattening of the adhesion pattern in the overlap region, where it appears that a dip has been superimposed on the tall peak in adhesion usually seen between the dips of the X2 and X3 bands, thus resulting in either in multiple small peaks at its position or a totally flat adhesion with no peaks.(Table 3.3, Figure 3.17, 3.18) An accumulation of AGEs is also expected in the gap region, albeit lower than seen in the overlap. However, it was only at week 3 of the experiment that the ribose sample displayed some changes in the gap region, where the visibility of the X1 band in adhesion was more frequent than the corresponding control sample and the previous ribose samples. A possible explanation for this observation is that the AGEs accumulate at or near the position of the X1 band in the gap, thus increasing its strength. Moreover, the fact that the overlap-gap adhesion was higher in the ribose samples as compared to the respective control samples also shows that one of the regions is getting more affected due to glycation than the other, which, from the qualitative results, appears to be the overlap region. And since the gap region also showed prominent changes in week 3, unlike the previous samples, the overlap-gap adhesion contrast for this ribose sample was not significantly different from the control sample.

Contrary to CDE, SDF did not display a significant alteration in the qualitative features

observed in the height and adhesion profiles upon incubation with ribose until week 3. The ribose-treated SDF sample at week 3 displayed instances of flattened adhesion pattern in the overlap that were previously observed in CDE at week 2. Although these instances were rare (Table 3.3), it appears that it was after 3 weeks that the effect of ribose started to become apparent in SDF. There may be three reasons for this delay.

First, SDF has a higher intermolecular crosslink density compared to CDE.[104] Since glycation causes the molecular packing to expand in collagen fibrils by generating intermolecular crosslinks,[57] the higher number of pre-existing crosslinks in SDF might impede this process, resulting in the impression of a delayed effect.

Second, the surface of SDF fibrils has a higher amount of proteoglycans compared to CDE fibrils. If proteoglycans cause the binding sites for glycation to become inaccessible, then it is likely that SDF fibrils will be less affected by ribose compared to CDE fibrils.

Third, the effect of PBS was negligible on SDF fibrils.(Table 3.2) Consequently, if PBS is accountable for the removal of the proteoglycans and thus augmenting the effect of ribose, it is plausible that lack of influence from PBS could impact the efficacy of ribose. Finally, considering the signs of fungal or bacterial degradation in the samples, the effect of ribose may have been modified due to such microbial activity.

Chapter 4

Conclusion

4.1 Summary of main results

In this study, we investigated the modulation of adhesion force measured between an AFM tip and collagen fibrils and discussed how various interactions may affect this force to demonstrate that adhesion force microscopy is likely sensitive to the presence of charges implanted at the surface of a material even in the absence of an applied voltage. Taking advantage of the periodic nature of the fibril surface, we also reveal subtle differences in fibril architecture and possibly surface charge distribution for *in vitro* and *in vivo* assembled fibrils.

We also examined the impact of glycation on fibrils in tendon sections and explored the potential use of adhesion force microscopy to detect these changes. Our observations revealed significant differences between the extensor fibrils in tendon sections and the extracted fibrils, which we attribute to the removal of surface-bound material during the mechanical extraction process. This distinction was not observed in flexor fibrils. Additionally, we demonstrated that long-term incubation in PBS can potentially lead to surface changes in the fibrils. Furthermore, our findings indicated that ribose-induced glycation affects extensor and flexor fibrils in tendon sections differently. The accumulation of advanced glycation end products (AGEs) at documented binding sites was evident in the extensor fibrils from the first week of the experiment, while in flexor fibrils, this accumulation was observed only in the third week and on fewer fibrils.

4.2 Addressing the initial hypotheses

The study was performed to verify the two hypotheses mentioned at the start. The outcomes provide a deeper understanding of the factors involved in adhesion force microscopy, potential uses of the technique, and also its limitations. While there are certain conflicting observations that need further exploration to fully understand, these results do validate the

hypotheses, as discussed below.

4.2.1 Is adhesion force microscopy sensitive to surface charge distribution along a single collagen fibril?

This hypothesis holds true due to three main reasons. First, the fact that KPFM has showed that overlap (gap) is negatively (positively) charged, and this is in line with our results. Second, the three major electron dense bands (X1, X2 and X3) and some of the other negatively-charged minor bands (a, b, c, d, and e) mapped by TEM are visible as dips in the adhesion profiles. Third, forces other than the electrostatic force governing the adhesion force (Van der Waal's and Capillary force) cannot explain these results.

There are different ways to corroborate this technique further which could not be performed due to time limitations. These include measurement of adhesion force in the presence of an applied voltage on the sample or as a function of pH, since the surface charge distribution is known to change with pH.[34]

4.2.2 Can adhesion force microscopy detect glycation induced changes at the collagen fibril surface?

As a result of glycation, it was expected that the surface of the fibril would get more negatively-charged and this should therefore make the fibrils less adhesive. Such an effect was not observed in our results. As explained earlier, this can be due to multiple factors related to the unexpected effect of PBS, degradation of samples or a potential uneven impact of ribose throughout the tendon. We believe that one or more of these factors contributed to the changes observed in mean adhesion of samples and therefore, the effect of ribose alone could not be ascertained quantitatively. A study to understand or eliminate the effects of other agents first could lead to an unbiased quantitative analysis. Nevertheless, another expected result was that the accumulation of AGEs would lead to dips in adhesion near the proposed glycation sites. This observation holds true, especially for the extensor samples. This qualitative result is important to consider since it was exclusive to the ribose-treated samples. Therefore, even under the influence of the aforementioned factors, the adhesion force was able to reflect the changes induced at the surface due to glycation and hence, we believe that the hypothesis is correct.

4.3 Applications and future directions

The applications of this technique and/or some of the possible next steps are as follows:

1. Following this study, different experiments, like mentioned earlier, can be performed to further understand the contribution of electrostatic interactions on adhesion force measured by the AFM. For example, the capillary force, while not the primary contributor in modulating the adhesion force, still does affect it. Hence, an independent experiment to study the adhesion force as a function of humidity can also be performed to determine the effect of capillary force on adhesion. Understanding the true effect of electrostatic forces alone on adhesion would yield a novel way to accurately map the charge distribution on a surface, with a resolution of less than 10 nm.

2. In principle, our approach can also be applied towards characterizing changes in surface charge distribution induced due to other phenomena, like the binding of proteins such as decorin. Another example is mechanical exploitation, such as strain, which has been shown to alter the charge profile of collagen fibrils.[32] Using this technique, these changes in surface charges can be visualized at a higher resolution.

3. This technique also breaks new ground in the measurement of charges distribution on other solid surfaces of materials such as polymers or polyelectrolytes.

4. Since our results suggest that the long-term incubation of tendons in PBS may change the fibrils surface, an independent study can be performed to understand this effect. However, it is recommended that as a way to limit microbial activity, measures be taken, such as increasing the concentration of antimycotic solution or incubating individual tendon samples in separate containers.

5. Moreover, following this study, the effect of glycation can be investigated on extracted fibrils, *in vitro* assembled fibrils or even single collagen molecules. This can help understand the impact of glycation on fibrils in the absence of the bound non-collagenous material.

6. As the results show that the effect of glycation can differ between extensor and flexor fibrils, this discrepancy can be explored further with other techniques, such as the study performed by Tanaka and co-workers using X-ray diffraction.[57]

Bibliography

[1] I. Tresoldi, F. Oliva, M. Benvenuto, M. Fantini, L. Masuelli, R. Bei, and A. Modesti, "Tendon's ultrastructure," *Muscles, ligaments and tendons journal*, vol. 3, no. 1, p. 2, 2013.

[2] J. Gosline, M. Lillie, E. Carrington, P. Guerette, C. Ortlepp, and K. Savage, "Elastic proteins: biological roles and mechanical properties," *Philosophical Transactions of the Royal Society of London. Series B: Biological Sciences*, vol. 357, no. 1418, pp. 121–132, 2002.

[3] S. Rauscher and R. Pomès, "Structural disorder and protein elasticity," *Fuzziness: Structural Disorder in Protein Complexes*, pp. 159–183, 2012.

[4] G. S. Schultz, G. A. Chin, L. Moldawer, and R. F. Diegelmann, "23 principles of wound healing," *Mechanisms of vascular disease: a reference book for vascular specialists*, p. 423, 2011.

[5] M. D. Shoulders and R. T. Raines, "Collagen structure and stability," *Annual review of biochemistry*, vol. 78, pp. 929–958, 2009.

[6] S. Bandyopadhyay-Ghosh, "Bone as a collagen-hydroxyapatite composite and its repair," *Trends in Biomaterials and Artificial Organs*, vol. 22, no. 2, pp. 112–121, 2008.

[7] S. V. Sandhu, S. Gupta, H. Bansal, and K. Singla, "Collagen in health and disease," *Journal of Orofacial research*, pp. 153–159, 2012.

[8] R. Parenteau-Bareil, R. Gauvin, and F. Berthod, "Collagen-based biomaterials for tissue engineering applications," *Materials*, vol. 3, no. 3, pp. 1863–1887, 2010.

[9] E. G. Canty and K. E. Kadler, "Procollagen trafficking, processing and fibrillogenesis," *Journal of cell science*, vol. 118, no. 7, pp. 1341–1353, 2005.

[10] R. A. Gjaltema and R. A. Bank, "Molecular insights into prolyl and lysyl hydroxylation of fibrillar collagens in health and disease," *Critical reviews in biochemistry and molecular biology*, vol. 52, no. 1, pp. 74–95, 2017.

[11] E. G. Canty-Laird, Y. Lu, and K. E. Kadler, "Stepwise proteolytic activation of type I procollagen to collagen within the secretory pathway of tendon fibroblasts in situ," *Biochemical journal*, vol. 441, no. 2, pp. 707–717, 2012.

[12] G. N. Ramachandran and G. Kartha, "Structure of collagen," *Nature*, vol. 174, pp. 269–270, 1954.

[13] J. A. Petruska and A. J. Hodge, "A subunit model for the tropocollagen macromolecule," *Proceedings of the National Academy of Sciences*, vol. 51, no. 5, pp. 871–876, 1964.

[14] A. Ellingson, N. Pancheri, and N. Schiele, "Regulators of collagen crosslinking in developing and adult tendons," *Eur. Cell. Mater*, vol. 43, pp. 130–152, 2022.

[15] D. R. Eyre, M. A. Paz, and P. M. Gallop, "Cross-linking in collagen and elastin," *Annual review of biochemistry*, vol. 53, no. 1, pp. 717–748, 1984.

[16] G. Wood and M. K. Keech, "The formation of fibrils from collagen solutions 1. the effect of experimental conditions: kinetic and electron-microscope studies," *Biochemical Journal*, vol. 75, no. 3, p. 588, 1960.

[17] J. R. Harris, A. Soliakov, and R. J. Lewis, "In vitro fibrillogenesis of collagen type I in varying ionic and pH conditions," *Micron*, vol. 49, pp. 60–68, 2013.

[18] G. Mosser, A. Anglo, C. Helary, Y. Bouligand, and M.-M. Giraud-Guille, "Dense tissue-like collagen matrices formed in cell-free conditions," *Matrix Biology*, vol. 25, no. 1, pp. 3–13, 2006.

[19] D. Holmes, M. Capaldi, and J. Chapman, "Reconstitution of collagen fibrils in vitro; the assembly process depends on the initiating procedure," *International Journal of Biological Macromolecules*, vol. 8, no. 3, pp. 161–166, 1986.

[20] M. J. Capaldi and J. A. Chapman, "The C-terminal extrahelical peptide of type I collagen and its role in fibrillogenesis in vitro," *Biopolymers: Original Research on Biomolecules*, vol. 21, no. 11, pp. 2291–2313, 1982.

[21] V. C. Chan, J. A. Ramshaw, A. Kirkpatrick, K. Beck, and B. Brodsky, "Positional preferences of ionizable residues in Gly-X-Y triplets of the collagen triple-helix," *Journal of Biological Chemistry*, vol. 272, no. 50, pp. 31441–31446, 1997.

[22] J. H. Bowes and R. Kenten, "The effect of alkalis on collagen," *Biochemical Journal*, vol. 43, no. 3, p. 365, 1948.

[23] J. Heino, "The collagen family members as cell adhesion proteins," *Bioessays*, vol. 29, no. 10, pp. 1001–1010, 2007.

[24] S. V. Plotnikov, A. M. Pasapera, B. Sabass, and C. M. Waterman, "Force fluctuations within focal adhesions mediate ECM-rigidity sensing to guide directed cell migration," *Cell*, vol. 151, no. 7, pp. 1513–1527, 2012.

[25] K. Poole, K. Khairy, J. Friedrichs, C. Franz, D. A. Cisneros, J. Howard, and D. Mueller, "Molecular-scale topographic cues induce the orientation and directional movement of fibroblasts on two-dimensional collagen surfaces," *Journal of molecular biology*, vol. 349, no. 2, pp. 380–386, 2005.

[26] H.-Y. Chang, C.-C. Huang, K.-Y. Lin, W.-L. Kao, H.-Y. Liao, Y.-W. You, J.-H. Lin, Y.-T. Kuo, D.-Y. Kuo, and J.-J. Shyue, "Effect of surface potential on NIH_3T_3 cell adhesion and proliferation," *The Journal of Physical Chemistry C*, vol. 118, no. 26, pp. 14464–14470, 2014.

[27] H.-Y. Chang, W.-L. Kao, Y.-W. You, Y.-H. Chu, K.-J. Chu, P.-J. Chen, C.-Y. Wu, Y.-H. Lee, and J.-J. Shyue, "Effect of surface potential on epithelial cell adhesion, proliferation and morphology," *Colloids and Surfaces B: Biointerfaces*, vol. 141, pp. 179–186, 2016.

[28] E. Fukada and I. Yasuda, "Piezoelectric effects in collagen," *Japanese Journal of Applied Physics*, vol. 3, no. 2, p. 117, 1964.

[29] M. Minary-Jolandan and M.-F. Yu, "Nanoscale characterization of isolated individual type I collagen fibrils: polarization and piezoelectricity," *Nanotechnology*, vol. 20, no. 8, p. 085706, 2009.

[30] C. Halperin, S. Mutchnik, A. Agronin, M. Molotskii, P. Urenski, M. Salai, and G. Rosenman, "Piezoelectric effect in human bones studied in nanometer scale," *Nano Letters*, vol. 4, no. 7, pp. 1253–1256, 2004.

[31] M. Nair, Y. Calahorra, S. Kar-Narayan, S. M. Best, and R. E. Cameron, "Self-assembly of collagen bundles and enhanced piezoelectricity induced by chemical crosslinking," *Nanoscale*, vol. 11, no. 32, pp. 15120–15130, 2019.

[32] E. Gachon and P. Mesquida, "Mechanical strain alters the surface charge of collagen fibrils," *ACS nano*, vol. 15, no. 6, pp. 9820–9826, 2021.

[33] A. Gautieri, S. Uzel, S. Vesentini, A. Redaelli, and M. J. Buehler, "Molecular and mesoscale mechanisms of osteogenesis imperfecta disease in collagen fibrils," *Biophysical Journal*, vol. 97, no. 3, pp. 857–865, 2009.

[34] A. D. Stone and P. Mesquida, "Kelvin-probe force microscopy of the pH-dependent charge of functional groups," *Applied Physics Letters*, vol. 108, no. 23, p. 233702, 2016.

[35] J. Muschler and C. H. Streuli, "Cell–matrix interactions in mammary gland development and breast cancer," *Cold Spring Harbor perspectives in biology*, vol. 2, no. 10, p. a003202, 2010.

[36] R. D. Semba, E. J. Nicklett, and L. Ferrucci, "Does accumulation of advanced glycation end products contribute to the aging phenotype?," *Journals of Gerontology Series A: Biomedical Sciences and Medical Sciences*, vol. 65, no. 9, pp. 963–975, 2010.

[37] R. G. PAUL, C. N. AVERY, A. D. SLATTER, J. T. SIMS, and J. A. BAILEY, "Isolation and characterization of advanced glycation end products derived from the in vitro reaction of ribose and collagen," *Biochemical Journal*, vol. 330, no. 3, pp. 1241–1248, 1998.

[38] R. Singh, A. Barden, T. Mori, and L. Beilin, "Advanced glycation end-products: a review," *Diabetologia*, vol. 44, pp. 129–146, 2001.

[39] N. Ahmed and P. Thornalley, "Advanced glycation end-products: what is their relevance to diabetic complications?," *Diabetes, Obesity and Metabolism*, vol. 9, no. 3, pp. 233–245, 2007.

[40] P. T. Bullock, D. G. Reid, W. Ying Chow, W. P. Lau, and M. J. Duer, "A new glycation product 'norpronyl-lysine,'and direct characterization of cross linking and other glycation adducts: NMR of model compounds and collagen," *Bioscience reports*, vol. 34, no. 2, 2014.

[41] A. Munanairi, S. K. O'Banion, R. Gamble, E. Breuer, A. W. Harris, and R. K. Sandwick, "The multiple Maillard reactions of ribose and deoxyribose sugars and sugar phosphates," *Carbohydrate research*, vol. 342, no. 17, pp. 2575–2592, 2007.

[42] P. J. Thornalley, A. Langborg, and H. S. Minhas, "Formation of glyoxal, methylglyoxal and 3-deoxyglucosone in the glycation of proteins by glucose," *Biochemical Journal*, vol. 344, no. 1, pp. 109–116, 1999.

[43] F. Ledl, "Chemical pathways of the Maillard reaction," *The Maillard reaction in food processing, human nutrition and physiology*, vol. 4, 1990.

[44] S. Grandhee and V. Monnier, "Mechanism of formation of the Maillard protein cross-link pentosidine. glucose, fructose, and ascorbate as pentosidine precursors," *Journal of Biological Chemistry*, vol. 266, no. 18, pp. 11649–11653, 1991.

[45] D. R. Sell, K. M. Biemel, O. Reihl, M. O. Lederer, C. M. Strauch, and V. M. Monnier, "Glucosepane is a major protein cross-link of the senescent human extracellular matrix: relationship with diabetes," *Journal of Biological Chemistry*, vol. 280, no. 13, pp. 12310–12315, 2005.

[46] L. De Caro, A. Terzi, L. Fusaro, D. Altamura, F. Boccafoschi, O. Bunk, and C. Giannini, "Time scale of glycation in collagen of bovine pericardium-derived bio-tissues," *IUCrJ*, vol. 8, no. 6, pp. 1024–1034, 2021.

[47] A. Gautieri, A. Redaelli, M. J. Buehler, and S. Vesentini, "Age-and diabetes-related nonenzymatic crosslinks in collagen fibrils: candidate amino acids involved in advanced glycation end-products," *Matrix Biology*, vol. 34, pp. 89–95, 2014.

[48] D. M. Hudson, M. Archer, K. B. King, and D. R. Eyre, "Glycation of type I collagen selectively targets the same helical domain lysine sites as lysyl oxidase–mediated cross-linking," *Journal of Biological Chemistry*, vol. 293, no. 40, pp. 15620–15627, 2018.

[49] J. A. Chapman, M. Tzaphlidou, K. M. Meek, and K. E. Kadler, "The collagen fibril—a model system for studying the staining and fixation of a protein," *Electron microscopy reviews*, vol. 3, no. 1, pp. 143–182, 1990.

[50] B. B. Doyle, D. W. Hukins, D. J. Hulmes, A. Miller, C. J. Rattew, and J. Woodhead-Galloway, "Origins and implications of the D stagger in collagen," *Biochemical and biophysical research communications*, vol. 60, no. 2, pp. 858–864, 1974.

[51] S. Morozova and M. Muthukumar, "Electrostatic effects in collagen fibril formation," *The Journal of chemical physics*, vol. 149, no. 16, p. 163333, 2018.

[52] D. J. Hulmes and A. Miller, "Quasi-hexagonal molecular packing in collagen fibrils," *Nature*, vol. 282, no. 5741, pp. 878–880, 1979.

[53] R. Li, R. Rajan, W. Wong, D. Reid, M. Duer, V. Somovilla, N. Martinez-Saez, G. Bernardes, R. Hayward, and C. Shanahan, "In situ characterization of advanced glycation end products (AGEs) in collagen and model extracellular matrix by solid state NMR," *Chemical Communications*, vol. 53, no. 100, pp. 13316–13319, 2017.

[54] K. L. Reigle, G. Di Lullo, K. R. Turner, J. A. Last, I. Chervoneva, D. E. Birk, J. L. Funderburgh, E. Elrod, M. W. Germann, C. Surber, *et al.*, "Non-enzymatic glycation of type I collagen diminishes collagen–proteoglycan binding and weakens cell adhesion," *Journal of cellular biochemistry*, vol. 104, no. 5, pp. 1684–1698, 2008.

[55] S. Bansode, U. Bashtanova, R. Li, J. Clark, K. H. Müller, A. Puszkarska, I. Goldberga, H. H. Chetwood, D. G. Reid, L. J. Colwell, *et al.*, "Glycation changes molecular organization and charge distribution in type I collagen fibrils," *Scientific reports*, vol. 10, no. 1, pp. 1–13, 2020.

[56] G. J. Hildick-Smith, M. C. Downey, L. M. Gretebeck, R. A. Gersten, and R. K. Sandwick, "Ribose 5-phosphate glycation reduces cytochrome C respiratory activity and membrane affinity," *Biochemistry*, vol. 50, no. 51, pp. 11047–11057, 2011.

[57] S. Tanaka, G. Avigad, B. Brodsky, and E. F. Eikenberry, "Glycation induces expansion of the molecular packing of collagen," *Journal of molecular biology*, vol. 203, no. 2, pp. 495–505, 1988.

[58] T. T. Andreassen, H. Oxlund, and C. C. Danielsen, "The influence of non-enzymatic glycosylation and formation of fluorescent reaction products on the mechanical properties of rat tail tendons," *Connective tissue research*, vol. 17, no. 1, pp. 1–9, 1988.

[59] A. Galeski, J. Kastelic, E. Baer, and R. Kohn, "Mechanical and structural changes in rat tail tendon induced by alloxan diabetes and aging," *Journal of biomechanics*, vol. 10, no. 11-12, pp. 775–782, 1977.

[60] A. J. Fox, A. Bedi, X.-H. Deng, L. Ying, P. E. Harris, R. F. Warren, and S. A. Rodeo, "Diabetes Mellitus alters the mechanical properties of the native tendon in an experimental rat model," *Journal of Orthopaedic Research*, vol. 29, no. 6, pp. 880–885, 2011.

[61] G. K. Reddy, L. Stehno-Bittel, and C. S. Enwemeka, "Glycation-induced matrix stability in the rabbit achilles tendon," *Archives of biochemistry and biophysics*, vol. 399, no. 2, pp. 174–180, 2002.

[62] G. K. Reddy, "Cross-linking in collagen by nonenzymatic glycation increases the matrix stiffness in rabbit achilles tendon," *Experimental diabesity research*, vol. 5, no. 2, pp. 143–153, 2004.

[63] N. Avery and A. Bailey, "Enzymic and non-enzymic cross-linking mechanisms in relation to turnover of collagen: relevance to aging and exercise," *Scandinavian journal of medicine & science in sports*, vol. 15, no. 4, pp. 231–240, 2005.

[64] N. Avery and A. Bailey, "Restraining cross-links responsible for the mechanical properties of collagen fibers: natural and artificial," *Collagen: structure and mechanics*, pp. 81–110, 2008.

[65] S. J. Zieman and D. A. Kass, "Advanced glycation end-product crosslinking in the cardiovascular system: potential therapeutic target for cardiovascular disease," *Drugs*, vol. 64, pp. 459–470, 2004.

[66] S. McLennan, D. Yue, M. Marsh, B. Swanson, L. Delbridge, T. Reeve, and J. Turtle, "The prevention and reversibility of tissue non-enzymatic glycosylation in diabetes," *Diabetic medicine*, vol. 3, no. 2, pp. 141–146, 1986.

[67] B. K. Connizzo, P. R. Bhatt, K. W. Liechty, and L. J. Soslowsky, "Diabetes alters mechanical properties and collagen fiber re-alignment in multiple mouse tendons," *Annals of biomedical engineering*, vol. 42, pp. 1880–1888, 2014.

[68] N. Ahmed, "Advanced glycation end-products—role in pathology of diabetic complications," *Diabetes research and clinical practice*, vol. 67, no. 1, pp. 3–21, 2005.

[69] J. W. Baynes, "The role of AGEs in aging: causation or correlation," *Experimental gerontology*, vol. 36, no. 9, pp. 1527–1537, 2001.

[70] V. P. Reddy, X. Zhu, G. Perry, and M. A. Smith, "Oxidative stress in diabetes and alzheimer's disease," *Journal of Alzheimer's Disease*, vol. 16, no. 4, pp. 763–774, 2009.

[71] S. F. Yan, R. Ramasamy, Y. Naka, and A. M. Schmidt, "Glycation, inflammation, and RAGE: a scaffold for the macrovascular complications of diabetes and beyond," *Circulation research*, vol. 93, no. 12, pp. 1159–1169, 2003.

[72] J. K. Buchanan, Y. Zhang, G. Holmes, A. D. Covington, and S. Prabakar, "Role of x-ray scattering techniques in understanding the collagen structure of leather," *ChemistrySelect*, vol. 4, no. 48, pp. 14091–14102, 2019.

[73] J. P. Orgel, T. C. Irving, A. Miller, and T. J. Wess, "Microfibrillar structure of type I collagen in situ," *Proceedings of the National Academy of Sciences*, vol. 103, no. 24, pp. 9001–9005, 2006.

[74] P. Frederik, M. Stuart, P. Bomans, W. Busing, K. Burger, and A. Verkleij, "Perspective and limitations of cryo-electron microscopy: From model systems to biological specimens," *Journal of microscopy*, vol. 161, no. 2, pp. 253–262, 1991.

[75] B. D. Quan and E. D. Sone, "Structural changes in collagen fibrils across a mineralized interface revealed by cryo-TEM," *Bone*, vol. 77, pp. 42–49, 2015.

[76] M. Marchini, M. Morocutti, P. Castellani, L. Leonardi, and A. Ruggeri, "The banding pattern of rat tail tendon freeze-etched collagen fibril," *Connective tissue research*, vol. 11, no. 2-3, pp. 175–184, 1983.

[77] J. Zhu, C. L. Hoop, D. A. Case, and J. Baum, "Cryptic binding sites become accessible through surface reconstruction of the type I collagen fibril," *Scientific reports*, vol. 8, no. 1, pp. 1–12, 2018.

[78] M. Griepentrog, G. Krämer, and B. Cappella, "Comparison of nanoindentation and AFM methods for the determination of mechanical properties of polymers," *Polymer testing*, vol. 32, no. 3, pp. 455–460, 2013.

[79] L.-Z. Cheong, W. Zhao, S. Song, and C. Shen, "Lab on a tip: Applications of functional Atomic Force Microscopy for the study of electrical properties in biology," *Acta Biomaterialia*, vol. 99, pp. 33–52, 2019.

[80] O. Vatel and M. Tanimoto, "Kelvin Probe Force Microscopy for potential distribution measurement of semiconductor devices," *Journal of applied physics*, vol. 77, no. 6, pp. 2358–2362, 1995.

[81] D. S. Jakob, H. Wang, and X. G. Xu, "Pulsed force Kelvin Probe Force Microscopy," *ACS nano*, vol. 14, no. 4, pp. 4839–4848, 2020.

[82] J. Lyklema, "Fundamentals of interface and colloid science: soft colloids," *Elsevier*, vol. 5, 2005.

[83] J. Lyklema, "Surface charges and Electrokinetic charges: Distinctions and juxtapositionings," *Colloids and Surfaces A: Physicochemical and Engineering Aspects*, vol. 376, no. 1-3, pp. 2–8, 2011.

[84] A. Trache and G. A. Meininger, "Atomic Force Microscopy (AFM)," *Current protocols in microbiology*, vol. 8, no. 1, pp. 2C–2, 2008.

[85] J. Friedrichs, K. R. Legate, R. Schubert, M. Bharadwaj, C. Werner, D. J. Müller, and M. Benoit, "A practical guide to quantify cell adhesion using single-cell force spectroscopy," *Methods*, vol. 60, no. 2, pp. 169–178, 2013.

[86] P.-H. Puech, K. Poole, D. Knebel, and D. J. Muller, "A new technical approach to quantify cell–cell adhesion forces by AFM," *Ultramicroscopy*, vol. 106, no. 8-9, pp. 637–644, 2006.

[87] J. Helenius, C.-P. Heisenberg, H. E. Gaub, and D. J. Muller, "Single-cell force spectroscopy," *Journal of cell science*, vol. 121, no. 11, pp. 1785–1791, 2008.

[88] O. H. Willemsen, M. M. Snel, A. Cambi, J. Greve, B. G. De Grooth, and C. G. Figdor, "Biomolecular interactions measured by Atomic Force Microscopy," *Biophysical journal*, vol. 79, no. 6, pp. 3267–3281, 2000.

[89] E. P. Wojcikiewicz, X. Zhang, and V. T. Moy, "Force and compliance measurements on living cells using Atomic Force Microscopy (AFM)," *Biological procedures online*, vol. 6, pp. 1–9, 2004.

[90] H. Kweon, S. Yiacoumi, and C. Tsouris, "The role of electrostatic charge in the adhesion of spherical particles onto planar surfaces in atmospheric systems," *Colloids and Surfaces A: Physicochemical and Engineering Aspects*, vol. 481, pp. 583–590, 2015.

[91] S. Rajupet, A. A. Riet, Q. Chen, M. Sow, and D. J. Lacks, "Relative importance of electrostatic and van der waals forces in particle adhesion to rough conducting surfaces," *Physical Review E*, vol. 103, no. 4, p. 042906, 2021.

[92] V. Mull and L. Kreplak, "Adhesion force microscopy is sensitive to the charge distribution at the surface of single collagen fibrils," *Nanoscale Advances*, vol. 4, no. 22, pp. 4829–4837, 2022.

[93] J. E. Sader and J. R. Friend, "Note: Calibration of Atomic Force Microscope cantilevers using only their resonant frequency and quality factor," *Review of Scientific Instruments*, vol. 85, no. 11, p. 116101, 2014.

[94] V. Mull and L. Kreplak, "Collagen fibril fingerprint analysis," *Github repository, https://github.com/vnk-m/Collagen-fingerprint*, 2023.

[95] S. J. Baldwin, J. Sampson, C. J. Peacock, M. L. Martin, S. P. Veres, J. M. Lee, and L. Kreplak, "A new longitudinal variation in the structure of collagen fibrils and its relationship to locations of mechanical damage susceptibility," *Journal of the mechanical behavior of biomedical materials*, vol. 110, p. 103849, 2020.

[96] S. YAMAMOTO, J. HITOMI, M. SHIGENO, S. SAWAGUCHI, H. ABE, and T. USHIKI, "Atomic force microscopic studies of isolated collagen fibrils of the bovine cornea and sclera," *Archives of histology and cytology*, vol. 60, no. 4, pp. 371–378, 1997.

[97] D. A. Cisneros, C. Hung, C. M. Franz, and D. J. Muller, "Observing growth steps of collagen self-assembly by time-lapse high-resolution Atomic Force Microscopy," *Journal of structural biology*, vol. 154, no. 3, pp. 232–245, 2006.

[98] M. R. Uhlig and R. Magerle, "Unraveling capillary interaction and viscoelastic response in Atomic Force Microscopy of hydrated collagen fibrils," *Nanoscale*, vol. 9, no. 3, pp. 1244–1256, 2017.

[99] M. Raspanti, A. Alessandrini, P. Gobbi, and A. Ruggeri, "Collagen fibril surface: TM-AFM, FEG-SEM and freeze-etching observations," *Microscopy research and technique*, vol. 35, no. 1, pp. 87–93, 1996.

[100] J. D. San Antonio, O. Jacenko, A. Fertala, and J. P. Orgel, "Collagen structure-function mapping informs applications for regenerative medicine," *Bioengineering*, vol. 8, no. 1, p. 3, 2020.

[101] L. Bozec and M. Horton, "Topography and mechanical properties of single molecules of type I collagen using Atomic Force Microscopy," *Biophysical journal*, vol. 88, no. 6, pp. 4223–4231, 2005.

[102] M. Raspanti, A. Alessandrini, V. Ottani, and A. Ruggeri, "Direct visualization of collagen-bound proteoglycans by tapping-mode Atomic Force Microscopy," *Journal of structural biology*, vol. 119, no. 2, pp. 118–122, 1997.

[103] P. G. Scott, P. A. McEwan, C. M. Dodd, E. M. Bergmann, P. N. Bishop, and J. Bella, "Crystal structure of the dimeric protein core of decorin, the archetypal small leucine-rich repeat proteoglycan," *Proceedings of the National Academy of Sciences*, vol. 101, no. 44, pp. 15633–15638, 2004.

[104] T. W. Herod, N. C. Chambers, and S. P. Veres, "Collagen fibrils in functionally distinct tendons have differing structural responses to tendon rupture and fatigue loading," *Acta Biomaterialia*, vol. 42, pp. 296–307, 2016.

[105] D. F. Holmes, Y. Lu, T. Starborg, and K. E. Kadler, "Collagen fibril assembly and function," *Current topics in developmental biology*, vol. 130, pp. 107–142, 2018.

[106] A. J. Hodge and F. O. Schmitt, "The charge profile of the tropocollagen macromolecule and the packing arrangement in native-type collagen fibrils," *Proceedings of the National Academy of Sciences*, vol. 46, no. 2, pp. 186–197, 1960.

[107] M. Rivard, M. Laliberté, A. Bertrand-Grenier, C. Harnagea, C. P. Pfeffer, M. Vallières, Y. St-Pierre, A. Pignolet, M. A. El Khakani, and F. Légaré, "The structural origin of Second Harmonic Generation in fascia," *Biomedical optics express*, vol. 2, no. 1, pp. 26–36, 2011.

[108] C.-A. Couture, S. Bancelin, J. Van der Kolk, K. Popov, M. Rivard, K. Légaré, G. Martel, H. Richard, C. Brown, S. Laverty, *et al.*, "The impact of collagen fibril polarity on Second Harmonic Generation microscopy," *Biophysical journal*, vol. 109, no. 12, pp. 2501–2510, 2015.

[109] M. Fang, E. L. Goldstein, A. S. Turner, C. M. Les, B. G. Orr, G. J. Fisher, K. B. Welch, E. D. Rothman, and M. M. Banaszak Holl, "Type I collagen D-spacing in fibril bundles of dermis, tendon, and bone: bridging between nano-and micro-level tissue hierarchy," *ACS nano*, vol. 6, no. 11, pp. 9503–9514, 2012.

[110] F. Yang, D. Das, K. Karunakaran, G. M. Genin, S. Thomopoulos, and I. Chasiotis, "Nonlinear time-dependent mechanical behavior of mammalian collagen fibrils," *Acta Biomaterialia*, 2022.

[111] J. Scott and M. Haigh, "'Small'-proteoglycan: collagen interactions: Keratan sulphate proteoglycan associates with rabbit corneal collagen fibrils at the 'a'and 'c' bands," *Bioscience reports*, vol. 5, pp. 765–774, 1985.

[112] Z. L. Shen, M. R. Dodge, H. Kahn, R. Ballarini, and S. J. Eppell, "In vitro fracture testing of submicron diameter collagen fibril specimens," *Biophysical journal*, vol. 99, no. 6, pp. 1986–1995, 2010.

[113] E. Hedbom and D. Heinegård, "Binding of Fibromodulin and Decorin to separate sites on fibrillar collagens.," *Journal of Biological Chemistry*, vol. 268, no. 36, pp. 27307–27312, 1993.

[114] H. Hedlund, S. Mengarelli-Widholm, D. Heinegård, F. P. Reinholt, and O. Svensson, "Fibromodulin distribution and association with collagen," *Matrix Biology*, vol. 14, no. 3, pp. 227–232, 1994.

[115] J. Scott and M. Haigh, "Proteoglycan-type I collagen fibril interactions in bone and non-calcifying connective tissues," *Bioscience Reports*, vol. 5, no. 1, pp. 71–81, 1985.

[116] J. E. Scott, C. R. Orford, and E. W. Hughes, "Proteoglycan-collagen arrangements in developing rat tail tendon. an electron microscopical and biochemical investigation," *Biochemical Journal*, vol. 195, no. 3, pp. 573–581, 1981.

[117] C. Thorpe, R. Stark, A. Goodship, and H. Birch, "Mechanical properties of the equine superficial digital flexor tendon relate to specific collagen cross-link levels," *Equine Veterinary Journal*, vol. 42, pp. 538–543, 2010.

[118] H. L. Birch, "Tendon matrix composition and turnover in relation to functional requirements," *International journal of experimental pathology*, vol. 88, no. 4, pp. 241–248, 2007.

[119] E. Batson, R. Paramour, T. Smith, H. Birch, J. Patterson-Kane, and A. Goodship, "Are the material properties and matrix composition of equine flexor and extensor tendons determined by their functions?," *Equine veterinary journal*, vol. 35, no. 3, pp. 314–318, 2003.

[120] J. G. Snedeker and A. Gautieri, "The role of collagen crosslinks in ageing and diabetes-the good, the bad, and the ugly," *Muscles, ligaments and tendons journal*, vol. 4, no. 3, p. 303, 2014.

[121] J. H. Lillie, D. K. MacCallum, L. J. Scaletta, and J. C. Occhino, "Collagen structure: evidence for a helical organization of the collagen fibril," *Journal of ultrastructure research*, vol. 58, no. 2, pp. 134–143, 1977.

Appendix

Copyright Permissions

Critical Reviews in Biochemistry and Molecular Biology >
Volume 52, 2017 - Issue 1

Review Article

Molecular insights into prolyl and lysyl hydroxylation of fibrillar collagens in health and disease

Rutger A. F. Gjaltema & Ruud A. Bank

Pages 74-95 | Received 01 Aug 2016, Accepted 05 Dec 2016, Published online: 23 Dec 2016

Licensing

Not-for-Profit Open Access
Created by Scientists, for Scientists

ISSN:1473-2262 NLM:100973416 (link) DOI:10.22203/eCM

2021 Volume No 43 – pages 130-152

Title: Regulators of collagen crosslinking in developing and adult tendons

Authors: AJ Ellingson, NM Pancheri, NR Schiele

Address: Chemical and Biological Engineering, University of Idaho, 875 Perimeter Dr. MS 0904, Moscow, ID, USA

E-mail: gaskon.ibarretxe **at** ehu.eus

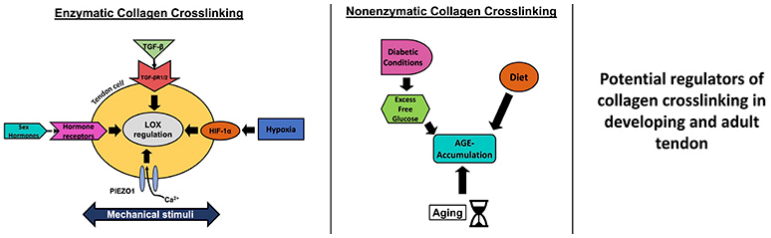

Abstract: Tendons are collagen-rich musculoskeletal tissues that possess the mechanical strength needed to transfer forces between muscles and bones. The mechanical development and function of tendons are impacted by collagen crosslinks. However, there is a limited understanding of how collagen crosslinking is regulated in tendon during development and aging. Therefore, the objective of the present review was to highlight potential regulators of enzymatic and non-enzymatic collagen crosslinking and how they impact tendon function. The main collagen crosslinking enzymes include lysyl oxidase (LOX) and the lysyl oxidase-like isoforms (LOXL), whereas non-enzymatic crosslinking is mainly mediated by the formation of advanced glycation end products (AGEs). Regulators of the LOX and LOXL enzymes may include mechanical stimuli, mechanotransducive cell signaling pathways, sex hormones, transforming growth factor (TGF)β family, hypoxia, and interactions with intracellular or extracellular proteins. AGE accumulation in tendon is due to diabetic conditions and aging, and can be mediated by diet and mechanical stimuli. The formation of these enzymatic and non-enzymatic collagen

crosslinks plays a major role in tendon biomechanics and in the mechanisms of force transfer. A more complete understanding of how enzymatic and non-enzymatic collagen crosslinking is regulated in tendon will better inform tissue engineering and regenerative therapies aimed at restoring the mechanical function of damaged tendons.

Keywords: Tendon, development, collagen, crosslinking, advanced glycation end products (AGEs), lysyl oxidase (LOX).

Publication date: April 5th 2022

Article download: Pages 130-152 (PDF file)
DOI: 10.22203/eCM.v043a11

Not-for-Profit Open Access
Created by Scientists, for Scientists

ISSN:1473-2262 NLM:100973416 (link) DOI:10.22203/eCM

Open Access Compliant

All publications in **eCM** have been immediately freely available upon publication since **eCM** first paper in 2001: articles are freely accessible to the public without any embargo period, irrespective of who funded the research. This is equivalent to the new term **"Gold Open Access"**, where articles are immediately available for others to read, download and share (e.g. can be uploaded on ResearchGate).

The European Research Council (ERC) and the The SNSF (Swiss National Science Foundation) are two of the funders of Europe PMC (Europe PubMed Central). ERC and SNSF are committed to open access. **eCM**, as an open access journal, is compliant for SNSF and ERC funded projects. Every **eCM** publication is held as a copy within this repository, which also has direct access to each paper on the **eCM** website. Europe PMC enriches the publications with information such as citation data and links from other databases. See **eCM** on European PMC. eCM is now indexed in the China Knowledge Resource Integrated (CNKI) Database.

Info on eCM
eCM Conferences
Editors
Societies
Sponsors
Privacy Policy
Donate
Contact

ELSEVIER LICENSE
TERMS AND CONDITIONS

May 23, 2023

This Agreement between Mr. VINAYAK MULL ("You") and Elsevier ("Elsevier") consists of your license details and the terms and conditions provided by Elsevier and Copyright Clearance Center.

License Number	5554971283244
License date	May 23, 2023
Licensed Content Publisher	Elsevier
Licensed Content Publication	International Journal of Biological Macromolecules
Licensed Content Title	Reconstitution of collagen fibrils in vitro; the assembly process depends on the initiating procedure
Licensed Content Author	D.F. Holmes,M.J. Capaldi,J.A. Chapman
Licensed Content Date	Jun 1, 1986
Licensed Content Volume	8
Licensed Content Issue	3
Licensed Content Pages	6
Start Page	161
End Page	166
Type of Use	reuse in a thesis/dissertation

Portion	figures/tables/illustrations
Number of figures/tables/illustrations	4
Format	electronic
Are you the author of this Elsevier article?	No
Will you be translating?	No
Title	Development of adhesion force microscopy for surface charge analysis of collagen fibrils in vivo and in vitro
Institution name	Dalhousie University
Expected presentation date	Jun 2023
Portions	Figures 1,2,3, and 5
Requestor Location	Dalhousie University 2073 Oxford Street Halifax, NS B3L2T3 Canada Attn: Dalhousie University
Publisher Tax ID	GB 494 6272 12
Total	0.00 CAD

Terms and Conditions

INTRODUCTION

1. The publisher for this copyrighted material is Elsevier. By clicking "accept" in connection with completing this licensing transaction, you agree that the following terms and conditions apply to this transaction (along with the Billing and Payment terms and conditions

IUCr Journals

Time scale of glycation in collagen of bovine pericardium-derived bio-tissues

[De Caro et al. (2021). IUCrJ, **8**, 1024-1034
https://doi.org/10.1107/S2052252521010344]

ELSEVIER LICENSE
TERMS AND CONDITIONS

May 23, 2023

This Agreement between Mr. VINAYAK MULL ("You") and Elsevier ("Elsevier") consists of your license details and the terms and conditions provided by Elsevier and Copyright Clearance Center.

License Number	5552621211477
License date	May 19, 2023
Licensed Content Publisher	Elsevier
Licensed Content Publication	Bone
Licensed Content Title	Structural changes in collagen fibrils across a mineralized interface revealed by cryo-TEM
Licensed Content Author	Bryan D. Quan,Eli D. Sone
Licensed Content Date	Aug 1, 2015
Licensed Content Volume	77
Licensed Content Issue	n/a
Licensed Content Pages	8
Start Page	42
End Page	49
Type of Use	reuse in a thesis/dissertation

Portion	figures/tables/illustrations
Number of figures/tables/illustrations	1
Format	electronic
Are you the author of this Elsevier article?	No
Will you be translating?	No
Title	Development of adhesion force microscopy for surface charge analysis of collagen fibrils in vivo and in vitro
Institution name	Dalhousie University
Expected presentation date	Jun 2023
Portions	Fig 2 on Page 44
Requestor Location	Dalhousie University 2073 Oxford Street Halifax, NS B3L2T3 Canada Attn: Dalhousie University
Publisher Tax ID	GB 494 6272 12
Total	0.00 CAD

Terms and Conditions

INTRODUCTION

1. The publisher for this copyrighted material is Elsevier. By clicking "accept" in connection with completing this licensing transaction, you agree that the following terms and conditions apply to this transaction (along with the Billing and Payment terms and conditions

CCC Marketplace

Order Date	24-May-2023	**Type of Use**	Republish in a thesis/dissertation
Order License ID	1358237-1		
ISSN	1077-3118	**Publisher**	AMERICAN INSTITUTE OF PHYSICS,
		Portion	Image/photo/illustration

LICENSED CONTENT

Publication Title	Applied physics letters	**Rightsholder**	American Institute of Physics
Article Title	Kelvin-probe force microscopy of the pH-dependent charge of functional groups	**Publication Type**	e-Journal
		Start Page	233702
Author/Editor	American Institute of Physics., American Institute of Physics.Online Journal Publishing Service	**Issue**	23
		Volume	108
		URL	http://aip.scitation.org/journal/apl
Date	01/01/1962		
Language	English		
Country	United States of America		

REQUEST DETAILS

Portion Type	Image/photo/illustration	**Distribution**	Canada
Number of Images / Photos / Illustrations	1	**Translation**	Original language of publication
Format (select all that apply)	Electronic	**Copies for the Disabled?**	No
		Minor Editing Privileges?	Yes
Who Will Republish the Content?	Academic institution	**Incidental Promotional Use?**	No
Duration of Use	Life of current and all future editions	**Currency**	CAD
Lifetime Unit Quantity	Up to 499		
Rights Requested	Main product		

NEW WORK DETAILS

Title	Development of adhesion force microscopy for surface charge analysis of collagen fibrils in vivo and in vitro	**Institution Name**	Dalhousie University
		Expected Presentation Date	2023-06-06
Instructor Name	Laurent Kreplak		

ADDITIONAL DETAILS

Order Reference Number	N/A	**The Requesting Person/Organization to Appear on the License**	Vinayak A. Mull

REQUESTED CONTENT DETAILS

Title, Description or Numeric Reference of the Portion(s)	Figure 4 on page 233702-3	**Title of the Article/Chapter the Portion Is From**	Kelvin-probe force microscopy of the pH-dependent charge of functional groups
Editor of Portion(s)	Stone, Alexander D. D.; Mesquida, Patrick	**Author of Portion(s)**	Stone, Alexander D. D.; Mesquida, Patrick
Volume of Serial or Monograph	108	**Issue, if Republishing an Article From a Serial**	23
Page or Page Range of Portion	233702	**Publication Date of Portion**	2016-06-06

SPECIAL RIGHTSHOLDER TERMS AND CONDITIONS

Please include a credit line referencing the original publication. Our preferred format is (please fill in the citation information): “Reproduced from [FULL CITATION], with the permission of AIP Publishing.”

Marketplace Permissions General Terms and Conditions

The following terms and conditions (“General Terms”), together with any applicable Publisher Terms and Conditions, govern User’s use of Works pursuant to the Licenses granted by Copyright Clearance Center, Inc. (“CCC”) on behalf of the applicable Rightsholders of such Works through CCC’s applicable Marketplace transactional licensing services (each, a “Service”).

1) **Definitions.** For purposes of these General Terms, the following definitions apply:

“License” is the licensed use the User obtains via the Marketplace platform in a particular licensing transaction, as set forth in the Order Confirmation.

“Order Confirmation” is the confirmation CCC provides to the User at the conclusion of each Marketplace transaction. “Order Confirmation Terms” are additional terms set forth on specific Order Confirmations not set forth in the General Terms that can include terms applicable to a particular CCC transactional licensing service and/or any Rightsholder-specific terms.

“Rightsholder(s)” are the holders of copyright rights in the Works for which a User obtains licenses via the Marketplace platform, which are displayed on specific Order Confirmations.

Marketplace

Order Date	12-Jun-2023	Type of Use	Republish in a thesis/dissertation
Order License ID	1364498-1		
ISSN	2516-0230	Publisher	Royal Society of Chemistry
		Portion	Chapter/article

LICENSED CONTENT

Publication Title	Nanoscale Advances	Start Page	4829
Article Title	Adhesion force microscopy is sensitive to the charge distribution at the surface of single collagen fibrils	End Page	4837
		Issue	22
		Volume	4
Date	01/01/2018		
Rightsholder	Royal Society of Chemistry		
Publication Type	Journal		

REQUEST DETAILS

Portion Type	Chapter/article	Rights Requested	Main product
Page Range(s)	4829-4836	Distribution	Worldwide
Total Number of Pages	7	Translation	Original language of publication
Format (select all that apply)	Electronic	Copies for the Disabled?	No
Who Will Republish the Content?	Author of requested content	Minor Editing Privileges?	No
Duration of Use	Life of current edition	Incidental Promotional Use?	No
Lifetime Unit Quantity	Up to 1,000,000	Currency	CAD

NEW WORK DETAILS

Title	Development of adhesion force microscopy for the surface charge analysis of collagen fibrils in vivo and in vitro	Institution Name	Dalhousie University
		Expected Presentation Date	2023-06-12
Instructor Name	Laurent Kreplak		

ADDITIONAL DETAILS

Order Reference Number	N/A	**The Requesting Person/Organization to Appear on the License**	Dalhousie University

REQUESTED CONTENT DETAILS

Title, Description or Numeric Reference of the Portion(s)	Page 4829-4937	**Title of the Article/Chapter the Portion Is From**	Adhesion force microscopy is sensitive to the charge distribution at the surface of single collagen fibrils
Editor of Portion(s)	Mull, Vinayak; Kreplak, Laurent	**Author of Portion(s)**	Mull, Vinayak; Kreplak, Laurent
Volume / Edition	4	**Issue, if Republishing an Article From a Serial**	22
Page or Page Range of Portion	4829-4837	**Publication Date of Portion**	2022-11-08

Marketplace Permissions General Terms and Conditions

The following terms and conditions ("General Terms"), together with any applicable Publisher Terms and Conditions, govern User's use of Works pursuant to the Licenses granted by Copyright Clearance Center, Inc. ("CCC") on behalf of the applicable Rightsholders of such Works through CCC's applicable Marketplace transactional licensing services (each, a "Service").

1) **Definitions.** For purposes of these General Terms, the following definitions apply:

"License" is the licensed use the User obtains via the Marketplace platform in a particular licensing transaction, as set forth in the Order Confirmation.

"Order Confirmation" is the confirmation CCC provides to the User at the conclusion of each Marketplace transaction. "Order Confirmation Terms" are additional terms set forth on specific Order Confirmations not set forth in the General Terms that can include terms applicable to a particular CCC transactional licensing service and/or any Rightsholder-specific terms.

"Rightsholder(s)" are the holders of copyright rights in the Works for which a User obtains licenses via the Marketplace platform, which are displayed on specific Order Confirmations.

"Terms" means the terms and conditions set forth in these General Terms and any additional Order Confirmation Terms collectively.

"User" or "you" is the person or entity making the use granted under the relevant License. Where the person accepting the Terms on behalf of a User is a freelancer or other third party who the User authorized to accept the General Terms on the User's behalf, such person shall be deemed jointly a User for purposes of such Terms.

"Work(s)" are the copyright protected works described in relevant Order Confirmations.

2) **Description of Service.** CCC's Marketplace enables Users to obtain Licenses to use one or more Works in accordance with all relevant Terms. CCC grants Licenses as an agent on behalf of the copyright rightsholder identified in the relevant Order Confirmation.

3) **Applicability of Terms.** The Terms govern User's use of Works in connection with the relevant License. In the event of any conflict between General Terms and Order Confirmation Terms, the latter shall govern. User acknowledges that Rightsholders have complete discretion whether to grant any permission, and whether to place any limitations on any grant, and that CCC has no right to supersede or to modify any such discretionary act by a Rightsholder.

4) **Representations; Acceptance.** By using the Service, User represents and warrants that User has been duly authorized by the User to accept, and hereby does accept, all Terms.